UDK 66:54(05) CODEN HMIDA 8 ISSN 0367–598X

1

Hemijska industrija

Vol. 78

Časopis Saveza hemijskih inženjera Srbije

Chemical Industry

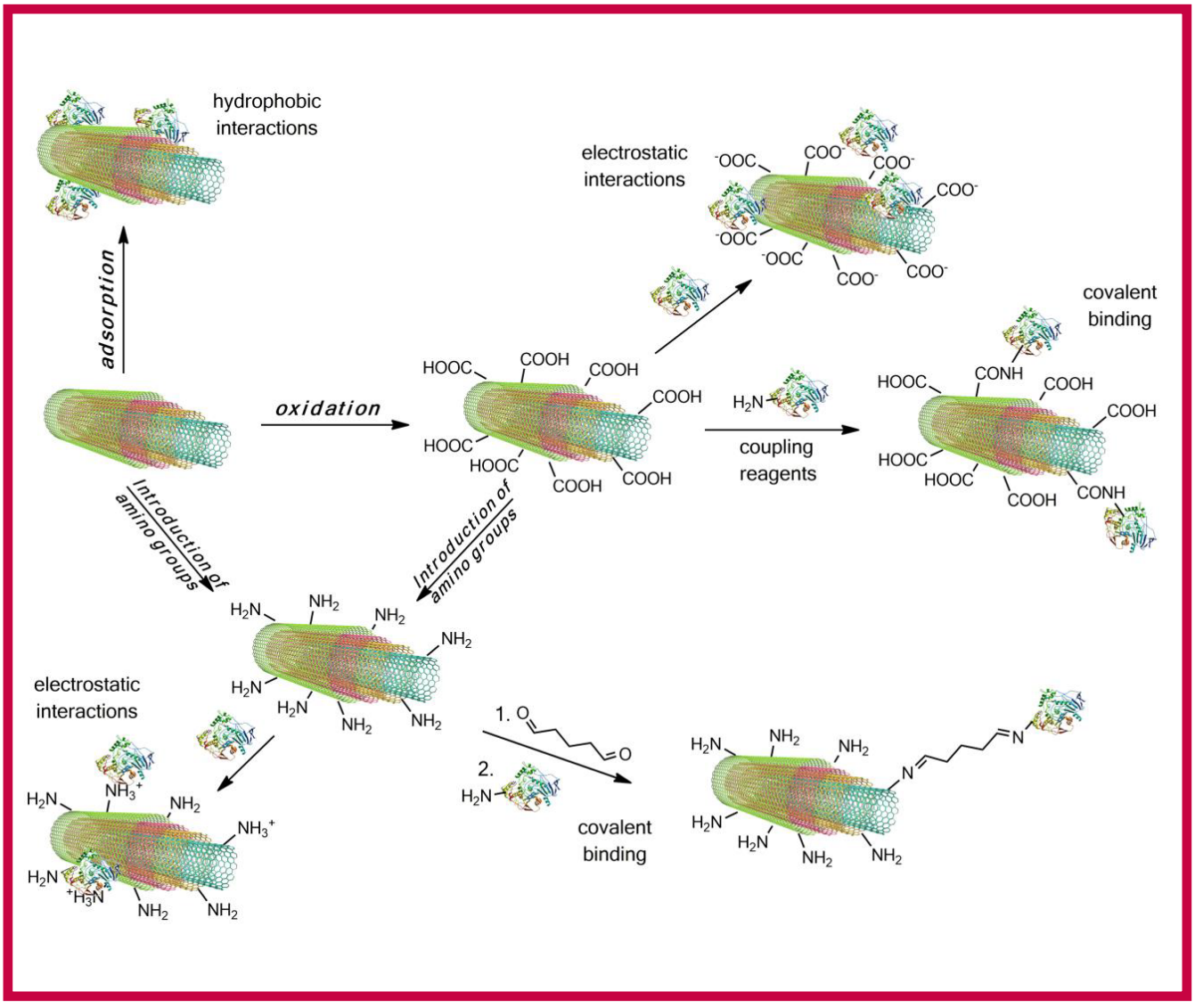

BEOGRAD, JANUAR - MART 2024. HMIDA 8, 78(1) 1-74 (2024)

Aktivnosti Saveza hemijskih inženjera Srbije pomažu:

**MINISTARSTVO NAUKE,
TEHNOLOŠKOG RAZVOJA
I INOVACIJA
REPUBLIKE SRBIJE**

Tehnološko-metalurški fakultet
Univerziteta u Beogradu

Prirodno-matematički fakultet
Univerziteta u Novom Sadu

Institut za tehnologiju nuklearnih i
drugih mineralnih sirovina, Beograd

Tehnološki fakultet
Univerziteta u Novom Sadu

Institut za hemiju, tehnologiju i metalurgiju
Univerziteta u Beogradu

Fakultet tehničkih nauka
Univerziteta u Novom Sadu

Tehnološki fakultet
Univerziteta u Nišu, Leskovac

Fakultet tehničkih nauka
Univerziteta u Prištini
Kosovska Mitrovica

Institut IMS, Beograd

DCP HEMIGAL
Leskovac

Barič

Elixir Prahovo

Chemical Industry
Химическая промышленность

Hemijska industrija

Časopis Saveza hemijskih inženjera Srbije
Journal of the Association of Chemical Engineers of Serbia
Журнал Союза химических инженеров Сербии

VOL. 78 **Beograd, januar – mart 2024.** **Broj 1**

Izdavač
Savez hemijskih inženjera Srbije
Beograd, Kneza Miloša 9/I

Glavni urednik
Bojana Obradović

Zamenica glavnog i odgovornog urednika
Emila Živković

Pomoćnik glavnog i odgovornog urednika
Ivana Drvenica

Urednici
Jelena Bajat, Dejan Bezbradica, Ivana Banković-Ilić, Dušan Mijin, Marija Nikolić, Đorđe Veljović, Tatjana Volkov-Husović

Članovi uredništva
Nikolaj Ostrovski, Milorad Cakić, Željko Čupić, Miodrag Lazić, Slobodan Petrović, Milovan Purenović, Aleksandar Spasić, Dragoslav Stoiljković, Radmila Šećerov-Sokolović, Slobodan Šerbanović, Nikola Nikačević, Svetomir Milojević

Članovi uredništva iz inostranstva
Dragomir Bukur (SAD), Jiri Hanika (Češka Republika), Valerij Meshalkin (Rusija), Ljubiša Radović (SAD), Constantinos Vayenas (Grčka)

Likovno-grafičko rešenje naslovne strane
Milan Jovanović

Redakcija
11000 Beograd, Kneza Miloša 9/I
Tel/fax: 011/3240-018
E-pošta: shi@ache.org.rs
www.ache.org.rs

Izlazi kvartalno, rukopisi se ne vraćaju

Za izdavača: Ivana T. Drvenica

Sekretar redakcije: Slavica Desnica

Izdavanje časopisa pomaže
Republika Srbija, Ministarstvo nauke, tehnološkog razvoja i inovacija

Uplata pretplate i oglasnog prostora vrši se na tekući račun Saveza hemijskih inženjera Srbije, Beograd, broj 205-2172-71, Komercijalna banka a.d., Beograd

Menadžer časopisa i kompjuterska priprema
Aleksandar Dekanski

Štampa
Razvojno-istraživački centar grafičkog inženjerstva, Tehnološko-metalurški fakultet, Univerzitet u Beogradu, Karnegijeva 4, 11000 Beograd

Indeksiranje
Radovi koji se publikuju u časopisu *Hemijska Industrija* ideksiraju se preko *Thompson Reuters Scietific®* servisa *Science Citation Index - Expanded™* i *Journal Citation Report (JCR)*

SADRŽAJ/CONTENTS

Multi-walled carbon nanotubes as lipase carriers for organic synthesis: current trends and recent update

Nevena Ž. Prlainović[1], Jelena S. Milovanović[2], Nikola Z. Milašinović[3], Dejan I. Bezbradica[1] and Dušan Ž. Mijin[1]

[1]*University of Belgrade, Faculty of Technology and Metallurgy, Belgrade, Serbia*
[2]*University of Belgrade, Institute of Molecular Genetics and Genetic Engineering, Belgrade, Serbia*
[3]*University of Criminal Investigation and Police Studies, Belgrade, Serbia*

Abstract

Lipase-catalyzed organic reactions have been widely practiced in the past three decades. Especially interesting are insoluble/immobilized forms due to providing a possibility of facile use and recyclability, thus reducing process costs, and making the procedure more environmentally friendly. Carbon-based supports have been extensively exploited for this purpose, because of neutral and biodegradable nature and thermal and chemical stability. Their high specific surface area, characteristic surface morphology and lower mass transfer resistances play a vital role in the performance of the attached enzyme. This review paper presents an overview of the main aspects of lipase immobilized on multi-walled carbon nanotubes (MWCNTs). Moreover, different immobilization strategies to achieve a biocatalyst with improved performances are discussed. Furthermore, as lipases are considered to have high commercial worth for synthesis of valuable organic molecules, the second part of the paper is dedicated to the overview of the most important industrial sectors in which these nanobiocatalysts have been used. In specific, applications in biodiesel production, flavour ester synthesis and racemization are summarized.

Keywords: Enzyme immobilization; biocatalysis; biodiesel; flavour esters; racemization.

Available on-line at the Journal web address: http://www.ache.org.rs/HI/

REVIEW PAPER

UDC: 577.152.3:544.478.3

Hem. Ind. **78(1)** 1-16 (2024)

1. INTRODUCTION

Organic syntheses strongly influence the quality of our lives because they have become an essential tool for preparing numerous molecules, which, due to their wide applicability, increase the modern living standard [1]. Considering that fundamental organic synthesis mostly harms the environment, attention is drawn to using enzymes as practical alternatives to fulfill the principles of green chemistry and sustainability [2-4]. The concept of enzymes as catalysts was introduced in the 1830s, while their importance in modern organic synthesis was recognized in the second half of the 20th century when the techniques for enzyme isolation and purification were developed [5]. Enzyme-based technology has been attracting substantial interest in many scientific fields as a substitute for conventional synthetic methods due to high specific activity and selectivity [6]. However, a couple of serious drawbacks at large-scale application, limited stability under working conditions in organic synthesis, and challenged recovery from reaction media restricted miscellaneous usage of enzymes.

Different cost-reduction techniques have been appraised to make biotechnological processes more favorable and to enhance enzyme stability and utilization [7]. The most elegant solution is enzyme immobilization and transformation into a heterogeneous solid catalyst which can be readily recovered from the reaction medium and reused [8]. Immobilization also decreases the mobility of the enzyme molecule by adjusting to the solid support surface, making the conformation more rigid and the preparation of biocatalysts more resistant to elevated temperatures and organic solvents. In short, immobilization can enable applications that would not be economically viable with the use of free enzyme, and it can facilitate the use of enzymes in cost-effective continuous flow technologies [9].

Corresponding authors: : Nevena Ž. Prlainović, University of Belgrade, Faculty of Technology and Metallurgy, Belgrade, Serbia
E-mail: nprlainovic@tmf.bg.ac.rs
Paper received: 14 June 2023; Paper accepted: 3 January 2024; Paper published: 25 January 2024.
https://doi.org/10.2298/HEMIND230614003P

The most widely used enzymes in organic synthesis are hydrolases [10]. Amongst them, especially important are lipases, triacylglycerol acylhydrolase, EC 3.1.1.3, which can catalyze the reactions of ester synthesis, hydrolysis, inter-esterification, and trans-esterification, [11-15] as well as some unconventional interesting reactions [16]. The valuable selective properties of lipases allow them to serve as highly adaptable catalysts in industrial biotechnology, particularly in the food, chemical, and pharmaceutical industries. The first scientific research on enzyme immobilization dates back to 1916 [17], while during the 1950s and 1960s, modern enzyme immobilization methods were developed [18]. One of the most critical tasks for developing insoluble/immobilized enzymes is selecting a suitable carrier [19,20], and a variety of supports for lipase immobilization have been synthesized [21,22]. Although conventional mesoporous resins are the most frequently used [23,24], typically micron-sized, nanostructured materials have received extensive attention in recent years. Among them especially significant are carbon nanotubes (CNTs). CNTs generally provide a large surface area, low mass transfer resistance, and high enzyme loading capacity, while proper functionalization of their surface with specific groups makes it even more suitable for further lipase attachment.

The present review focuses on lipase immobilization on multi-walled carbon nanotubes MWCNTs, starting from 2010. The aim is to provide a comprehensive guide on different immobilization strategies and further application of such prepared catalysts. Special attention will be paid to applying these biocatalytic systems in typical lipase catalyzed esterification/transesterification processes: biodiesel production, flavor esters synthesis, and racemization reaction.

2. NANOSCALED MATERIALS AS SUPPORTS FOR LIPASE IMMOBILIZATION

One of the most important issues for successfully applying immobilized systems in organic syntheses is selecting a suitable material to support enzyme attachment. Clear and precise classification of materials is a very complex and complicated task because materials science has been expanding for the last 20 years. The most general division is based on chemical composition, *i.e.* materials can be organic or inorganic [25]. Additionally, different organic and inorganic materials can be combined to create novel hybrid/composite materials [26]. According to the origin, materials can be natural, artificial (man-made), or a combination. Furthermore, all mentioned types of materials can be grouped based on the particle size: bulk (size above 100 nm) and nanomaterials (at least one dimension in the range 1 to 100 nm). Based on dimensionality, shape and number of nanoscale dimensions, nanomaterials can be divided into four classes (Fig. 1).

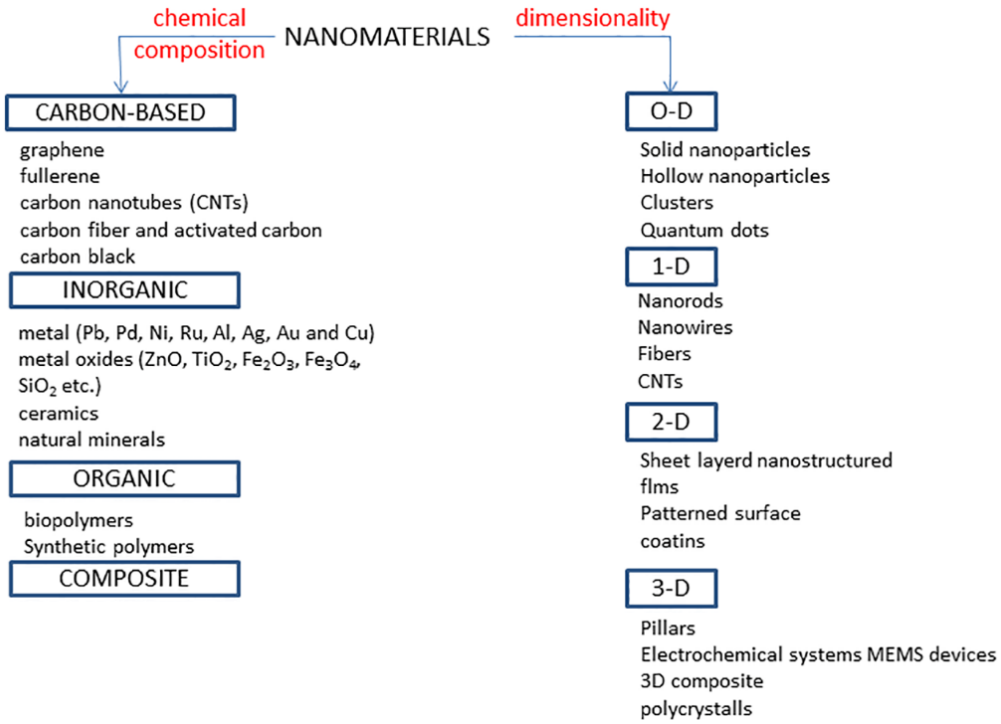

Figure 1. Classification of nanomaterials based on chemical composition and dimensionality (note that carbon materials are classified in a separate group)

Zero-dimensional (O-D) nanomaterials have all their dimensions within the nanoscale, one-dimensional (1-D) have one dimension outside the nanoscale, two-dimensional (2-D) have two dimensions outside the nanoscale and the three-dimensional (3-D) nanomaterials are composed of a multiple arrangement of nanosized crystals in different orientations [27]. Nanomaterials have proven to be ideal supports for enzyme immobilization, considering the possibility of balancing the key factors that determine the efficiency of biocatalysts. Many studies have reported that high specific surface area, characteristic surface morphology, and lower mass transfer resistances achieved by reducing the size of the enzyme immobilizing support play a vital role to achieve high enzyme loading, stabilization, and better performance of the attached enzyme [28,29]. Classification and examples of materials regarding composition and dimensionality are presented in Figure 1. It should be noted that carbon materials are classified in a separate group due to their variety of forms and distinctive properties.

2. 1. Carbon nanomaterials for lipase immobilization

Carbon is the most abundant element in the environment, and due to the possibility to exist in several allotropic modifications, carbon-based materials are considered a separate class of nanomaterials [30]. They include graphene, nanotubes (single- and multi-walled), fibers, activated carbon, and carbon black. Carbon-based supports have been extensively exploited because of neutral and biodegradable nature and thermal and chemical stability [31]. Due to the hydrophobic nature of the surface, these materials are particularly suitable for lipase immobilization. MWCNTs and graphene oxide (GO) are the most widely used, with the former being the focus of this review including modification routes for improving lipase performances.

Carbon nanotubes (CNTs), also called buckytubes, were discovered in 1991 [32]. Since then, they have been considered the most intensively studied nanostructured materials [33]. Structurally, CNTs consist of a two-dimensional hexagonal network of carbon atoms rolled up into a cylinder, with diameters typically measured in nanometers [34]. There are two types of CNTs, *i.e.* single-walled carbon nanotubes (SWCNTs) and multi-walled carbon nanotubes (MWCNTs). Due to lower costs and easier dispersibility immobilization research was almost exclusively performed on MWCNTs [35]. Structure of the MWCTs is presented in Figure 2.

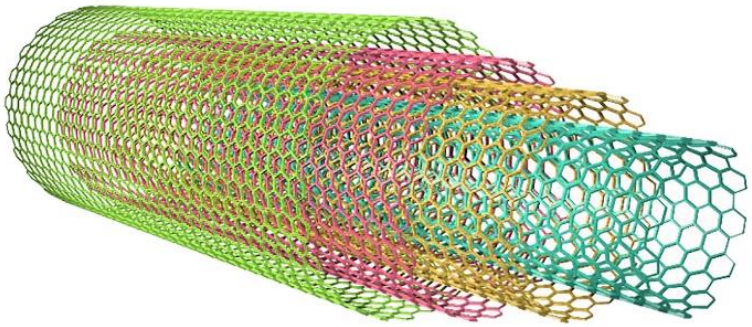

Figure 2. Schematic presentation of multi-walled carbon nanotubes (MWCNTs)

MWCNTs have one nanoscale dimension, providing a high specific area and possibility to load high amounts of the enzyme. Their length can be controlled, thus, providing the possibility for recovery by simple filtration [36]. Within various applications, due to their remarkable mechanical strength and specific surface chemistry, carbon nanotubes are recognized as unique and practical support for lipase immobilization. The success of lipase immobilization on a hydrophobic support greatly depends on the specific mobile structural domain called "lid", located over the active site. As a result, lipases show two different states in catalytic activity: closed - inactive and open - active form. Movement of the lid in the interaction with hydrophobic surfaces is a phenomenon known as "interfacial activation" and related to the increased lipase activity [37]. Hydrophobicity of the CNT surface can shift the structural balance of lipase to the open form, thus improving the catalytic activity [36]. MWCNTs became superior carbon nanomaterials for lipase immobilization due to greater hydrophobicity. At almost the same enzyme loading as on graphene oxide, MWCNT-composite showed higher activity by 1200 % [38].

2. 2. Strategies for lipase immobilization on carbon nanotubes

Summary of various lipase immobilization methods onto MWCNTs, together with the tested catalytic properties and biotechnological applications, is given in Table 1, while the immobilization strategies are illustrated in Figure 3. Immobilization on MWCNTs can be generally classified as non-covalent and covalent; regardless of the interaction type, they have a great lipase loading capacity. Direct coupling or physical adsorption on unmodified (*i.e.* raw or pristine) nanotubes is driven by hydrophobic interaction and π-π stacking. Results of a dozen of papers published since 2010 [39], have demonstrated that MWCNTs could adsorb high amounts of lipase [40-44]. Interfacial activation of lipases has led scientists to make CNTs surfaces even more hydrophobic. A heterogeneous biocatalyst was developed by adsorbing type B *Candida antarctica* lipase (CALB) on MWCNTs modified with hydrophobic polytetrafluoroethylene (PTFE), which showed high activity and stability in the synthesis of levulinate esters [45,46]. Adsorption on raw-MWCNTs can be also enhanced by the addition of surfactants such as Tween 80 and Triton X-100 [47,48]. Even though the very hydrophobic surface of the MWCNTs has a positive effect on increasing lipase activity, the major disadvantage of adsorption on the unmodified surface is the agglomeration of both the particles of the carrier and the enzyme molecules. This problem can be easily overcome by increasing hydrophilicity of the surface by functionalization [49]. Further improvement of enzyme immobilization in the sense of stabilization and better orientation of the molecule and higher dispersibility in aqueous media is induced by functionalization of the CNTs surface providing positively and/or negatively charged moieties. Among various techniques, acid treatment has been the most widely used. A carrier modified in this way (o-MWCNT) has polar carboxylic groups on its surface (negatively charged under all immobilization conditions), which, in addition to the mentioned π-π stacking, enable hydrogen bonding and electrostatic interactions with polar moieties present on the enzyme surface [35,39,40,50,51]. In addition to carboxyl, amino groups can be also introduced to the surface directly to raw-MWCNTs by using amino plasma treatment [52,53], or indirectly starting from o-MWCNTs, using bifunctional reagents [38,54-58].

Table 1. Summary of various lipase immobilization methods onto MWCNTs, together with the tested catalytic properties and biotechnological applications

Support	Lipase source	Modification reagents / surface group	Immobilization method	Application	Ref.
MWCNT	CRL	-	Hydrophobic interactions	*p*-NPP hydrolysis	[41]
MWCNT N-MWCNT Fe-MWCNT	CALB	-	Hydrophobic interactions	Baeyer-Villager oxidation	[42]
MWCNT	CRL	-	Hydrophobic interactions	Olive oil hydrolysis	[75]
MWCNT	CALB	-	Hydrophobic interactions	Diester plasticizers synthesis	[43]
MWCNT	PFL	-	Hydrophobic interactions	Commercially important esters	[76]
m-MWCNT	RML	-	Hydrophobic interactions	(OPO)-Rich human milk fat	[44]
MWCNT	CALB	→PTFE	Hydrophobic interactions	Levulinate esters synthesis	[45,46]
MWCNT	CALB	→plasma treated/-COOH → amine/-NH_2	Adsorption	Biodiesel (rapeseed oil)	[56]
MWCNT	PCL	→Tween 80	Adsorption	*p*-NPP hydrolysis	[47]
MWCNT	CRL	→Triton X-100	Adsorption	Emulsifier synthesis (methyl oleate)	[48]
MWCNT	*Pseudomonas sp.*	→acid treatment/-COOH	Adsorption	Flavor ester synthesis (ethyl butyrate)	[40]
MWCNT	CRL	→acid treatment/ -COOH	Adsorption	Emulsifier synthesis (methyl oleate)	[50]
MWCNT	CRL	→acid treatment/-COOH	Adsorption	Flavor ester synthesis (geranyl propionate	[51]

Support	Lipase source	Modification reagents / surface group	Immobilization method	Application	Ref.
MWCNT	CRL	→acid treatment/-COOH	Adsorption Covalent (coupling with EDC+NHS)	*p*-NPP hydrolysis	[66]
MWCNT	CALB	→acid treatment/-COOH →acid treatment; HMDA/-NH_2 →acid treatment; OABr and HDBr/-COOR	Adsorption	Ester synthesis (butyl caprylate)	[39]
MWCNT	CRL	→acid treatment/-COOH	Adsorption Covalent (coupling with EDC+NHS)	Oily waste water treatment	[49]
MWCNT	CALB	→acid treatment/-COOH	AdsorptionCovalent (coupling with EDC+NHS)	Ester synthesis (geranyl acetate)	[61]
MWCNT	Alkaline PFL	→acid treatment/-COOH	Adsorption Covalent (coupling with EDC+NHS)	Solketal esters	[63]
MWCNT	PFL	→acid treatment/-COOH	Covalent (coupling with EDC+NHS)	Resolution of (*RS*)-1-phenylethanol	[62]
MWCNT	Amano AK from PFL	→acid treatment/-COOH	Covalent (coupling with EDC+NHS)	Biodiesel (Jatropha seed oil)	[64]
MWCNT	YLL	→acid treatment/-COOH	Covalent (coupling with EDC+NHS)	Resolution of (*RS*)-1-phenylethanol	[65]
MWCNT	Isolated lipase	→acid treatment/-COOH	Covalent (coupling with EDC+NHS)	Resolution of (*RS*)-1-phenylethanol	[67]
MWCNT	CALB	→acid treatment/-COOH →acid treatment; APTES; succinic acid/-COOH	Covalent (coupling with EDC+NHS)	Flavor ester synthesis (pentyl valerate)	[55]
MWCNT	Amano AK from PFL	→acid treatment/-COOH →$Fe_2SO_4{\cdot}6H_2O$; H_2O_2/-OH →AZDA/-NH_2	Covalent(coupling with CDI, DVS or GA)	Solketal esters	[38]
MWCNT	Amano AK from PFL	urea/-NH_2	Covalent (crosslinking with GA)	Biodiesel (sunflower oil)	[77]
m-MWCNT	RML	→acid treatment; APTES; PAMAM/-NH_2	Covalent (crosslinking with GA)	Biodiesel (vegetable oil)	[73]
m-MWCNT	BCL	→acid treatment; $SOCl_2$; EDA; methyl acrylate; PAMAM/-NH_2	Covalent (crosslinking with GA)	Biodiesel	[74]
MWCNT	CRL	→acid treatment; PDA/-NH_2	Covalent (crosslinking with GA)	Flavor ester synthesis (ethyl butyrate and isoamyl acetate)	[54]
MWCNT	CALB	-NH_2	Covalent (crosslinking with GA)	Biodiesel (Jatropha seed oil)	[70]
MWCNT	TLL	→acid treatment; EDA/-NH_2	Covalent (crosslinking with GA)	Hydrolysis long chain ester	[71]
MWCNT	CRL, CALA, CALB	→acid treatment; HMDA/-NH_2	Covalent (crosslinking with GA)	Ester synthesis (butyl caprylate)	[72]
MWCNT	CALB	→D-glucose based IL treatment	Adsorption Covalent	Ester synthesis (n-butyl acrylate)	[69]
MWCNT	CALB, CRL, AOL	→ IL treatment	Adsorption Covalent	Baeyer-Villiger oxidation of ketones	[68]

CRL - *Candida rugosa* lipase; CALB - *Candida antarctica* lipase B; PFL - *Psudomonas fluorescens* lipase; m-MWCNT - magnetic MWCNT; RML -*Rhizomucor miehei* lipase; PCL - *Pseudomonas cepacia* lipase; BCL - *Burkholderia cepacia* lipase; YLL -*Yarrowia lipolitica* lipase; TLL - *Thermomyces lanuginosus* lipase; CALA - *Candida antarctica* lipase A;AOL - *Aspergilus oryzae* lipase PTFE - Polytetrafluoroethylene; OABr - tetra-n-Octylammonium bromide; HDBr - Hexadecyl bromide EDC - 1-Ethyl-3-(3-dimethylaminopropyl)carbodiimide; NHS - N-Hydroxysuccinimide; APTES - (3-Aminopropyl)triethoxysilane; AZDA - 10-Azidodecan-1-amine CDI - 1,1'-Carbonyldiimidazole; DVS - Divinyl sulfone; GA - Glutaraldehyde; PAMAM - Poly(amidoamine); PDA - Polydopamine; EDA - Ethylenediamine; HMDA - Hexamethylenediamine; *p*-NPP - *p*-Nitrophenyl palmitate, IL - ionic liquids

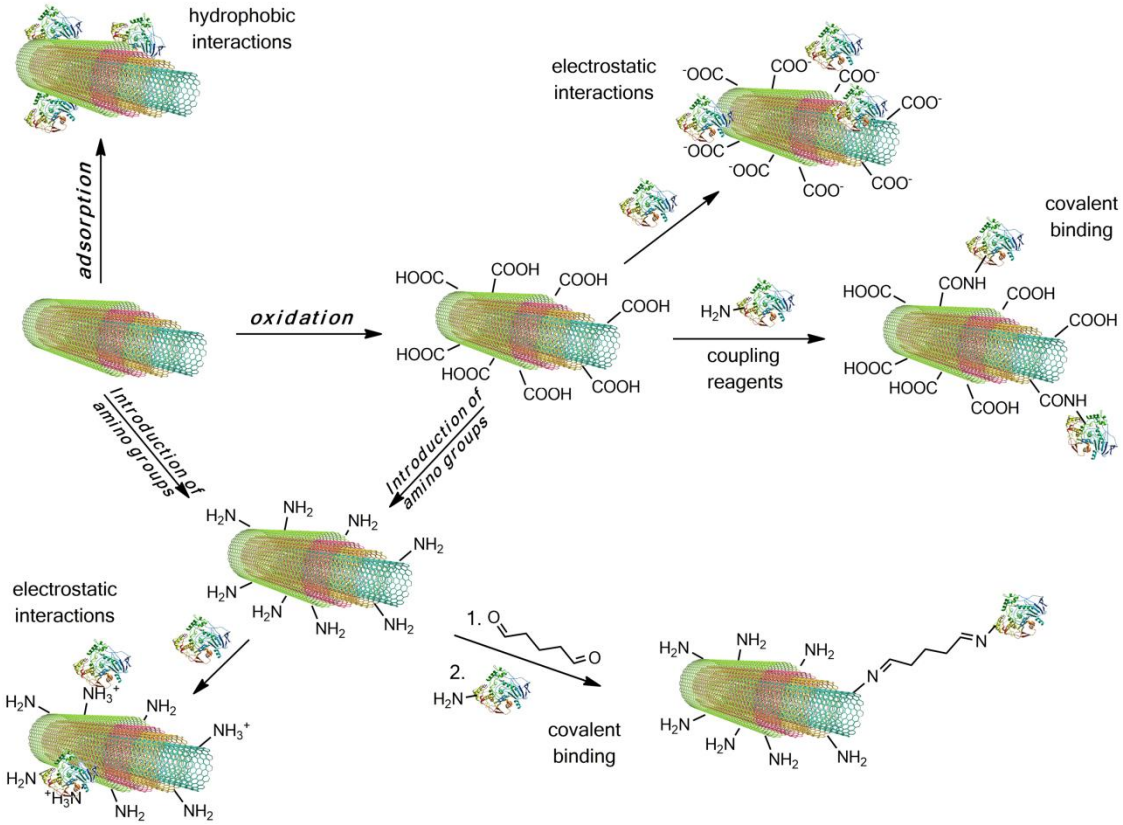

Figure 3. Lipase immobilization strategies onto MWCNTs

Modification of o-MWCNTs first implies formation of chloride (with the aid of thionyl chloride), and reaction with various diamines afterwards, or direct reaction with diamines using coupling reagents. In both ways, one amino group of diamine forms an amide bond with the carbonyl group at the MWCNTs surface, and the other remains free. Such a more hydrophilic surface with positively charged amino groups enables electrostatic interactions with oppositely charged groups from the lipase molecule surface. By a comparative study of lipase adsorption on MWCNTs functionalized with carboxyl-, amine-, and ester-terminal groups, it has been shown that a more hydrophilic surface can load a higher lipase amount, while a more hydrophobic surface provides biocatalysts with greater activity [39]. Covalent conjugation between the enzyme and support is recognized to provide durable attachment, enhanced stability, selectivity, and accessibility, and prevents enzyme leaching [59,60]. The most commonly used covalent method for immobilizing lipase is amide bond formation between carboxylic groups on MWCNTs and amino groups on the enzyme *via* carbodiimide chemistry [38,49,55,61-66]. Numerous examples can be mentioned to illustrate the advantages of this method. Lipolytic activity of MWCNT immobilized *Candida rugosa* lipase (CRL) was shown to be almost 3-fold higher under covalent promoting conditions compared to only adsorption [67]. At the same time, it was reported that covalently attached CRL retained 98 % activity of the native lipase, which is significantly higher than other usually used supports [49]. Raghavendra *et al*. used (3-aminopropyl)triethoxysilane (APTES) as a spacer arm to position lipase molecules away from the MWCNTs surface, but the biocatalyst activity was not improved [55]. Excellent results were obtained by covalently coupled Amano lipase AK on oxidized MWCNTs resulting in a biocatalyst with 100 % retained native activity [64].

As stability of the immobilized enzyme appears to be the most significant factor for industrial application, an interesting approach for lipase stabilization using ionic liquids (IL) has been developed [68,69]. The obtained biocatalysts showed exceptional properties, and the synthesis process fully corresponds to the sustainable development.

Amino functionalized surface of MWCNTs can be further activated by using glutaraldehyde (GA). To avoid cross-linking of the enzyme molecule, the nanomaterial is activated first. After that, aldehyde groups of GA can form stable covalent, imine, bond with amino groups of the enzyme. Various lipases have been attached using this approach [54,70-72]. Although biocatalysts obtained by forming a covalent bond typically express lower catalytic activity than the free lipase, their higher

stability and reusability justify the immobilization process. For example, *Thermomyces lanuginosus* lipase (TLL) immobilized by GA cross-linking exhibited significantly improved thermal stability and could be reused in up to 10 cycles for hydrolysis of long-chain esters [71]. The improved stability of lipase–MWCNTs conjugates over the free lipase is considered a consequence of a more rigid protein, resistant towards rapid unraveling for longer periods of time. Such property is useful, especially when dealing with extensive esterification process under harsh conditions.

Another interesting immobilization approach feasible for amino-functionalized MWCNTs (not depicted in Fig. 3), which significantly increases surface, represents dendrimer formation using a nanoscaled hyperbranched polymer as poly(amidoamine) (PAMAM). *Rhizomucor miehei* (RML) and *Burkholderia cepacia* lipases (BCL) immobilized on magnetic-MWCNT-PAMAM nanocomposites exhibited good stability and recycling performance [73,74].

Influence of different functionalized MWCNTs, namely alkylamino-, hydroxyl- and carboxyl- MWCNTs, was explored regarding the biocatalytic performance [38]. Nanobiocatalysts obtained by covalent immobilization of alkaline lipase from *P. fluoerscens* on MWCNT-NH_2 have been the most active (12 times higher than the native lipase), while MWCNT-COOH based bioconjugates emerged as the most enantioselective. Such results corroborate the finding that different properties of biocatalysts can be achieved by controlling the immobilization conditions, especially surface groups involved in the immobilization process.

3. APPLICATIONS

Lipases primarily catalyze hydrolysis of triacylglycerols to free fatty acids, di- and monoacylglycerols and glycerol. Still, their versatile nature enables them to catalyze hydrolysis of various other esters, as well as the formation of ester bonds between acids and alcohols (Fig. 4). Lipases occupy third place in the total world enzyme production, just behind proteases and enzymes that catalyze the hydrolysis of carbohydrates, while they are the most widely exploited enzymes in organic synthesis [78].

Transesterification *via* lipase use is referred to as a ping-pong bi-bi mechanism, where the lipase enzyme reacts with two substrates, triglyceride and the enzyme-substrate intermediate resulting in the formation of two products. The lipase active site has two functional groups vital for the catalytic activity: the hydroxyl group of serine that performs a nucleophilic addition forming an enzyme-substrate complex, and the second is a nitrogen atom on histidine acting as a proton acceptor [79].

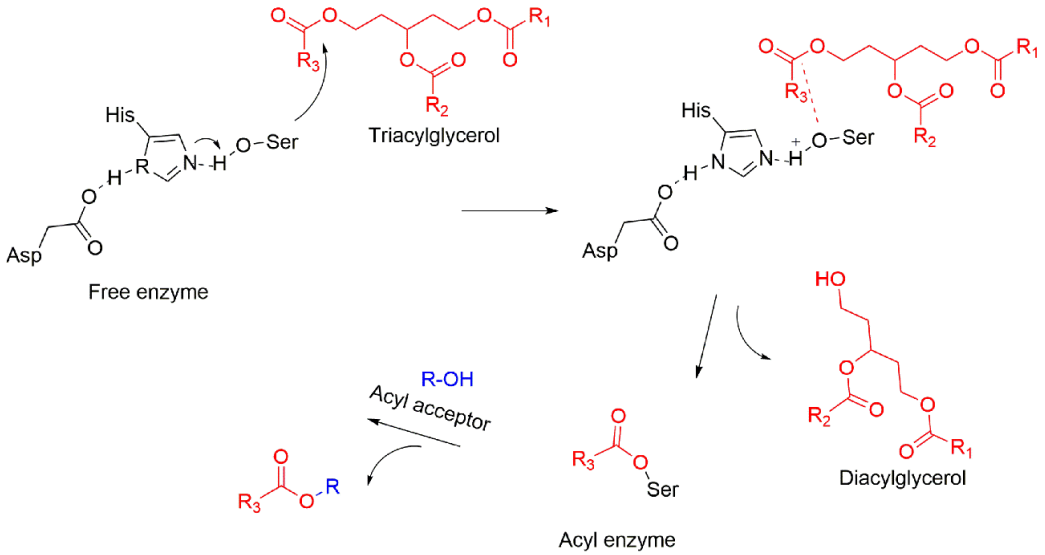

Figure 4. Schematic Illustration of lipase catalyzed transesterification reaction

An amphiphilic polypeptide loop covers the active center (in most lipases), the lid. In contact with hydrophobic substrates such as oil droplets, the lid acquires the open conformation for the active center and creates a large hydrophobic pocket [80]. In aqueous media, lipases in the open form can create dimeric and multimeric aggregates, which can lead to the lower lipase activity [81]. This can be overcome by enzyme immobilization [82] providing also

lower costs by possibilities of reuse [83] as the high cost of lipases has slowed down its commercialization for the production of bulk chemicals. Synthesis of biodiesel and other bulk chemicals is generally carried out in a non-aqueous or organic environment; hence, many researchers focus on obtaining novel lipases with enhanced activity and stability in organic solvents. High activity and stability of CALB in the presence of alcohols have drawn attention to this enzyme as a biocatalyst for biodiesel production [84]. However, some challenges need to be resolved. The immobilized lipase on a hydrophilic carrier may show low activity in biodiesel production because of the low accessibility of oil as the hydrophobic substrate. Also, the hydrophilic matrix has a higher affinity for methanol than oil, and methanol may easily deactivate the immobilized lipase. On the other hand, immobilization of lipase on the hydrophobic surface induce conformational changes of protein which result in increased stability [85].It is required to improve the existing methods and to explore new techniques to make immobilized lipase useful for industrial applications. Many papers deal with advanced techniques of enzyme immobilization and their application to obtain commercially valuable compounds [86].

3. 1. Lipase immobilized on MWCNTs for biodiesel production

Biodiesel (fatty acid alkyl esters, FAAE) is one of the best alternatives to fossil fuels. It has similar physical and chemical properties to petroleum diesel but it is renewable and sustainable with lower carbon dioxide, sulfur, and particulate emissions [82]. Biodiesel can be derived *via* transesterification of vegetable oil, animal fats, or microbial oil with alcohol by either chemical or enzymatic catalysis [87].

Most of the scientific studies and patents filed on biodiesel production have focused on improving the catalyst technology for efficient conversion. Other biodiesel research areas predominantly deal with feedstock, reactor configuration, byproduct recovery, and combustion performance [89]. Generally, biodiesel is produced *via* the transesterification/esterification reaction of acylglycerols and free fatty acids into fatty acid alkyl esters using short-chain alcohols (methanol) (Fig. 4). The acyl migration with short-chain alcohols is a time-consuming process, and, therefore, catalysts or pre-conditions (super/subcritical) are required for quicker alkyl ester formation. The formed FAAE (biodiesel) has a lower viscosity and pour point than its precursor oil/fat [89].

Chemical catalysts, consisting mainly of acids (H_2SO_4, BF_3, H_3PO_4) and bases (KOH, NaOH), are industrially used in biodiesel production. High temperatures are required, and wastewater is generated in large volumes. Using chemical catalysts also produces metal ions and salts that present a disposal challenge [88]. To reduce energy consumption and the amount of wastewater generated and to avoid producing inefficient end products, classes of enzymes, especially lipases, are being successfully explored as substitutes for chemical catalysts [89]. Compared with chemical catalysis, biodiesel production by lipase displays numerous advantages, such as easy product separation, minimal wastewater treatment requirements, easy glycerol recovery, and the absence of side reactions [90]. Recently, acidic, alkaline, and immobilized lipase catalysts were compared regarding efficiency in converting waste cooking oil to biodiesel. Alkaline and lipase catalysts showed >85 % biodiesel conversion in <120 min. Unlike the alkaline catalyst, the immobilized TLL used for the study was recycled three times [91].

As described previously, enzymes can be immobilized on the surface of MWCNTs by adsorption or covalent binding, resulting in improved catalytic performance and stability and showing great potential in biodiesel synthesis. A biocatalytic Pickering emulsion using MWCNT-immobilized CALB (CALB@PE) was developed to produce biodiesel, with *Jatrophacurcas L*. seed oil and methanol as substrates. A yield of 95.2 %, consistent with the predicted 95.5 %, was obtained. CALB@PE could be reused up to 10 times without substantial activity loss; it also exhibited better reusability than the commercial Novozym 435 in biodiesel production [70].

A nanoscale carrier was created as a support for CALB immobilization, and the catalytic performance was evaluated in methanolysis of rapeseed oil using *terc*-butanol as the reaction solvent. The carrier was plasma-treated MWCNTs (MWCNT-COOH), while further functionalization of the obtained oxidized MWCNTs was performed by using butylamine (BA) and octadecylamine (OA). The yield of biodiesel for the two of these three supports, namely, MWCNT-COOH and MWCNT-BA was similar at about 92 %, while 86 % was the yield for the reaction catalyzed by the lipase immobilized on MWCNT-OA [56].

The small size of carbon nanotubes, one of its best properties, is also one of its disadvantages because the recovery after the end of the reaction is challenging. A solution for this problem could be combination of carbon nanotubes with magnetic nanoparticles, or functionalization with other molecules [92]. Magnetic multiwalled carbon nanotubes (m-MWCNT) were used to immobilize RML. The obtained esterification activity was 27-fold higher than that of the free lipase. The immobilized lipase was employed as a biocatalyst in biodiesel production from waste cooking oil in a *tert*-butanol solvent system yielding high biodiesel conversion of 94 % under optimal conditions. Additionally, the immobilized lipase could be recovered easily without showing a significant decrease in conversion rates after 10 cycles of reuse [73]. Same authors made superparamagnetic MWCNTs by filling the nanotubes with iron oxide and further modified them by linking polyamidoamine dendrimers (m-MWCNTs-PAMAM) on the surface. BCL was successfully immobilized on the obtained carrier *via* a covalent method. The maximal activity of the immobilized lipase was 17-fold higher than that of the free enzyme. The immobilized lipase displayed significantly enhanced thermostability and pH-resistance and could efficiently catalyze transesterification to produce biodiesel at a conversion rate of ~93 % [74].

Deep *et al*. demonstrated preparation of a lipase-conjugated MWCNT catalyst *via* a chemical reaction. They examined the catalyst efficiency for biodiesel production *via* methanolysis of crude Jatropha oil and compared it with that of free lipase. The results revealed that the production of fatty acid methyl esters (FAME) (1 h reaction time) increased linearly with increasing the fraction of the catalyst support. The maximum yield of the desired product was achieved in the presence of 15 % of the immobilized catalyst (calculated as the mass of catalyst in the total reaction mixture). Moreover, it was also reported that the developed carbon-based nanocatalysts could be reused up to 10 times without any loss of enzyme activity. A maximum 90 % FAME yield was recorded for lipase-conjugated MWCNT catalyst, compared to only 10-15 % obtained with the free lipase [64].

3. 2. Flavor esters

Although several flavors and fragrances are obtained either by chemical synthesis or by extraction from plants, applying biocatalysts for the sake of a safe and productive pathway by more sustainable chemical processes is the main alternative. Optimization of variables that influence this lipase-catalyzed synthesis, such as enzyme formulations, solvent-free media, and acetylating agents, is crucial to achieving higher conversions[93].

Lipase from *C. rugosa* was immobilized by surface modified MWCNTs and used to synthesize ethyl butyrate and isoamyl acetate, which have characteristic pineapple and banana flavors. Magnetic MWCNTs were produced by incorporating cobalt and functionalized with aminated polydopamine. The immobilized CRL retained around 84 % of its initial hydrolytic activity and showed high-yields in enzymatic synthesis of ethyl butyrate and isoamyl acetate, amounting to 78 and 75 % ester yield, respectively [54].

Compared with geraniol, geranyl esters are preferred for their lower toxicity and higher bioactivity in food, pharmaceutical, cosmetic, and other fields. Enzymatic synthesis of geranyl esters is the most effective, especially with lipase as a catalyst [94]. Geranyl propionate was enzymatically synthesized from geraniol and propionic acid using CRL immobilized on acid-functionalized MWCNTs [51]. Bourkaib*et al*. combined advantages of MWCNTs as a support and supercritical CO_2 as a solvent for the synthesis of geranyl acetate catalyzed by CALB [61].

CALB-MWCNT conjugates were shown to be highly efficient in synthesis of pentyl valerate under non-aqueous conditions as reflected by the esterification yields, storage stabilities and storage stabilities and reusability studies [55].

Alkyl esters of levulinic acid are important flavors and fragrances in pharmaceutical, cosmetic and food industries. Enzymatically, they are usually prepared in the conventional esterification reaction as demonstrated using CALB immobilized on commercially available MWCNTs and polytetrafluoroethylene (PTFE) - CALB/MWCNT-PTFE as a biocatalyst. n-Butyl levulinate has been synthesized in a high yield (99 %) and with high selectivity (>99 %). The catalyst used retained its activity and stability after sixth reaction cycles, with 69 % yield of ester[45]. However, as lipase can catalyze ester hydrolysis at the same time, to overcome limitations regarding equilibrium, lactones can be used as alternative substrates. Szelwicka et al. used the same CALB/MWCNT-PTFE conjugate as a biocatalyst and α-angelica lactone as a substrate and obtained quantitative yields of n-butyl levulinate. The developed biocatalyst was stable in the six consecutive reaction cycles [46].

3. 3. Racemization

One of the most complex and challenging problems in the field of synthesis of valuable chemicals is production of optically active compounds [95]. Due to the possibility of functional conformation lipases are capable for the resolution of racemic mixtures of optically active compounds. As the enantiomers of 1-phenylethanol represent valuable intermediates in several industries, the lipase catalyzed resolution of (*R*,*S*)-1-phenylethanol is a relevant research topic.

Pseudomonas fluorescens lipase (PFL) was covalently immobilized on oxidized MWCNTs and applied in the kinetic resolution of racemic 1-phenyl ethanol with good enantioselectivity and recyclability (8 cycles) [62].

To produce effective and recyclable catalysts for enantioselective transesterification of three vinyl esters (acyl donors) by racemic Solketal esters, PFL was non-covalently immobilized on raw and oxidized MWCNTs (MWCNTs and o-MWCNTs, respectively). Depending on the structure of the acyl donor, MWCNTs were found to be 2.2- to 4-fold more active than their oxidized counterparts (and up to 9 times more activating than the native enzyme), whereas enantioselectivity was higher for the composites based on o-MWCNTs [63]. The same research group chemically synthesized different functionalized MWCNTs for the same purpose. The studies revealed that different chemical functionalization of morphologically identical nanotube supports led to various enzyme loadings, catalytic activities, and enantioselectivities [38].

3. 4. Miscellaneous applications

Progressively demanding regulations of industrial processes concerning safety and waste disposal have compelled modification of several chemical processes. A new method for the chemo-enzymatic Baeyer–Villiger oxidation of cyclic ketones to lactones in the presence of a new heterogeneous nanobiocatalyst consisting of CALB immobilized on MWCNTs has been developed. Activities of the obtained biocatalysts were compared with the commercially available Novozyme-435. Recycling studies demonstrated the possibility of utilizing the most active MWCNTs-lipase biocatalyst five times without any significant activity loss [42]. The same nanobiocatalyst was used to synthesize diester plasticizers based on aliphatic diesters (dicarboxylates). The superior activity of the CALB immobilized on MWCNTs was obtained resulting in a significant reduction in reaction times compared to those reported in the literature [43].

Wastewater generated from various industries (food, paper, textile, oleochemical, pharmaceutical) contain high concentrations of oil and grease difficult to treat by using inadequate and costly conventional chemical and/or biological methods. Therefore, considering the primary function of lipase to catalyze hydrolysis of fat and oil it is not surprising that they represent an appropriate "green" choice for lipid-rich wastewater treatment. Lipase can degrade complex oily materials through hydrolysis to free fatty acids that are easier to extract. There are a number of studies about treatment of oily wastewater using lipases[49,96-101]. However, most of them are directed towards exploiting native enzyme and synthetically prepared/model wastewater. Only few studies used the immobilized lipase and/or real industrial water, among which application of CRL immobilized on MWCNTs was reported [49]. High thermal and operational stability of lipase immobilized on oxidized MWCNTs in the presence of EDC and NHS as cross-linkers demonstrated the potential for improved resistance to severe conditions in industrial applications [49]. In another study it was shown that immobilization of CRL on MWCNTs significantly improved its activity in olive oil hydrolysis reactions. MWCNTs affected diffusion and distribution of the substrate and products in the lipase reaction environment [75].

Production of methyl oleate, an important ester used in detergents, emulsifiers, wetting agents, and intermediate stabilizers was optimized by using the adsorbed CRL onto raw-MWCNT by dint of Triton X-100 and o-MWCNT. The obtained biocatalysts produced around 80 % of methyl oleate. o-MWCNT-CRL could be recycled up to 5 times, retaining 50 % of its activity [48,50].

Lipases have the capability to catalyze unconventional reactions as aldol condensation, Hantzsch, Canizzaro, Morita-Baylis-Hillman, Knoevenagel, UGI and Mannich reaction, Michael addition, perhydrolysis, oxidation and some cascade reactions [16,78]. It was shown that PPL immobilized on magnetic-MWCNT can catalyze a three-component reaction to obtain 2H-chromenes at high yields (95 %) [102], while Szelwicka et al. used biocatalyst designed in the presence of supported ionic liquid-like phase for chemo-enzymatic Baeyer-Villiger oxidation of cyclic ketones. The obtained

biocatalysts showed high conversion of substrate (92 %) in the model oxidation of 2-adamantanone, under favorable conditions [68].

4. CONCLUSION

This review aims to summarize and point out the most important advances in the lipase-catalyzed synthesis of biotechnologically important compounds, with a particular focus on MWCNTs-immobilized biocatalysts. According to the data presented in this review, it is clear that the development of processes catalyzed by immobilized lipase represents a focus for many researchers due to the high use of these reactions in important industries. Esterification is a well-established reaction type in organic synthesis used for manufacturing various valuable esters used prevalently as food ingredients, in skincare products, pharmaceuticals, and fuels. The fact that enzymatically synthesized products gain label of natural products makes this technology even more market appealing. Additionally, a lipase-immobilized process offers significant advantages, including higher chemical and thermal stabilities than the free form of lipase as well as easy recovery and reuse. However, many challenges need to be overcome. In the future, developing additional viable and cost-effective methods is required. This can be achievable by enhancing capabilities for biocatalyst recycling, minimizing lipase production costs using molecular biology and genetic engineering techniques, or by designing supports from inexpensive and readily available waste biomass (for example, MWCNT from cotton or corncobs).

Acknowledgements: *This work was supported by the Ministry of Science, Technological Development and Innovation of the Republic of Serbia (Contract No.451-03-47/2023-01/200135).*

REFERENCES

[1] Winkler CK, Schrittwieser JH, Kroutil W. Power of Biocatalysis for Organic Synthesis. *ACS Cent Sci.* 2021; 7(1): 55-71. https://doi.org/10.1021/acscentsci.0c01496
[2] Sutradhar M. Metal-based catalysts in organic synthesis. *Catalysts.* 2020; 10(12): 1429. https://doi.org/10.3390/catal10121429
[3] Cossy J. Biocatalyts: Catalysts of the future for organic synthesis and beyond? *Tetrahedron.* 2022; 123: 132966. https://doi.org/10.1016/j.tet.2022.132966
[4] Sheldon RA, Woodley JM. Role of Biocatalysis in Sustainable Chemistry. *Chem Rev.* 2018; 118(2): 801-838. https://doi.org/10.1021/acs.chemrev.7b00203
[5] Heckmann CM, Paradisi F. Looking Back: A Short History of the Discovery of Enzymes and How They Became Powerful Chemical Tools. *ChemCatChem.* 2020; 12(24): 6082-6102. https://doi.org/10.1002/cctc.202001107
[6] Koeller KM, Wong CH. Enzymes for chemical synthesis. *Nature.* 2001; 409(6817): 232-240. https://doi.org/10.1038/35051706
[7] Guisan JM, Fernandez-Lorente G, Rocha-Martin J, Moreno-Gamero D. Enzyme immobilization strategies for the design of robust and efficient biocatalysts. *Curr Opin Green Sustain Chem.* 2022; 35: 100593. https://doi.org/10.1016/j.cogsc.2022.100593
[8] Gutarra MLE, Miranda LSM, de Souza ROMA. Enzyme Immobilization for Organic Synthesis. In: Goswami A, Stewart JD, eds. *Organic Synthesis Using Biocatalysts*. Academic Press; Elsevier Inc.; 2016: 99-126. https://doi.org/10.1016/B978-0-12-411518-7.00004-4
[9] Padrosa DR, Benítez-Mateos AI, Paradisi F. Back to the future: taking enzymes to the next level of sustainability. *Biochem (Lond).* 2022; 44(3): 19-22. https://doi.org/10.1042/bio_2022_109
[10] Kazlauskas R. Hydrolysis and Formation of Carboxylic Acid and Alcohol Derivatives. In: Goswami A, Stewart JD, eds. *Organic Synthesis Using Biocatalysts*. Academic Press; Elsevier; 2016: 127-148. https://doi.org/10.1016/B978-0-12-411518-7.00005-6
[11] Prlainović NŽ., Bezbradica DI., Knežević-Jugović ZD., Kozlowska RT., Mijin D Ž. A Kinetic Study of *Candida rugosa* Lipase-Catalyzed Synthesis of 4,6-Dimethyl-3-cyano-2-pyridone. *J Brazilian Chem Soc.* 2010; 21(12): 2285-2293. https://doi.org/10.1016/0096-3003(83)90011-5
[12] Prlainović NŽ, Bezbradica DI, Knežević-Jugović ZD, Marinković AD, Mijin DŽ. Imobilizacija enzima na ugljenične nanocevi. *Hem Ind.* 2011; 65(4): 423-430. https://doi.org/10.2298/HEMIND110330028P (in Serbian)
[13] Prlainović NŽ, Bezbradica DI, Knežević-Jugović ZD, Veličković D V., Mijin DŽ. Enzymatic synthesis of a vitamin B6 precursor. *J Serb Chem Soc.* 2013; 78(10): 1491-1501. https://doi.org/10.2298/JSC130322050P
[14] Milašinović N, Jakovetić S, Knežević-Jugović Z, Milosavljević N, Lučić M, Filipović J, Kalagasidis Krušić M. Catalyzed ester synthesis using *Candida rugosa* lipase entrapped by poly(N-isopropylacrylamide-co-itaconic Acid) hydrogel. *Sci World J.* 2014; 2014: 142123. https://doi.org/10.1155/2014/142123

[15] Milašinović N, Knežević-Jugović Z, Jakovljević Ž, Filipović J, Kalagasidis Krušić M. Synthesis of n-amyl isobutyrate catalyzed by *Candida rugosa* lipase immobilized into poly(N-isopropylacrylamide-co-itaconic acid) hydrogels. *Chem Eng J.* 2012; 181-182: 614-623. https://doi.org/10.1016/J.CEJ.2011.11.115

[16] Dwivedee BP, Soni S, Sharma M, Bhaumik J, Laha JK, Banerjee UC. Promiscuity of Lipase-Catalyzed Reactions for Organic Synthesis: A Recent Update. *ChemistrySelect.* 2018; 3(9): 2441-2466. https://doi.org/10.1002/slct.201702954

[17] Chibata I, Tosa T. Immobilized Cells: Historical Background. *Appl Biochem Bioeng.* 1983; 4: 1-9. https://doi.org/10.1016/b978-0-12-041104-7.50007-5

[18] Homaei AA, Sariri R, Vianello F, Stevanato R. Enzyme immobilization: An update. *J Chem Biol.* 2013; 6(4): 185-205. https://doi.org/10.1007/s12154-013-0102-9

[19] Cao L. Introduction: Immobilized Enzymes: Past, Present and Prospects. In: *Carrier-bound Immobilized Enzymes*, Wiley; 2005; 1-52. https://doi.org/10.1002/3527607668.ch1

[20] Zdarta J, Meyer AS, Jesionowski T, Pinelo M. A general overview of support materials for enzyme immobilization: Characteristics, properties, practical utility. *Catalysts.* 2018; 8(2): 92. https://doi.org/10.3390/catal8020092

[21] Spasojević M, Prodanović O, Pantić N, Popović N, Balaž AM, Prodanović R. The Enzyme Immobilization: Carriers and Immobilization methods. *J Eng Process Manag.* 2019; 11(2): 89-105. https://doi.org/10.7251/jepm1902089s

[22] Ismail AR, Baek KH. Lipase immobilization with support materials, preparation techniques, and applications: Present and future aspects. *Int J Biol Macromol.* 2020; 163: 1624-1639. https://doi.org/10.1016/j.ijbiomac.2020.09.021

[23] Mihailović M, Stojanović M, Banjanac K, Carević M, Prlainović N, Milosavić N, Bezbradica D. Immobilization of lipase on epoxy-activated Purolite® A109 and its post-immobilization stabilization. *Process Biochem.* 2014; 49(4): 637-646. https://doi.org/10.1016/j.procbio.2014.01.013

[24] Prlainović NŽ, Knežević-Jugović ZD, Mijin DŽ, Bezbradica DI. Immobilization of lipase from *Candida rugosa* on Sepabeads®: The effect of lipase oxidation by periodates. *Bioprocess Biosyst Eng.* 2011; 34(7): 803-810. https://doi.org/10.1007/s00449-011-0530-2

[25] Jeevanandam J, Barhoum A, Chan YS, Dufresne A, Danquah MK. Review on nanoparticles and nanostructured materials: History, sources, toxicity and regulations. *Beilstein J Nanotechnol.* 2018; 9(1): 1050-1074. https://doi.org/10.3762/bjnano.9.98

[26] Veličić Z, Rusmirović J, Prlainović N, Tomić N, Veličković Z, Taleb K, Marinković AD. The optimization of glycidyl methacrylate based terpolymer monolith synthesis: an effective *Candida rugosa* lipase immobilization support. *J Polym Res.* 2020; 27(5): 127. https://doi.org/10.1007/s10965-020-02127-z

[27] Buzea C, Pacheco I. Nanomaterials and their classification. *Adv Struct Mater.* 2017; 62: 3-45. https://doi.org/10.1007/978-81-322-3655-9_1

[28] Meryam Sardar RA. Enzyme Immobilization: An Overview on Nanoparticles as Immobilization Matrix. *Biochem Anal Biochem.* 2015; 4(2): 1000178. https://doi.org/10.4172/2161-1009.1000178

[29] Banjanac K, Carević M, Ćorović M, Milivojević A, Prlainović N, Marinković A, Bezbradica D. Novel β-galactosidase nanobiocatalyst systems for application in the synthesis of bioactive galactosides. *RSC Adv.* 2016; 6(99): 97216-97225. https://doi.org/10.1039/c6ra20409k

[30] Rao N, Singh R, Bashambu L. Carbon-based nanomaterials: Synthesis and prospective applications. *Mater Today Proc.* 2021; 44: 608-614. https://doi.org/10.1016/j.matpr.2020.10.593

[31] Romero-Arcos M, Pérez-Robles JF, Guadalupe Garnica-Romo M, Luna-Martinez MS, Gonzalez-Reyna MA. Synthesis and functionalization of carbon nanotubes and nanospheres as a support for the immobilization of an enzyme extract from the mushroom Trametes versicolor. *J Mater Sci.* 2019; 54(17): 11671-11681. https://doi.org/10.1007/s10853-019-03722-2

[32] Iijima S. Helical microtubules of graphitic carbon. *Nature.* 1991; 354: 56-58. https://doi.org/10.1038/354056a0

[33] Khan M, Husain Q. Multiwalled carbon nanotubes bound beta-galactosidase: It's activity, stability and reusability. *Methods Enzymol.* 2020; 630: 365-405. https://doi.org/10.1016/bs.mie.2019.10.018

[34] Taib NAB, Uddin J, Khusairy M, Bakri B. A Review on Carbon Nanotubes (CNT): Structure, Synthesis, Purification and Properties for Modern day Applications. *Res Sq.* 2021: 1-22. https://doi.org/10.21203/rs.3.rs-930166/v1

[35] Bilal M, Anh Nguyen T, Iqbal HMN. Multifunctional carbon nanotubes and their derived nano-constructs for enzyme immobilization - A paradigm shift in biocatalyst design. *Coord Chem Rev.* 2020; 422: 213475. https://doi.org/10.1016/j.ccr.2020.213475

[36] Shuai W, Kumar Das R, Naghdi M, Kaur Brar S, Verma M. A Review on the ImportantAspects of Lipase Immobilization on Nanomaterials. *Biotechnol Appl Biochem Appl Biochem.* 2017; 64(4): 496-508. https://doi.org/10.1002/bab.1515

[37] Mokhtar NF, Raja Noor Zaliha RNZR, Muhd Noor ND, Mohd Shariff F, Ali MSM. The immobilization of lipases on porous support by adsorption and hydrophobic interaction method. *Catalysts.* 2020; 10(7): 1-17. https://doi.org/10.3390/catal10070744

[38] Zniszczoł A, Herman AP, Szymańska K, Mrowiec-Białoń J, Walczak KZ, Jarzebski A, Boncel S. Covalently immobilized lipase on aminoalkyl-, carboxy- and hydroxy-multi-wall carbon nanotubes in the enantioselective synthesis of Solketal esters. *Enzyme Microb Technol.* 2016; 87-88: 61-69. https://doi.org/10.1016/j.enzmictec.2016.02.015

[39] Pavlidis IV, Tsoufis T, Enotiadis A, Gournis D, Stamatis H. Functionalized multi-wall carbon nanotubes for lipase immobilization. *Adv Eng Mater.* 2010; 12(5): 179-183. https://doi.org/10.1002/adem.200980021

[40] Vrutika P, Datta M. Lipase from Solvent-Tolerant *Pseudomonas* sp. DMVR46 Strain Adsorb on Multiwalled Carbon Nanotubes: Application for Enzymatic Biotransformation in Organic Solvents. *Appl Biochem Biotechnol.* 2015; 177(6): 1313-1326. https://doi.org/10.1007/s12010-015-1816-7

[41] Prlainović NŽ, Bezbradica DI, Knežević-Jugović ZD, Stevanović SI, Avramov Ivić ML, Uskoković PS, Mijin DŽ. Adsorption of lipase from *Candida rugosa* on multi walled carbon nanotubes. *J Ind Eng Chem.* 2013; 19(1): 279-285. https://doi.org/10.1016/j.jiec.2012.08.012

[42] Markiton M, Boncel S, Janas D, Chrobok A. Highly active nanobiocatalyst from lipase noncovalently immobilized on multiwalled carbon nanotubes for Baeyer-Villiger synthesis of lactones. *ACS Sustain Chem Eng.* 2017; 5(2): 1685-1691. https://doi.org/10.1021/acssuschemeng.6b02433

[43] Szelwicka A, Boncel S, Jurczyk S, Chrobok A. Exceptionally active and reusable nanobiocatalyst comprising lipase non-covalently immobilized on multi-wall carbon nanotubes for the synthesis of diester plasticizers. *Appl Catal A Gen.* 2019; 574: 41-47. https://doi.org/10.1016/j.apcata.2019.01.030

[44] Ghide MK, Yan Y. 1,3-Dioleoyl-2-palmitoyl glycerol (OPO)—Enzymatic synthesis and use as an important supplement in infant formulas. *J Food Biochem.* 2021; 45(7): 13799. https://doi.org/10.1111/jfbc.13799

[45] Szelwicka A, Siewniak A, Kolanowska A, Boncel S. Selective Synthesis of Levulinate Esters. *Materials (Basel).* 2021; 14: 1518. https://doi.org/10.3390/ma14061518

[46] Szelwicka A, Kolanowska A, Latos P, Jurczyk S, Boncel S, Chrobok A. Carbon nanotube/PTFE as a hybrid platform for lipase B from *Candida antarctica*in transformation of α-angelica lactone into alkyl levulinates. *Catal Sci Technol.* 2020; 10(10): 3255-3264. https://doi.org/10.1039/d0cy00545b

[47] Ameri A, Forootanfar H, Behnam B, Shakibaie M, Ameri A, Daneshpajooh M, Najafi A, Amirheidari B. Optimization of immobilization of *Pseudomonas cepacia* lipase on multiwalled carbon nanotubes functionalized with glycyrrhizin and Tween 80. *3 Biotech.* 2021; 11(6): 1-13. https://doi.org/10.1007/s13205-021-02813-9

[48] Che Marzuki NH, Mahat NA, Huyop F, Aboul-Enein HY, Wahab RA. Sustainable production of the emulsifier methyl oleate by *Candida rugosa* lipase nanoconjugates. *Food Bioprod Process.* 2015; 96: 211-220. https://doi.org/10.1016/j.fbp.2015.08.005

[49] Jamie A, Alshami AS, Maliabari ZO, Ateih MA, Al Hamouz OCS. Immobilization and Enhanced Catalytic Activity of Lipase on Modified MWCNT for Oily Wastewater Treatment. *Environ Prog Sustain Energy.* 2016; 35(5): 1441-1449. https://doi.org/10.1002/ep

[50] Che Marzuki NH, Mahat NA, Huyop F, Buang NA, Wahab RA. *Candida rugosa* Lipase Immobilized onto Acid-Functionalized Multi-walled Carbon Nanotubes for Sustainable Production of Methyl Oleate. *Appl Biochem Biotechnol.* 2015; 177(4): 967-984. https://doi.org/10.1007/s12010-015-1791-z

[51] Mohamad NR, Buang NA, Mahat NA, Jamalis J, Huyop F, Aboul-Enein HY, Wahab RA. Simple adsorption of *Candida rugosa* lipase onto multi-walled carbon nanotubes for sustainable production of the flavor ester geranyl propionate. *J Ind Eng Chem.* 2015; 32: 99-108. https://doi.org/10.1016/j.jiec.2015.08.001

[52] Mokhtarifar M, Arab H, Maghrebi M, Baniadam M. Amine-functionalization of carbon nanotubes assisted by electrochemical generation of chlorine. *Appl Phys A Mater Sci Process.* 2018; 124(1): 1-9. https://doi.org/10.1007/s00339-017-1438-8

[53] Yook JY, Jun J, Kwak S. Amino functionalization of carbon nanotube surfaces with NH 3 plasma treatment. *Appl Surf Sci.* 2010; 256(23): 6941-6944. https://doi.org/10.1016/j.apsusc.2010.04.075

[54] Asmat S, Anwer AH, Husain Q. Immobilization of lipase onto novel constructed polydopamine grafted multiwalled carbon nanotube impregnated with magnetic cobalt and its application in synthesis of fruit flavours. *Int J Biol Macromol.* 2019; 140: 484-495. https://doi.org/10.1016/j.ijbiomac.2019.08.086

[55] Raghavendra T, Basak A, Manocha LM, Shah AR, Madamwar D. Robust nanobioconjugates of *Candida antarctica* lipase B - Multiwalled carbon nanotubes: Characterization and application for multiple usages in non-aqueous biocatalysis. *Bioresour Technol.* 2013; 140: 103-110. https://doi.org/10.1016/j.biortech.2013.04.071

[56] Rastian Z, Khodadadi AA, Guo Z, Vahabzadeh F, Mortazavi Y. Plasma Functionalized Multiwalled Carbon Nanotubes for Immobilization of *Candida antarctica* Lipase B: Production of Biodiesel from Methanolysis of Rapeseed Oil. *Appl Biochem Biotechnol.*2016; 178(5): 974-989. https://doi.org/10.1007/s12010-015-1922-6

[57] Salah LS, Ouslimani N, Bousba D, Huynen I, Danleé Y, Aksas H. Carbon Nanotubes (CNTs) from Synthesis to Functionalized (CNTs) Using Conventional and New Chemical Approaches. *J Nanomater.* 2021; 2021: 4972770. https://doi.org/10.1155/2021/4972770

[58] Thakur CK, Karthikeyan C, Abou-Dahech MS, Altabakha MMAM, Al Shahwan MJS, Ashby CR, Tiwari AK, Babu RJ, Moorthy NSHN. Microwave-Assisted Functionalization of Multi-Walled Carbon Nanotubes for Biosensor and Drug Delivery Applications. *Pharmaceutics.* 2023; 15(2): 335. https://doi.org/10.3390/pharmaceutics15020335

[59] Bié J, Sepodes B, Fernandes PCB, Ribeiro MHL. Enzyme Immobilization and Co-Immobilization: Main Framework, Advances and Some Applications. *Processes.* 2022; 10(3): 1-31. https://doi.org/10.3390/pr10030494

[60] Smith S, Goodge K, Delaney M, Struzyk A, Tansey N, Frey M. A comprehensive review of the covalent immobilization of biomolecules onto electrospun nanofibers. *Nanomaterials.* 2020; 10(11): 1-39. https://doi.org/10.3390/nano10112142

[61] Bourkaib MC, Guiavarc'h Y, Chevalot I, Delaunay S, Gleize J, Ghanbaja J, Valsaque F, Berrada N, Desforges A, Vigolo B. Non-covalent and covalent immobilization of *Candida antarctica* lipase B on chemically modified multiwalled carbon nanotubes for a green acylation process in supercritical CO2. *Catal Today.* 2020; 348: 26-36. https://doi.org/10.1016/j.cattod.2019.08.046

[62] Dwivedee BP, Bhaumik J, Rai SK, Laha JK, Banerjee UC. Development of nanobiocatalysts through the immobilization of *Pseudomonas fluorescens* lipase for applications in efficient kinetic resolution of racemic compounds. *Bioresour Technol.* 2017; 239: 464-471. https://doi.org/10.1016/j.biortech.2017.05.050

[63] Boncel S, Zniszczoł A, Szymańska K, Mrowiec-Białoń J, Jarzebski A, Walczak KZ. Alkaline lipase from *Pseudomonas fluorescens* non-covalently immobilised on pristine versus oxidised multi-wall carbon nanotubes as efficient and recyclable catalytic systems in the synthesis of Solketal esters. *Enzyme Microb Technol.* 2013; 53(4): 263-270. https://doi.org/10.1016/j.enzmictec.2013.05.003

[64] Deep A, Sharma AL, Kumar P. Lipase immobilized carbon nanotubes for conversion of Jatropha oil tofatty acid methyl esters. *Biomass and Bioenergy.* 2015; 81: 83-87. https://doi.org/10.1016/j.biombioe.2015.06.008

[65] Tan H, Feng W, Ji P. Lipase immobilized on magnetic multi-walled carbon nanotubes. *Bioresour Technol.* 2012; 115: 172-176. https://doi.org/10.1016/j.biortech.2011.10.066

[66] Prlainović NZ, Bezbradica DI, Rogan JR, Uskoković PS, Mijin D, Marinković AD. Surface functionalization of oxidized multi-walled carbon nanotubes: *Candida rugosa* lipase immobilization. *Comptes Rendus Chim.* 2016; 19(3): 363-370. https://doi.org/10.1016/j.crci.2015.10.008

[67] Ji P, Tan H, Xu X, Feng W. Lipase Covalently Attached to Multiwalled Carbon Nanotubes as an Efficient Catalyst in Organic Solvent. *AIChE J.* 2010; 56(11): 3005-3011. https://doi.org/10.1002/aic

[68] Szelwicka A, Wolny A, Grymel M, Jurczyk S, Boncel S, Chrobok A. Chemo-enzymatic baeyer-villiger oxidation facilitated with lipases immobilized in the supported ionic liquid phase. *Materials (Basel).* 2021; 14(13): 3443. https://doi.org/10.3390/ma14133443

[69] Szelwicka A, Erfurt K, Jurczyk S, Boncel S, Chrobok A. Outperformance in acrylation: Supported d-glucose-based ionic liquid phase on mwcnts for immobilized lipase B from *Candida antarctica* as catalytic system. *Materials (Basel).* 2021; 14(11): 3090. https://doi.org/10.3390/ma14113090

[70] Wang L, Liu X, Jiang Y, Zhou L, Ma L, He Y, Gao J. Biocatalytic pickering emulsions stabilized by lipase-immobilized carbon nanotubes for biodiesel production. *Catalysts.* 2018; 8(12): 587. https://doi.org/10.3390/catal8120587

[71] Verma ML, Naebe M, Barrow CJ, Puri M. Enzyme Immobilisation on Amino-Functionalised Multi-Walled Carbon Nanotubes: Structural and Biocatalytic Characterisation. *PLoS One.* 2013; 8(9): 16-18. https://doi.org/10.1371/journal.pone.0073642

[72] Pavlidis I V., Vorhaben T, Tsoufis T, Rudolf P, Bornscheuer UT, Gournis D, Stamatis H. Development of effective nanobiocatalytic systems through the immobilization of hydrolases on functionalized carbon-based nanomaterials. *Bioresour Technol.* 2012; 115: 164-171. https://doi.org/10.1016/j.biortech.2011.11.007

[73] Fan Y, Wu G, Su F, Li K, Xu L, Han X, Yan Y. Lipase oriented-immobilized on dendrimer-coated magnetic multi-walled carbon nanotubes toward catalyzing biodiesel production from waste vegetable oil. *Fuel.* 2016; 178: 172-178. https://doi.org/10.1016/j.fuel.2016.03.071

[74] Fan Y, Su F, Li K, Ke C, Yan Y. Carbon nanotube filled with magnetic iron oxide and modified with polyamidoamine dendrimers for immobilizing lipase toward application in biodiesel production. *Sci Rep.* 2017; 7: 1-13. https://doi.org/10.1038/srep45643

[75] Malaibari ZO. Effect of MWCNTs surface properties on lipase immobilization and its catalytic activity. *Mater Express.* 2018; 8(2): 123-132. https://doi.org/10.1166/mex.2018.1414

[76] Badgujar KC, Sasaki T, Bhanage BM. Synthesis of lipase nano-bio-conjugates as an efficient biocatalyst: Characterization and activity-stability studies with potential biocatalytic applications. *RSC Adv.* 2015; 5: 55238-55251. https://doi.org/10.1039/C5RA10032A

[77] Bartha-Vári JH, Moisă ME, Bencze LC, Irimie FD, Paizs C, Toşa MI. Efficient biodiesel production catalyzed by nanobioconjugate of lipase from *Pseudomonas fluorescens*. *Molecules.* 2020; 25(3): 651. https://doi.org/10.3390/molecules25030651

[78] Kapoor M, Gupta MN. Lipase promiscuity and its biochemical applications. *Process Biochem.* 2012; 47(4): 555-569. https://doi.org/10.1016/j.procbio.2012.01.011

[79] Al-Zuhair S, Ling FW, Jun LS. Proposed kinetic mechanism of the production of biodiesel from palm oil using lipase. *Process Biochem.* 2007; 42(6): 951-960. https://doi.org/10.1016/j.procbio.2007.03.002

[80] Brzozowski AM, Derewenda U, Derewenda ZS, Dodson GG, Lawson DM, Turkenburg JP, Bjorkling F, Huge-Jensen B, Patkar SA, Thim L. A model for interfacial activation in lipases from the structure of a fungal lipase-inhibitor complex. *Nature.* 1991; 351(6326): 491-494. https://doi.org/10.1038/351491a0

[81] Adlercreutz P. Immobilisation and application of lipases in organic media. *Chem Soc Rev.* 2013; 42(15): 6406-6436. https://doi.org/10.1039/c3cs35446f

[82] Sankaran R, Show PL, Chang J-S. Biodiesel production using immobilized lipase: feasibility and challenges. *Biofuels, Bioprod Biorefining.* 2016; 10(6): 896-916. https://doi.org/10.1002/BBB

[83] Zhong L, Feng Y, Wang G, Wang Z, Bilal M, Lv H, Jia S, Cui J. Production and use of immobilized lipases in/on nanomaterials: A review from the waste to biodiesel production. *Int J Biol Macromol.* 2020; 152: 207-222. https://doi.org/10.1016/j.ijbiomac.2020.02.258

[84] Idris A, Bukhari A. Immobilized *Candida antarctica* lipase B: Hydration, stripping off and application in ring opening polyester synthesis. *Biotechnol Adv.* 2012; 30(3): 550-563. https://doi.org/10.1016/j.biotechadv.2011.10.002

[85] Singh N, Dhanya BS, Verma ML. Nano-immobilized biocatalysts and their potential biotechnological applications in bioenergy production. *Mater Sci Energy Technol.* 2020; 3: 808-824. https://doi.org/10.1016/j.mset.2020.09.006

[86] Basso A, Serban S. Industrial applications of immobilized enzymes—A review. *Mol Catal.* 2019; 479: 110607. https://doi.org/10.1016/j.mcat.2019.110607

[87] Atabani AE, Silitonga AS, Badruddin IA, Mahlia TMI, Masjuki HH, Mekhilef S. A comprehensive review on biodiesel as an alternative energy resource and its characteristics. *Renew Sustain Energy Rev.* 2012; 16(4): 2070-2093. https://doi.org/10.1016/j.rser.2012.01.003

[88] Hama S, Noda H, Kondo A. How lipase technology contributes to evolution of biodiesel production using multiple feedstocks. *Curr Opin Biotechnol.* 2018; 50: 57-64. https://doi.org/10.1016/j.copbio.2017.11.001

[89] Quayson E, Amoah J, Hama S, Kondo A, Ogino C. Immobilized lipases for biodiesel production: Current and future greening opportunities. *Renew Sustain Energy Rev.* 2020; 134: 110355. https://doi.org/10.1016/j.rser.2020.110355

[90] Avhad MR, Marchetti JM. Uses of enzymes for biodiesel production. In: Hoseini M, ed. *Advanced Bioprocessing for Alternative Fuels, Biobased Chemicals and Bioproducts*. Woodhead Publishing, Elsevier; 2019; 135-152. https://doi.org/10.1016/B978-0-12-817941-3.00007-3

[91] Tacias-Pascacio VG, Torrestiana-Sánchez B, Dal Magro L, Virgen-Ortíz JJ, Suárez-Ruíz FJ, Rodrigues RC, Fernandez-Lafuente R. Comparison of acid, basic and enzymatic catalysis on the production of biodiesel after RSM optimization. *Renew Energy.* 2019; 135: 1-9. https://doi.org/10.1016/J.RENENE.2018.11.107

[92] Shim M, Kam NWS, Chen RJ, Li Y, Dai H. Functionalization of Carbon Nanotubes for Biocompatibility and Biomolecular Recognition. *Nano Lett.* 2002; 2(4): 285-288. https://doi.org/10.1021/nl015692j

[93] Bayout I, Bouzemi N, Guo N, Mao X, Serra S, Riva S, Secundo F. Natural flavor ester synthesis catalyzed by lipases. *Flavour Fragr J.* 2020; 35(2): 209-218. https://doi.org/10.1002/ffj.3554

[94] Liu YQ, WeiZhuo X, Wei X. A review on lipase-catalyzed synthesis of geranyl esters as flavor additives for food, pharmaceutical and cosmetic applications. *Food Chem Adv.* 2022; 1: 100052. https://doi.org/10.1016/j.focha.2022.100052

[95] Muralidhar R, Marchant R, Nigam P. Lipases in racemic resolutions. *J Chem Technol Biotechnol.* 2001; 76(1): 3-8. https://doi.org/10.1002/1097-4660(200101)76:1<3::AID-JCTB336>3.0.CO;2-8

[96] Cammarota MC, Teixeira GA, Freire DMG. Enzymatic pre-hydrolysis and anaerobic degradation of wastewaters with high fat contents. *Biotechnol Lett.* 2001; 23(19): 1591-1595. https://doi.org/10.1023/A:1011973428489

[97] Scioli C, Vollaro L. The use of Yarrowia lipolytica to reduce pollution in olive mill wastewaters. *Water Res.* 1997; 31(10): 2520-2524. https://doi.org/10.1016/S0043-1354(97)00083-3

[98] Masse L, Massé DI, Kennedy KJ. Effect of hydrolysis pretreatment on fat degradation during anaerobic digestion of slaughterhouse wastewater. *Process Biochem.* 2003; 38(9): 1365-1372. https://doi.org/10.1016/S0032-9592(03)00020-7

[99] Masse L, Kennedy KJ, Chou S. Testing of alkaline and enzymatic hydrolysis pretreatments for fat particles in slaughterhouse wastewater. *Bioresour Technol.* 2001; 77(2): 145-155. https://doi.org/10.1016/S0960-8524(00)00146-2

[100] MongkolthanarukW, DharmsthitiS. Biodegradation of lipid-rich wastewater by a mixed bacterial consortium Biodegradation of lipid-rich wastewater by a mixed bacterial consortium. *Int Biodeterior Biodegrad.* 2012; 50: 101-105. https://doi.org/10.1016/S0964-8305(02)00057-4

[101] Jeganathan J, Bassi A, Nakhla G. Pre-treatment of high oil and grease pet food industrial wastewaters using immobilized lipase hydrolyzation. *J Hazard Mater.* 2006; 137(1): 121-128. https://doi.org/10.1016/j.jhazmat.2005.11.106

[102] Liu J, Zhao W, Zhang L, Zhang M, Chen Y, Xu Y, Li Y, Wang L. Synthesis of substituted 2H-chromenes catalyzed by lipase immobilized on magnetic multiwalled carbon nanotubes. *Biotechnol Appl Biochem.* 2021; 68(2): 411-416. https://doi.org/10.1002/bab.1939

Višeslojne ugljenične nanocevi kao nosač lipaza za organsku sintezu: pregled najnovijih trendova

Nevena Ž. Prlainović[1], Jelena S. Milovanović[2], Nikola Z. Milašinović[3], Dejan I. Bezbradica[1] i Dušan Ž. Mijin[1]

[1]*Univerzitet u Belgradu, Tehnološko-metalurški fakultet, Beograd, Srbija*

[2]*Univerzitet u Beogradu, Institut za molekularnu genetiku i genetičko inženjerstvo, Beograd, Srbija*

[3]*Kriminalističko-policijski Univerzitet, Beograd, Srbija*

(Pregledni rad)

Izvod

Lipaze su poslednjih decenija široko rasprostanjeni katalizatoriu raznovrsnim organskim reakcijama. Posebno su interesantne u imobilisanom/nerastvornom obliku jer je na ovaj način olakšana njihova upotreba uz mogućnost recikliranja i ponovne upotrebe čime se smanjuju troškovi samog procesa i postupak je ekološki prihvatljiviji. Kao nosači za vezivanje nanomaterijali na bazi ugljenika, posebno ugljenične nanocevi, su našli primenu zbog svojih izuzetnih fizičkih, mehaničkih i hemijskih svojstava. Njihova velika specifična površina, karakteristična površinska morfologija i smanjen otpor prenosu mase igraju vitalnu ulogu u performansama vezanog enzima. Ovaj pregledni rad predstavlja prikaz glavnih aspekata lipaze imobilisane na višeslojne ugljenične nanocevi i različitih strategija imobilizacije za dobijanje biokatalizatora sa poboljšanim svojstvima. Takođe, kako su lipaze enzimi od velikog komercijalnog značaja za organsku sintezu i primenu u biotehnologiji, drugi deo rada posvećen je pregledu najvažnijih industrijskih sektora u kojima su ovi nanobiokatalizatori našli primenu. Shodno tome, dat je pregled proizvodnje biodizela, mirisnih estara i racemizacije.

Ključne reči: Imobilizacija enzima; biokataliza; biodizel; mirisni estri; racemizacija

Use of a mixture of coal and oil as an additive for selective reduction of lateritic ore by the Caron process

Hugo Javier Angulo-Palma[1,3], Ángel Legrá Legrá[1], Alisa Lamorú Urgellés[1], Carlos Hernández Pedrera[4], Sandra Gallegos[2], Felipe M. Galleguillos Madrid[5] and Norman Toro[2]

[1]*Centro de Investigaciones del Níquel ``Alberto Fernández Montes de Oca´´ (CEDINIQ), Moa, Holguín, Cuba*
[2]*Faculty of Engineering and Architecture, Universidad Arturo Prat, Iquique 1110939, Chile*
[3]*Departamento de Metalurgia Química, Universidad de Moa, Holguín, Cuba*
[4]*Facultad de Ingeniería Química y Agronomía, Universidad de Oriente, Santiago de Cuba, Cuba*
[5]*Centro de Desarrollo Energético Antofagasta, Universidad de Antofagasta, Antofagasta 1271155, Chile*

Abstract

Lateritic ores constitute the main source of raw material for extraction of Ni and Co by the Caron process. Consumption of oil in the reduction furnace is one of the key indicators if the metallurgical process is economical. To date it has not been possible to replace the additive fuel oil that is used at commercial scales, therefore, the aim of this study was to partially replace the oil with bituminous coal on a pilot scale by using a mixture of 2 % coal and 1.25 % oil as the reducer additive. Phases of the reduced/leached ores were analyzed by powder X-ray diffraction, while the metallic state of the ore was determined by leaching the reacted samples with a bromine-ethanol solution followed by the atomic absorption spectrometry analysis. Extractions of Ni and Co were confirmed by leaching the reduced ore with ammoniacal-ammonium carbonate solutions. It was observed that the mixture used as a reducer additive can replace the fuel oil since it allows the adequate transformation of the main mineralogical phases of the laterite ore during the reduction process and the average extraction yields of Ni and Co for ~3 and ~8 %, respectively. Although the effect of bituminous coal particle size in the process was not analyzed, the reducing mixture ensured that the Caron process was more efficient.

Keywords: nickel and cobalt recovery, furnaces operation, pyrometallurgy.

Available on-line at the Journal web address: http://www.ache.org.rs/HI/

TECHNICAL PAPER

UDC: 553.3/.4:622.348.1:669.25

Hem. Ind. **78(1)** 17-27 (2024)

1. INTRODUCTION

Nickel and cobalt are critical elements that are currently in high demand in the production of special steels, aerospace alloys, and lithium-ion batteries for electric vehicles because they improve material properties such as durability, resistance to corrosion, ductility, and thermal and electrical conductivities. Predominant ore types in nature are sulfides and laterites, with a world reserve of the latter close to 60 % [1,2]. Currently, lateritic ores are considered as the main sources of these metals, concentrating Ni in more than 0.7 % by weight [3]. These deposits are produced by prolonged and deep weathering of Ni silica containing ultramafic rocks, usually in humid tropical or subtropical climates. The mineral ores shall be classified as hydrated silicates, clay silicates, and oxide deposits; those are processed by using a variety of processes, including the Caron process. [4-7]

The Caron process is a technology that combines the pyrometallurgical and hydrometallurgical processes, and is based on leaching of previously reduced lateritic ores with ammoniacal-ammonium carbonate solutions ($(NH_4)_2CO_3$) with the reduction being one of the stages that mostly influence the final extractions [8-10]. Also, the use of the Caron process is recommended when the contents of Ni, Fe, and MgO in the lateritic ore exceed 0.9, 25 and 2 %, respectively

Corresponding authors: Norman Toro, Faculty of Engineering and Architecture, Universidad Arturo Prat, Iquique 1110939, Chile
E-mail: notoro@unap.cl
Paper received: 28 October 2022; Paper accepted: 18 July 2023; Paper published: 18 October 2023.
https://doi.org/10.2298/HEMIND230118017A

[8,11]. Rodríguez *et al.* [12] recognize that the Caron process, generates high consumption of fuel oil during its operation, and the reduction stage in the production process induces one of the most important costs.

Reduction of lateritic ore is carried out in Herreschoff multiple hearth furnaces. The furnaces are oil-fired and are operated at air deficiency in order to produce the required ratio of carbon monoxide to carbon dioxide in each hearth. Temperatures in the reduction zone are maintained at 750-800 °C [13].

Main reactions involved in roasting/reduction in the Caron process are [11,14]:

$2FeOOH \rightarrow Fe_2O_3 + H_2O$ (1)

$3Fe_2O_3 + CO \rightarrow 2\ Fe_3O_4 + CO_2$ (2)

$Fe_3O_4 + CO \rightarrow 3FeO + CO_2$ (3)

$FeO + CO \rightarrow Fe + CO_2$ (4)

$NiO + CO \rightarrow Ni + CO_2$ (5)

$CoO + CO \rightarrow Co + CO_2$ (6)

$C + CO_2 \rightarrow 2CO$ (7)

Different studies focused on the reduction of lateritic minerals indicating that the particle size [15], temperature profile, and the composition of the reducing atmosphere are the most important variables in the process [16-19], which is why the use of reducing additives has been one of the most analyzed variables in recent years [20,21]. Some additives used during the reduction in the Caron process are FeS_2 [8], NaCl [8,20], $CaCl_2$ [8], S [21,22], Na_2SO_4 [22] and coal [23-25]. Still, it has not been possible to replace the 2.5% of fuel oil (denoted here as FO-2.5 [11,13,25] implemented at the industrial scale.

Specifically, the use of coal as a substitute for fuel oil in the roasting/reduction in the Caron process has been considered a technological alternative in recent years to reduce operating costs [22-27].

However, it was demonstrated [26] that the use of anthracite coal to replace 20 % of the additive fuel oil is not economically feasible.

Ilias *et al.* [22,27] evaluated coal (fixed carbon and sulfur contents of 58.6 and 7.5 % respectively) from Pakistan in the roasting/reduction of lateritic ores using the Caron process. The optimal reduction condition was found for the mixture of laterite ore with 10 wt.% coal and 9 wt.% of Na_2SO_4, roasted at 800 °C for 120 min. Leaching of the reduced roast product carried out in $NH_{3(ac)}$-$(NH_4)_2CO_3$ solutions (150 g dm^{-3} total NH_3) was influenced by the concentration of carbonate ions and produced >90 % Ni and 67 % Co. The research presented as a difficulty the use of a residence time and the concentration of NH_3 in the first stage of leaching higher than those that have been used on a pilot and industrial scale (residence time in the furnace: 70-80 min [25] and NH_3 concentration in the first leaching stage: 60-100 g dm^{-3} [28].

Angulo *et al.* [23,24,29] analyzed the use of bituminous coal (fixed carbon and sulfur contents of 55.40 and 0.55 %, respectively) to replace the fuel oil. The studies showed that the substitution is technically and economically feasible by using the coal content of less than 4 % in the grinding and roasting/reduction processes. The highest extractions of Ni (> 90 %) and Co (> 68 %) were achieved when using the mixture of coal and fuel oil at 2.0 and 1.25 %, respectively. The residence time in the furnace was of 80 min and the NH_3 concentration used in the leaching was in the range of 80 to 85 g dm^{-3} on a laboratory scale.

Consequently, in the present work, we investigate the reduction-roasting behaviour of the laterite sample of mixtures from different Moa-Cuba deposits when using the same mixture of coal and fuel oil at 2.0 and 1.25 %, denoted here as BC2-FO1.25 as a reducing additive in the Caron process on a pilot scale. The ultimate goal was to investigate the possibility to replace the fuel oil at 2.5 % currently used on commercial scales so to assess whether the Caron process could be carried out more economically and efficiently. Still, it should be noted that the effect of bituminous coal particle size on extractions was not studied.

2. MATERIALS AND METHODS

2. .1 Methodology

In this research, two lateritic ore processing schemes were evaluated in a pilot-scale reduction furnace. The first was the use of the reducing additive conventional fuel oil at 2.5 wt.% (denoted here as FO-2.5), while the second was based on analyzing the effect of the reducing additive mixture of bituminous coal at 2.0 wt.% and fuel oil at 1.25 wt.% (denoted

here as BC2-FO1.25) under similar operating conditions. For this purpose, the installation that simulates the Caron process was used in the Centro de Investigaciones del Niquel: Alberto Fernández Montes de Oca, Moa-Cuba (CEDINIQ) [11]. The reduction process was carried out in a Herreshoff furnace (Fig. 1) composed of 17 hearths, listed from top to bottom from hearth 0 (H-0) to 16 (H-16), enclosed in a metal cylinder 11 m high and 2.51 m in diameter, coated internally by a refractory material; the post-combustion air being fed by the furnace hearths 4 (H-4) and 6 (H-6). The study was based on comparing the results when using both reducing additives in the reduction-leaching processes. The evaluation of each reducing additive was carried out during five days of continuous operation. To analyze the effect of the modification 12 daily samples were taken in each experiment, which were averaged to obtain the daily behavior of the variables under study.

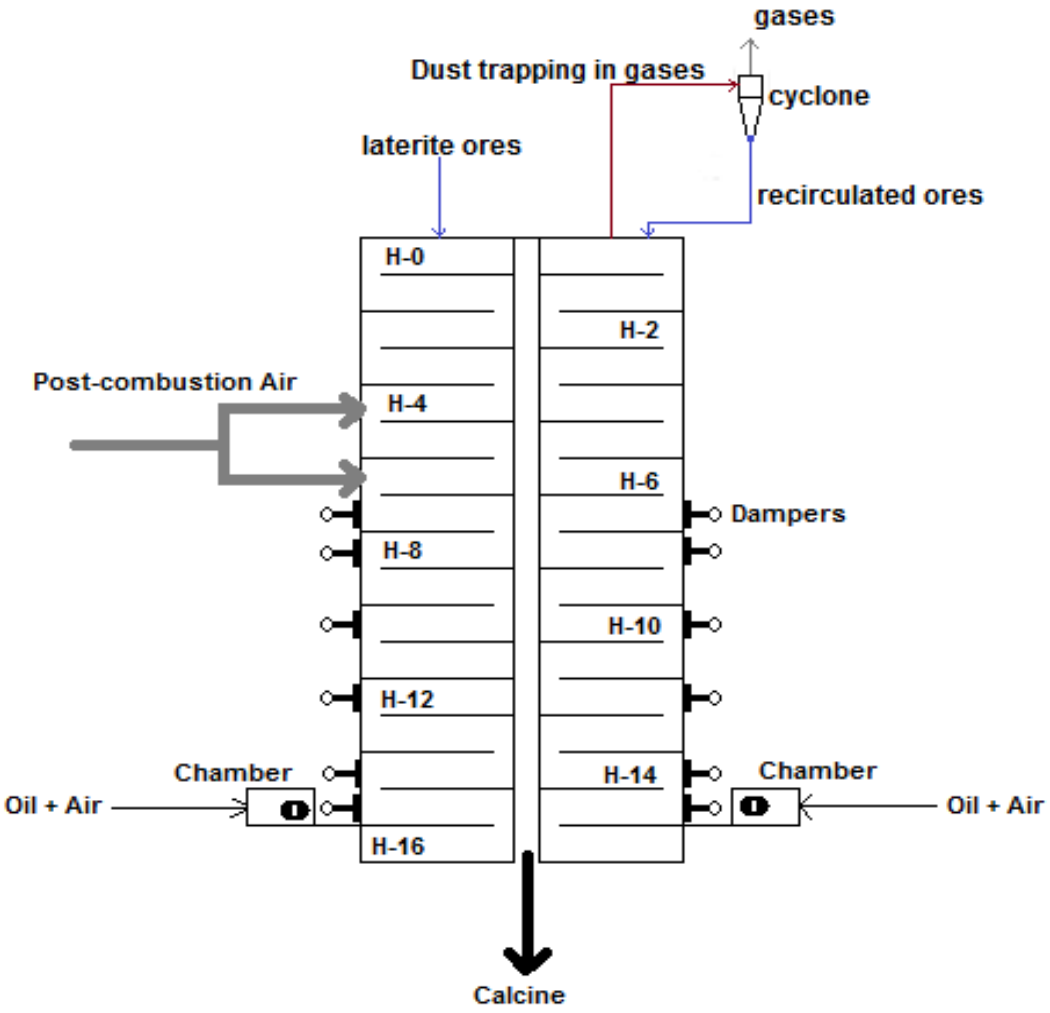

Figure 1. Pilot plant scale reduction furnace; letter H designate hearth [11]

2. 2. Physical chemistry characteristics of the fed lateritic ore

Lateritic ore with a degree of homogenization greater than 91 % was fed to the furnace at a rate of 750 kg h^{-1}, after being dried and ground until the moisture content was less than 4 % by weight and the size distribution of particle less than 75 μm it was from 84 to 88 %. Table 1 shows the main average (a) characteristics of the mineral where it is observed that there were insignificant differences between the processed samples used in the two experimental series in terms of the contents of Ni, Co, Fe, MgO, SiO_2, Al_2O_3, H_2O and S. Even so, there was a significant difference in the C content due to the type of additive used. In general, the results presented a low dispersion with standard deviation values lower than 1.8.

Table 1. Characteristics of lateritic ore with the two types of additive fed to the reduction process

Additive		Content, wt%									Particle size, μm			
											150	75	45	< 45
		Ni	Co	Fe	MgO	SiO_2	Al_2O_3	H_2O	S	C	Contribution, %			
FO-2.5	a	1.170	0.099	39.635	2.733	7.769	8.002	3.378	0.231	0.091	3.954	10.428	7.241	78.380
	σ	0.008	0.002	0.555	0.495	0.254	0.460	0.374	0.009	0.009	0.678	1.340	1.234	1.754
BC2-FO1.25	a	1.167	0.099	39.323	2.828	7.788	8.080	3.660	0.251	2.088	3.425	9.783	7.392	79.400
	σ	0.013	0.001	0.416	0.513	0.249	0.228	0.190	0.018	0.032	0.698	0.585	1.133	1.500

2. 3. Chemical analysis and mineralogical characteristics of the reduced/leached samples

The reduced ore samples were taken from the even hearths of the furnace using the procedure proposed by previously [11,25] Each sample was then leached with the ammonium carbonate solution with a concentration of NH_3 from 80 to 85 g dm^{-3} and CO_2 from 40 to 42 g dm^{-3} for 2 h at a liquid/solid mass ratio (L/S) of 10/1.

The individual elements of interest in the leached mineral were determined by atomic absorption spectrometry (AAS, model SOLAR 929, Solar System ATI, Unicam Analytical Technology Inc., Cambridge, UK).

The crystalline structure and composition of the reduced/leached minerals were analysed by powder X-ray diffraction (XRD) by a PANalytical X'PERT3 diffractometer (Malvern Panalytical, UK) with Gonio scanning at 2θ angular log from 4.0042 to 79.9962° and a distance step in 2θ = 0.0080°, potential difference of 40 kV, current of 30 mA and a calibration checked with an external silicon standard. Fractions of nickel, iron, and cobalt reduced to the metallic state of the ore in H16 were determined by leaching the reacted samples with a bromine-ethanol solution [30] followed by AAS analysis with flame and generator hydride, (model SOLAR 929, Solar System ATI, Unicam Analytical Technology Inc., Cambridge, UK).

2. 4. Temperature profile and reducing atmosphere in the reduction process

The thermal profile shown in Figure 2 was used in the investigation, regardless of the type of additive under study. Temperature measurements within different hearths were made by using K-type thermocouples (producer, country). To determine the effect of the additives FO-2.5 and BC2-FO1.25 in the reducing atmosphere of the furnace, the CO/CO_2 volumetric ratio was determined in each even hearth by the method used previously [25].

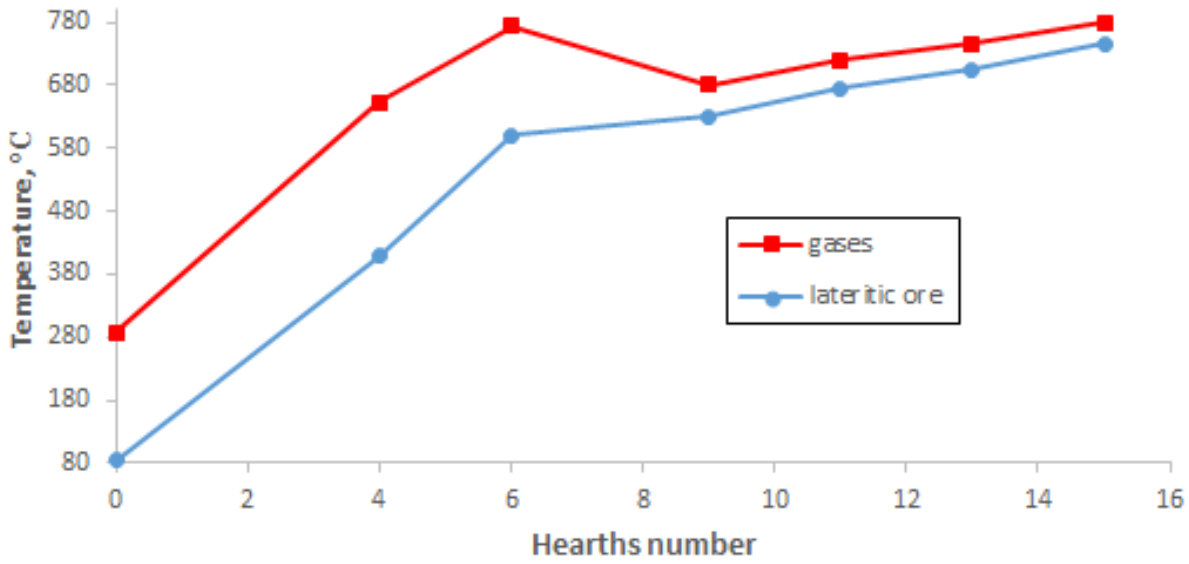

Figure 2. Temperature profile in the reduction furnace

2. 5. Nickel and cobalt extractions

Ni and Co extraction content were determined by the following equation, with an estimate of the error for Ni and Co of ±1.5 and ±2.5 %, respectively:

$$c_{\text{Ext-Met}} = \left(1 - \frac{c_{\text{Met-leached ore}}\ c_{\text{Fe-fed}}}{c_{\text{Met-fed}}\ c_{\text{Fr-leached ore}}}\right)100 \quad (8)$$

where:

$c_{\text{Ext-Met}}$ is the extracted content of the metal under analysis, Ni or Co;

$c_{\text{Met-leached ore}}$ is the content of the Ni or Co in the ore after leaching

$c_{\text{Met-fed}}$ is the content of Ni or Co in the ore fed to the reduction furnace

$c_{\text{Fe-fed}}$ is the content of iron in the ore fed to the reduction furnace

$c_{\text{Fe-leached ore}}$ is the content of iron in the ore after leaching

3. RESULTS AND DISCUSSIONS

3. 1. Effect of BC2-FO1.25 additive on the mineralogical composition and structure of reduced/leached ore

Figures 3 and 4 show the XRD patterns of the reduced/leached lateritic ore samples corresponding to each even hearth of the reduction furnace.

It is observed that the processed lateritic ore is characterized by the predominance of iron oxides and oxy-hydroxides (goethite, maghemite, and hematite), as well as aluminium hydroxide (gibbsite). Silicon and magnesium contents are mainly expressed in the phase of magnesium silicate hydrate (lizardite), magnesium aluminium oxide (spinel,) and some silicon oxide (quartz).

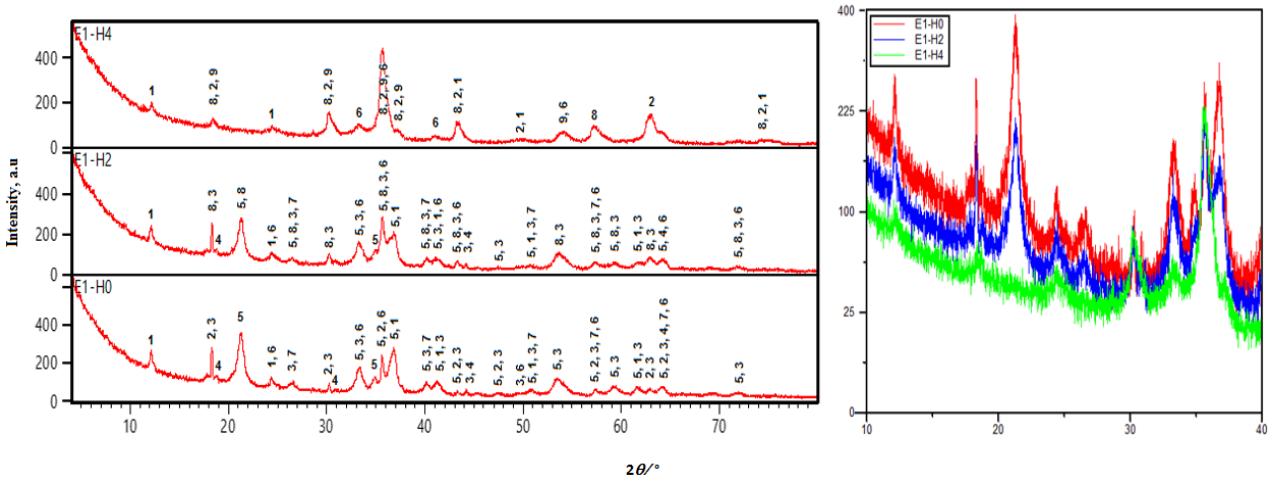

Figure 3. XRD patterns of reduced/leached lateritic ore samples from hearths H-0 through H-4 with the use of additive BC2-FO1.25. 1-Lizardite: $Mg_3Si_2O_5(OH)_4$; 2-Maghemite: $Fe_{21.16}O_{31.92}$; 3-Gibbsite: $Al(OH)_3$; 4-Spinel: $MgAl_2O_4$; 5-Goethite: FeOOH; 6-Hematite: Fe_2O_3; 7-Quartz: SiO_2; 8-Magnetite, syn: Fe_3O_4; 9-Chromite, aluminian: $Fe(Cr, Al)_2O_4$.

The furnace heating zone (from H-0 to H-4) is characterized by the loss of crystalline mineral water linked to the dehydroxylation process, with a predominance of transformations of goethite into hematite-magnetite, gibbsite in spinels containing aluminum and the decomposition of lizardite in H-4. The identification of hematite in the feed ore justifies the low presence of magnetite in H-2.

Different investigations agree that the goethite dehydroxylation process occurs in the temperature range of 250 to 400 °C to release iron oxide in the form of Fe_2O_3 as well as NiO [14,20,21,31-34].

In the literature [21] it was recognized that saprolite dehydroxylation has to be achieved between approximately 400 and 800 °C to obtain the complete recovery of Ni and Co.

The main mineralogical phases identified in the furnace reduction zone (from H-6 to H-16) were iron oxides (magnetite and maghemite, syn) and magnesium iron aluminum chromium oxide (magnesiochromite, ferroan). Magnesium iron silicate (fayalite) was only observed in hearths H-14 and H-16 (Fig. 4). The mineralogical phases detected in this study coincide with the investigations carried out previously [35,36], which identified maghemite, magnetite, magnesiochromite and fayalite as the main phases in the residues of the Caron process.

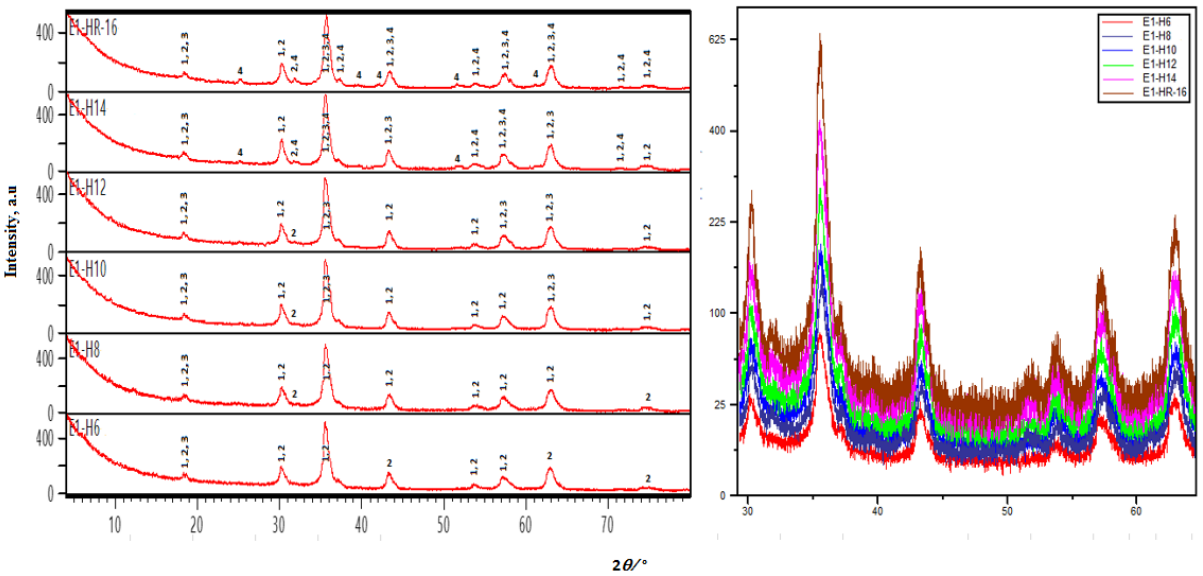

Figure 4. XRD patterns of reduced/leached lateritic ore samples from hearths H-6 through H-16 with the use of additive BC2-FO1.25. 1-Magnetite: Fe_3O_4; 2-Maghemite, syn: Fe_2O_3; 3-Magnesiochromite, ferroan: $[(Mg, Fe)(Cr, Al)_2O_4]$; 4-Fayalite: $Mg_{26}Fe_{1,74}(SiO_4)$

Magnetite increased in the content as each hearth corresponding to the reduction zone was passed. In the case of maghemite, loss of a part of oxygen from the $Fe_{21.16}O_{31.92}$ phase (heating zone) to Fe_2O_3 (H-6 to H-16) is observed, characteristic for the reduction process. Identification of magnesiochromite, ferroan, and fayalite indicates the formation of FeO and Fe^{2+}, and that the reduced ore reaches temperatures above 700 °C.

Similar magnetite content trend in the furnace reduction zone was described in a previous study on the Caron process with using 2.5 % fuel oil as the reducing additive [37]. Sanchez et al. [38] associated the identification of magnesiochromite and ferroane with processes in which partial substitution of Fe^{2+} by Mg, Cr, Al, and even by Fe^{3+} occurs in lower proportion. Also, it was recognized that fayalite is a product of transformation of the serpentine phase occurring at the highest reduction temperatures (600-800 °C) [21].

3. 2. Effect of substituting the reducing additive FO-2.5 with BC2-FO1.25 on chemical and physical characteristics of the reduced lateritic ore

Average chemical and physical characteristics of the reduced ore that were obtained when using each type of reducing additive are presented in Table 2 and Supplementary Material Tables S-1 and S-2.

Table 2. Chemical and physical characteristics of the reduced ore

Additive		Content, wt.%									ρ / kg m^{-3}	Magnetic fraction, %
		Ni	Co	Fe	Ni°	Fe°	Fe^{2+}	FeO	S	C		
FO-2.5	a	1.378	0.111	46.162	1.032	2.414	25.628	19.612	0.798	1.274	4690	59.584
	σ	0.022	0.003	0.277	0.034	0.213	1.387	0.543	0.036	0.053	8.843	1.268
BC2-FO1.25	a	1.344	0.112	46.534	1.067	2.782	25.058	19.896	0.604	1.368	4560	59.632
	σ	0.034	0.005	0.267	0.585	0.064	0.235	0.235	0.055	0.049	9.418	1.859

It is observed that regardless of the type of reducing additive used, chemical characteristics of the compounds correspond to an adequate reduction process where the conversion of NiO into metallic nickel (Ni°) is maximized, with contents of metallic iron (Fe^0) lower than 2.85 %. Also, Ni, Co, Fe, Fe^{2+}, FeO, and C contents, density and the magnetic fraction have shown similar values and were indicative that the substitution of the standard additive does not negatively affect the reducibility of the lateritic ores. It should be noted that the sulfur content was significantly lower when using the coal-oil mixture.

Different researchers [39,40] characterized the reduced ore when using FO-2.5 as a reducing additive and the reported values are close to those reported in this study.

Rojas *et al.* [41] recognized the negative effect caused by the increase in the sulfur content in the reduced ore in Ni and Co extractions due to the effect generated by passivation of the combined Fe-Ni-Co alloys during leaching. Therefore, implementation of the BC2-FO1.25 mixture on an industrial scale would benefit the leaching process.

3. 3. Effect of substituting the reducing additive FO-2.5 with BC2-FO1.25 on the CO/CO_2 profile in the furnace atmosphere

Figure 5 shows how the CO/CO_2 volumetric ratio varies in the even hearths of the pilot reduction furnace when using the reducing additives under analysis, see Supplementary Material Tables S-3 and S-4. The two zones described by Angulo *et al.* [25] were observed in correspondence with the content of reducing agents.

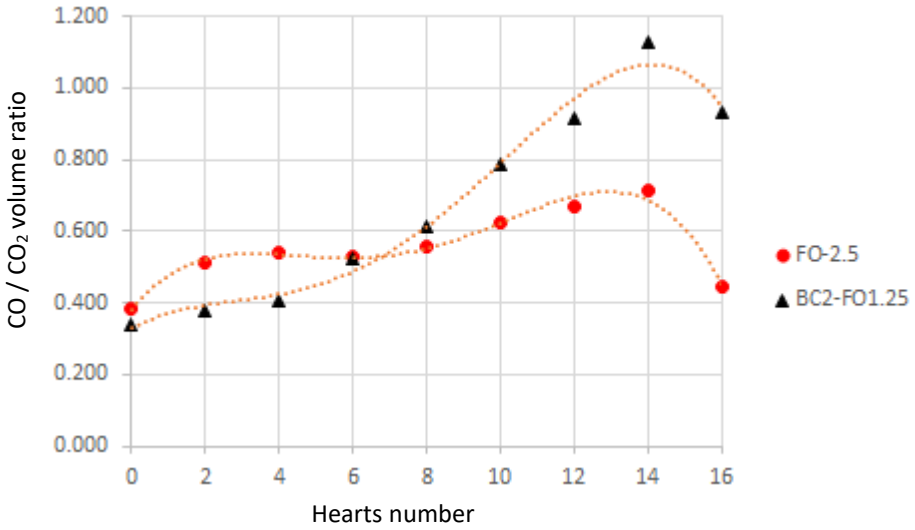

Figure 5. CO/CO_2 profile in the pilot furnace atmosphere

The first zone (from H-0 to H-6) is characterized by low CO/CO_2 volumetric ratios for both reducers resulting from the dilution generated by the post-combustion air supply in furnace hearths four and six. The average content of CO was higher by 16.4 % when using the FO-2.5 additive, justified by the fact that the temperatures in all furnaces are higher than the flash point of oil, while in the case of coal, the energy is not sufficient to provide the reductants from the dissociation process.

The second zone (from H-8 to H-16) is characterized by a gradual increase in the concentration of reducing gases. In all the hearths of the reduction zone (from H-8 to H-16) when using the BC2-FO1.25 additive, the average CO formation is increased by 22.4 % ($\sigma < 0.08$) compared to that achieved with the additive that is implemented currently on the industrial scale (FO-2.5).

Angulo *et al.* [11] report the average contents of CO in the chimney and the H-10 of the pilot furnace of 5.10 and 8.70 % respectively ($\sigma < 0.105$), values close to those achieved in this investigation (5.30 and 7.80 % for the H-0 and H-10, respectively). In the case of the BC2-FO1.25 mixture, no research was found to date that would allow comparisons to be made.

3. 4. Effect of replacing the reducing additive FO-2.5 for BC2-FO1.25 on nickel and cobalt extractions

During the evaluation of both additives, extraction content ranged from 78 to 84 % and 34 to 46 % for Ni and Co, respectively (Table 3 and Supplementary Material Tables S-5 and S-6). Different studies [11,13,16,25,37,39,40] reported values that coincide with those achieved in this investigation.

The average extraction of Ni and Co were higher by ~3 and ~8 %, respectively, when using the BC2-FO1.25 mixture as a reducing additive (Table 3), an aspect that is directly related to chemical and physical characteristics of the resulting reduced ore and the reducing atmosphere in the furnace in the process with this additive. The increases in Ni and Co extraction yields indicate that the used technological modification ensures more efficient operation of the reduction roasting process. These results confirm the values reported by Angulo *et al.* [23,24] for the laboratory scale experiments.

Table 3. Nickel and cobalt extraction results

Additive		Content, wt.% (Reduced and leached)			Extraction, wt.%	
		Ni	Co	Fe	Ni	Co
FO-2.5	a	0.295	0.077	48.11	79.22	35.74
	σ	0.004	0.001	0.598	0.428	1.130
BC2-FO1.25	a	0.254	0.069	48.37	82.30	43.90
	σ	0.015	0.002	0.253	1.104	1.388

5. CONCLUSIONS

The BC2-FO1.25 additive can reasonably increase the degree of recovery of nickel and cobalt from the laterite ore in the roasting/selective reduction process. The results of this study suggest that using this technological modification guarantees proper transformation of goethite in limonite to magnetite and serpentine minerals to olivine phases in saprolite. The use of this additive at a pilot scale showed that the industrially used additive fuel oil (FO-2.5) can be replaced since the main technological indicators of the process were improved. It should be stressed that the average formation of carbon monoxide in all hearths in the furnace reduction zone increased by ~22 % while the average extraction yields of Ni and Co were higher by ~3 and ~8 % respectively.

Declaration of interest statement: *The authors declare they have no conflict of interest.*

REFERENCES

[1] Bartzas G, Tsakiridis PE, Komnitsas K. Nickel industry: Heavy metal(loid)s contamination - sources, environmental impacts and recent advances on waste valorization. *Curr Opin Environ Sci Heal.* 2021; 21: 100253 https://doi.org/10.1016/j.coesh.2021.100253

[2] Mitterecker J, Košević M, Stopic S, Friedrich B, Panić V, Stevanović J, Mihailović M. Electrochemical Investigation of Lateritic Ore Leaching Solutions for Ni and Co Ions Extraction. *Metals (Basel).* 2022; 12(2): 325 https://doi.org/10.3390/met12020325

[3] Al-Khirbash SA. Mineralogical characterization of low-grade nickel laterites from the North Oman Mountains: Using mineral liberation analyses - scanning electron microscopy-based automated quantitative mineralogy. *Ore Geol Rev.* 2020; 120: 103429 https://doi.org/10.1016/j.oregeorev.2020.103429

[4] Gleeson SA, Butt CRM, Elias M. Nickel Laterites. *SEG Discov* 2003; (54): 1-18 https://doi.org/10.5382/SEGnews.2003-54.fea.

[5] Domenech C, Galí S, Villanova-de-Benavent C, Soler J, J P. Reactive transport model of the formation of oxide type Ni-laterite profiles (Punta Gorda, Moa Bay, Cuba. *Mineralium Deposita.* 2017; 52(7): 993-1010

[6] Aiglsperger T, Proenza JA, Lewis JF, *et al.* Critical metals (REE, Sc, PGE) in Ni laterites from Cuba and the Dominican Republic. *Ore Geol Rev*. 2016; 73: 127-147. https://doi.org/10.1016/j.oregeorev.2015.10.010

[7] Oxley A, Barcza N. Hydro-pyro integration in the processing of nickel laterites. *Miner Eng.* 2013; 54: 2-13. https://doi.org/10.1016/j.mineng.2013.02.012.

[8] Caron MH. "Fundamental and practical factors in ammonia leaching of nickel and cobalt ores" *JOM-Journal of the Minerals, Metals and Materials Society,* 1950; *2*(1): 67-90. https://doi.org/10.1007/BF03398981

[9] Caron MH. "Separation of Nickel and Cobalt" *JOM-Journal of the Minerals, Metals and Materials Society,* 1950; 2(1): 91-103. https://doi.org/10.1007/BF03398982

[10] Kießling F, Stopic S, Gürmen S, Friedrich B. Recovery of Diamond and Cobalt Powders from Polycrystalline Drawing Die Blanks via Ultrasound Assisted Leaching Process—Part 2: Kinetics and Mechanisms. *Metals (Basel),* 2020; 10(6): 741. https://doi.org/10.3390/met10060741

[11] Palma HJA, Legrá AL, Urgellés AL, Gálvez E, Castillo J. Post-combustion Effect on Nickel and Cobalt Extractions from the Caron Process. In: *Proceedings of Fourth International Conference on Inventive Material Science Applications, ICIMA 2021.* Coimbatore, India, 2022, pp. 515-527. https://doi.org/10.1007/978-981-16-4321-7_43

[12] Rodriguez R. Reduction in energy cost in Cuban Caron Process Plants. In: *International Laterite Nickel Symposium 2004 (as held during the 2004 TMS Annual Meeting)*. The Minerals, Metals & Materials Society 2004, pp. 657-664. ISBN: 0-87339-550-6.

[13] Canterford Jh. Oxide Ores of Nickel — The Australian Situation. *Miner Process Extr Metall Rev.* 1983; 1(1-2): 85-109. https://doi.org/10.1080/08827508308952590

[14] Shofi A, Supriyatna YI, Prasetyo AB. Selective Reduction of Southeast Sulawesi Nickel Laterite using Palm Kernel Shell Charcoal: Kinetic Studies with Addition of Na2SO4 and NaCl as Additives. *Bull Chem React Eng Catal.* 2020; 15(2): 501-513. https://doi.org/10.9767/bcrec.15.2.7733.501-513

[15] Coello-Velázquez AL, Quijano Arteaga V, Menéndez-Aguado JM, Pole FM, Llorente L. Use of the Swebrec Function to Model Particle Size Distribution in an Industrial-Scale Ni-Co Ore Grinding Circuit. *Metals (Basel).* 2019; 9(8): 882. https://doi.org/10.3390/met9080882

[16] De Graaf JE. The treatment of lateritic nickel ores — a further study of the caron process and other possible improvements. Part I. Effect of reduction conditions. *Hydrometallurgy.* 1979; 5(1): 47-65. https://doi.org/10.1016/0304-386X(79)90027-6

[17] Pickles CA, Elliott R. Thermodynamic analysis of selective reduction of nickeliferous limonitic laterite ore by carbon monoxide. *Miner Process Extr Metal.l* 2015; 124(4): 208-216. https://doi.org/10.1179/1743285515Y.0000000009

[18] Pickles CA, Anthony W. A Thermodynamic Study of the Reduction of a Limonitic Laterite Ore by Methane. *High Temp Mater Process.* 2018; 37(9-10): 909-19. https://doi.org/10.1515/htmp-2017-0106

[19] Pickles CA, Anthony W. Thermodynamic modelling of the reduction of a saprolitic laterite ore by methane. *Miner Eng.* 2018; 120: 47-59. https://doi.org/10.1016/j.mineng.2018.02.006

[20] de Alvarenga Oliveira V, dos Santos CG, de Albuquerque Brocchi E. Assessing the Influence of NaCl on the Reduction of a Siliceous Laterite Nickel Ore Under Caron Process Conditions. *Metall Mater Trans B.* 2019; 50(3): 1309-1321. https://doi.org/10.1007/s11663-019-01552-w

[21] Valix M, Cheung W. Effect of sulfur on the mineral phases of laterite ores at high temperature reduction. *Miner Eng.* 2002; 15(7): 523-530. https://doi.org/10.1016/S0892-6875(02)00069-9

[22] Ilyas S, Srivastava RR, Kim H, Ilyas N, Sattar R. Extraction of nickel and cobalt from a laterite ore using the carbothermic reduction roasting-ammoniacal leaching process. *Sep Purif Technol.* 2020; 232: 115971. https://doi.org/10.1016/j.seppur.2019.115971

[23] Angulo-Palma HJ, Legrá-Legrá A, Hernández-Pedrera C, Lamorú-Urgellés A, Vega-Cala RJ. Efecto de la sustitución del petróleo aditivo por carbón bituminoso en el proceso de reducción de lateritas. *Eff Substit Addit Oil with Bitum Coal Process Reducing Laterites.* 2018; 38(3): 750-764. (Spanish)

[24] Angulo-palma HJ, Legr A, Hern C, Lamor A, Toro-villarroel N. Reducción de menas lateríticas utilizando como aditivo mezclas de carbón bituminoso y petróleo. *Tecnol Química.* 2020; 40(1): 93-105. (Spanish)

[25] Angulo-palma HJ, Terencio-guevara PL, Legrá-Legrá A, Videaux-arcia L. Análisis especiales en un horno de reducción de níquel a escala de Planta Piloto Special Analysis in a Nickel Reduction Furnace at Pilot Plant scale. *Tecnol Química.* 2017; 37(3): 484-499. (Spanish)

[26] Basulto L. Evaluación de la sustitución de fuel-oil por finos de carbón antracita como aditivo en la empresa Comandante Ernesto Che Guevara 2018. http://ninive.ismm.edu.cu/handle/123456789/1706 (Spanish)

[27] Ilyas S, Kim H, Srivastava RR. Carbothermic Reduction Roasting of a Low-Grade Nickel Laterite Ore in the Modified Caron Process. In: *Ni-Co 2021 5th Int Symp Nickel Cobalt* 2021: 317-328. https://doi.org/10.1007/978-3-030-65647-8_27

[28] Suarez JC, Villanueva GAA, Fuxa AMDLC, González PM, Urtafe IL, Laurencio OP, Rodríguez ME. Hydrometallurgical process for the recovery of nickel and cobalt by ammoniacal leaching. US 6,524,367 B1, 2003

[29] Angulo-Palma HJ, Legrá-Legrá A, Hernández-Pedrera C. Modelos para determinar variables importantes en el proceso Caron. Parte I: Consumo específico de energía en molienda. *Opuntia Brava.* 2021; 13: 149-57. (Spanish)

[30] Sant B. Determination of metallic iron, iron(II) oxide, and iron(III) oxide in a mixture. *Talanta.* 1968; 15(12): 1483-1486. https://doi.org/10.1016/0039-9140(68)80211-5

[31] Chander S, Sharma VN. Reduction roasting/ammonia leaching of nickeliferous laterites. *Hydrometallurgy.* 1981; 7(4): 315-327. https://doi.org/10.1016/0304-386X(81)90029-3

[32] Valix M, Cheung WH. Study of phase transformation of laterite ores at high temperature. *Miner Eng.* 2002; 15(8): 607-612. https://doi.org/10.1016/S0892-6875(02)00068-7

[33] O'Connor F, Cheung WH, Valix M. Reduction roasting of limonite ores: effect of dehydroxylation. *Int J Miner Process.* 2006; 80(2-4): 88-99 https://doi.org/10.1016/j.minpro.2004.05.003

[34] Pintowantoro S, Widyartha AB, Setiyorini Y, Abdul F. Sodium Thiosulfate and Natural Sulfur: Novel Potential Additives for Selective Reduction of Limonitic Laterite Ore. *J Sustain Metall.* .2021; 7(2): 481-494. https://doi.org/10.1007/s40831-021-00352-4

[35] Cabrera G, Gómez JM, Hernández I, Coto O, Cantero D. Different strategies for recovering metals from CARON process residue. *J Hazard Mater.* 2011; 189(3): 836-842. https://doi.org/10.1016/j.jhazmat.2011.03.048

[36] Rojas-Purón AL, Turro-Breffe A. Composición mineralógica de las colas del proceso Caron en Moa, Holguín, Cuba. *Minería y Geol.* 2003; 19:8. (Spanish)
[37] Miranda J, Chaviano L, Miranda J. Nuevas interpretaciones quimico-mineralogicas de las menas lateriticas y serpentinicas a traves del proceso pirometalurgico en la tecnologia carbonato-amoniacal. *Rev Cuba Química.* 2002; 14: 42-51. (Spanish)
[38] Sánchez-Ramos S, Doménech-Carbó A, Gimeno-Adelantado JV, Peris-Vicente J, Valle-Algarra FM. Thermal decomposition of chromite spinel with chlorite admixture. *Thermochim Acta.* 2008; 476(1-2): 11-19. https://doi.org/10.1016/j.tca.2008.07.003
[39] Chang-Cardona AR, Rojas-Vargas A. Comportamiento electroquímico del Fe y sus iones durante la lixiviación estándar QT de minerales reducidos en el proceso "Caron" con diferentes aireaciones. *Tecnol Química.* 2014; 34: 117-127. (Spanish)
[40] Rojas-Vargas A, Sánchez-Guillen C, Magaña-Haynes ME, Hernández-Pedrera C. Extracción potencial de níquel y cobalto con mineral laterítico de mina "Pinares de Mayarí" en la tecnología Caron. Parte I. *Tecnol Química.* 2021; 41: 519531. (Spanish)
[41] [Rojas Vargas A, Magaña Haynes ME, Riverón AR. Lixiviación carbonato amoniacal: estimación del níquel disuelto en el efluente de destilación. *Rev Metal.* 2019; 55(3): 149.https://doi.org/10.3989/revmetalm.149. (Spanish)

Upotreba smeše uglja i nafte kao aditiva za selektivnu redukciju lateritne rude Caron procesom

Hugo Javier Angulo-Palma[1,3], Ángel Legrá Legrá[1], Alisa Lamorú Urgellés[1], Carlos Hernández Pedrera[4], Sandra Gallegos[2], Felipe M. Galleguillos Madrid[5] i Norman Toro[2]

[1]Centro de Investigaciones del Níquel ``Alberto Fernández Montes de Oca´´ (CEDINIQ), Moa, Holguín, Cuba
[2]Faculty of Engineering and Architecture, Universidad Arturo Prat, Iquique 1110939, Chile
[3]Departamento de Metalurgia Química, Universidad de Moa, Holguín, Cuba
[4]Facultad de Ingeniería Química y Agronomía, Universidad de Oriente, Santiago de Cuba, Cuba
[5]Centro de Desarrollo Energético Antofagasta, Universidad de Antofagasta, Antofagasta 1271155, Chile

(Stručni rad)

Izvod

Lateritne rude predstavljaju glavni izvor sirovine za ekstrakciju Ni i Co po Caron procesu. Potrošnja ulja u redukcionoj peći jedan je od ključnih pokazatelja da li je metalurški proces ekonomičan. Do danas nije bilo moguće zameniti aditiv lož ulje koji se koristi u komercijalnim razmerama, stoga je cilj ove studije bio da se delimično zameni nafta bitumenskim ugljem na pilot skali korišćenjem mešavine 2 % uglja i 1,25 % nafte kao redukcionog aditiva. Faze redukovanih/luženih ruda analizirane su difrakcijom rendgenskih zraka praha, dok je metalno stanje rude određivano luženjem izreagovanih uzoraka rastvorom brom-etanola nakon čega je usledila analiza atomske apsorpcione spektrometrije. Ekstrakcije Ni i Co potvrđene su luženjem redukovane rude rastvorima amonijum-amonijum karbonata. Uočeno je da smeša koja se koristi kao redukcioni aditiv može da zameni mazut jer omogućava adekvatnu transformaciju glavnih mineraloških faza lateritne rude tokom procesa redukcije i prosečne prinose ekstrakcije Ni i Co za ~3 i ~8. %, redom. Iako efekat veličine čestica bitumenskog uglja u procesu nije analiziran, redukciona smeša je obezbedila da je Caron proces efikasniji.

Ključne reči: ekstrakcija nikla i kobalta, rad peći, pirometalurgija

Analysis of the thermal behavior of a fixed bed reactor during the pyrolysis process

Milica Đurđević[1], Saša Papuga[2] and Aleksandra Kolundžija[2]

[1] *University of Banja Luka, Faculty of Mechanical Engineering, Banja Luka, Bosnia and Herzegovina*
[2] *University of Banja Luka, Faculty of Technology, Banja Luka, Bosnia and Herzegovina*

Abstract

Pyrolysis is a thermochemical process of degradation of organic compounds where the reaction takes place in an inert atmosphere. The process scale varies between industrial, semi-industrial or laboratory. During the pyrolysis process temperature has to be controlled, but, most of pyrolysis studies do not clearly state where the temperature is measured and weather the temperature field is uniform. In this paper thermal behavior of a laboratory scale fixed-bed reactor and energy consumption during pyrolysis processes were analyzed. Three different samples were used: mixture of plastic waste (sample 1), biomass (sample 2) and mixture of plastic waste and biomass (sample 3). The analysis of the thermal behavior of the reactor indicates that with careful regulation or temperature control of the process, one can obtain diagrams that can be used for the purpose of recording thermally intensive processes, similar to more complex thermogravimetric (TG) and derivative thermogravimetric (DTG) analyses. It has been shown that it is possible to change the heating rate and the overall energy efficiency of the process by simply choosing the appropriate raw material mixture.

Keywords: Waste plastics; waste recovering; thermal reaction; heating rate; energy consumption.

Available on-line at the Journal web address: http://www.ache.org.rs/HI/

ORIGINAL SCIENTIFIC PAPER

UDC: 66.092-97:628.4.043:678.028.6

Hem. Ind. **78(1)** 29-40-24 (2024)

1. INTRODUCTION

Plastic waste is a common part of municipal solid waste (MSW), which is composed of different mixtures of plastic, mostly consisting of: low-density polyethylene (LDPE), high-density polyethylene (HDPE), polypropylene (PP), polystyrene (PS), polyvinyl chloride (PVC), and polyethylene terephthalate (PET). The main components of municipal plastic waste are PE and PS [1]. Plastic waste is bulkier than other organic waste so that it occupies large spaces in landfills. Also, this is the main reason for the high costs of disposal and incineration of this type of waste. Waste-to-energy technologies convert plastic waste into heat, hydrocarbon fuels and chemicals [2]. Pyrolysis of plastic is a tertiary recycling method, whereby the polymer is heated in the absence of oxygen causing the polymer cracking [3]. Pyrolysis is also used for biomass conversion where the mostly used feedstock is plant matter, like forest residues, yard clippings, wood chips, and municipal solid waste [4].

Pyrolysis process represents a basis for production of the second generation of synthetic fuels, materials, and chemicals [5]. This reaction occurs in an inert atmosphere, in which organic compounds are decomposed, generating gaseous and liquid products that can be further utilized as fuels or chemicals. The inorganic material remains unchanged [6,7]. During pyrolysis of polymers, macromolecules are broken down into smaller molecules [8]. Biomass materials are mostly chemically and physically heterogeneous, whereby their components have various reactivities and yield different products [9].

Many studies have been published focusing on pyrolysis of plastic and biomass waste. A comprehensive bibliometric survey on pyrolysis of plastic waste has been done by Armenise *et al.* [10], while several studies provide detailed explanation on pyrolysis of plastic, pyrolytic reactors, effects of different parameters on the liquid oil yield and its

Corresponding authors: Milica Đurđević, Faculty of Mechanical Engineering, University of Banja Luka, Banja Luka, Bosnia and Herzegovina
E-mail: milica.preradovic@student.mf.unibl.org
Paper received: 17 December 2022; Paper accepted: 20 October 2023; Paper published: 16 November 2023.
https://doi.org/10.2298/HEMIND221217024D

characterization [11-16]. Interesting studies on the catalytic pyrolysis have been published by Budsaereechai *et al.* [17], and Suhartono *et al.* [18] showing that addition of natural catalysts lead to higher yields of liquid products with better properties (no wax formation, increased calorific value, and lower viscosity) compared to the pyrolysis runs without catalysts. Catalytic pyrolysis of plastic sample based on the plastic waste composition from Portuguese municipal solid waste has been conducted by Pinto *et al.* [19]. However, this study showed that there is no big difference between thermal and catalytic pyrolysis of selected plastic waste mix (68 % PE, 16 % PP, and 16 % PS). Uthpalani *et al.* [20] have reviewed the literature on pyrolysis of HDPE and LDPE wastes. Kalargaris *et al.* have been studied diesel engines powered by pyrolytic oil gained from pyrolysis of plastic waste throughout several studies [21-24]. Some papers [25-28] confirm and prove the success of pyrolysis of the mixture in the specific configuration of the reactor with a fixed bed that was used in this work as well.

Generally, pyrolysis can be divided into two phases, primary and secondary. When a solid biomass particle is heated in the absence of oxygen heat is firstly transferred to the particle surface by radiation and/or convection and then to the interiors of the particle by conduction. The temperature within the particle increases and contributes to the removal of moisture that is contained in biomass, and the pyrolysis reaction takes place. Due to the chemical reactions heat is generated/consumed, which with phase changes cause a temperature gradient as a function of time that is nonlinear. Volatiles and gas products flow through the particle pores. The rate of pyrolysis reactions depends on the local temperature [9].

Benefit of pyrolysis is production of high energy compounds (char, tar, and gas) from low energy materials (solid waste). The conversion depends on operating conditions, *e.g.* heating rate, maximum temperature, processing time at the maximum temperature, pressure, and catalysts used [29,30]. Additionally, the quality and yield of the oil products are depending on: operating temperature, the ratio of plastic waste and catalyst, and the type of reactor [31].

1. 1. Pyrolysis reactors

There are many different types of pyrolysis reactors and their classification can be based on: the final products achieved (oil, char, heat, electricity, gases), reactor mode of operation (batch or continuous), manner in which the reactor is heated (direct or indirect heating), method used to load the reactor (manually or mechanical), the pressure at which the unit operates (atmospheric, vacuum, pressurized), material used for the construction of the reactor (soil, brick, concrete, steel), reactor portability (stationary or mobile), and the reactor position [32].

Fixed-bed reactors are commonly used on a laboratory scale for pyrolysis of municipal solid waste, while industrial applications of this reactor type are rare. The heating rate is low, and the particles are not heated uniformly. This is due to the low heat transfer coefficient within the reactor and the absence of mixing of feedstock. So, the particles located near the heating source will gain more heat, whereas those more away from the heating source would be cooler [33]. Pyrolysis of biomass in fixed-bed reactors was studied in several studies [*e.g.* 34-36]. In another study that used fixed-bed reactors for pyrolysis of plastic waste, polystyrene and multilayer plastic were used in different ratios as raw materials. This research concluded that with the longer cracking time and the higher number of plastic multilayers, the fuel volume, viscosity, and heat value were increased. The addition of multilayer plastic also decreased percentage of benzene in the final product [37].

It is important to differentiate between the temperature of the reaction and the reactor temperature. The reactor temperature must be higher because of the need for a temperature gradient to provide heat transfer [38]. The temperature profile and heat transfer that occur during pyrolysis are decisive factors that determine the reactor performance, and consequently the oil yields [39]. Since pyrolysis is a thermal degradation process, efficient heat transfer increases the process efficiency. Plastic has low heat conductivity that leads to non-uniform heat distribution [40]. Temperature profile in the reactor is used to determine the area where thermal cracking happens, since cracking is the most important step during plastic pyrolysis to produce oil (fuel) [41]. In the work of Hartulistiyoso *et al.* [41], pyrolysis of waste plastic bottles was conducted in cylindrical reactor. Five thermocouples were used to monitor temperature at the bottom, top and in the middle part of the reactor, with different arrangements, while the temperature profile within the reactor was predicted by Computational Fluid Dynamic (CFD) modeling. Predicted temperature profiles were similar

to the experimentally measured temperature values. Accurate measurement of the particle temperature is important for the development of kinetic models. In most experiments temperature is measured by thermocouples close to the sample. However, there is less information on temperature profile inside the sample [42]. Fluidized bed is one of the reactors that can provide uniform temperature and uniform heating rate during high temperature operation [40].

Since the literature does not provide sufficient information on temperature distribution during plastic pyrolysis, this paper aims to investigate the uniformity of the temperature field in a pyrolytic reactor (fixed-bed reactor) that has been developed at the University of Banja Luka, at the Faculty of Technology. Energy consumption during pyrolysis of different samples was also analyzed.

2. EXPERIMENTAL

The experiments were carried out with plastic waste blends, originating from municipal solid waste, biomass sawdust and blends of plastic waste and sawdust. Plastic packaging waste originates from household waste from Banja Luka, Republic of Srpska, Bosna and Herzegovina, and the sawdust is from local sawmills from Banja Luka region. The ratio of plastic types in the blends was following: polypropylene (PP) 40 %, low-density polyethylene (LDPE), 35 %, and high-density polyethylene (HDPE) 25 %. A mixture of two typical types of waste wood biomass beech sawdust and spruce sawdust was used as the biomass sample, which were mixed in equal mass ratios (1:1).

Packaging household waste was used to prepare PP and HDPE samples, while LDPE granulates for the production of plastic bags was used as LDPE sample. The waste packaging was firstly thoroughly washed, dried, shredded and grounded in the laboratory mill. After grinding, a mixture of PP and HDPE was prepared in the selected ratios and a granulometric analysis was performed. The average diameter of the plastic mixture (PP + HDPE) was 1.40±0.02 mm. The prepared plastic mixture was then mixed with cylindrical LDPE granulates (2.20 mm diameter × 5.03 mm length). The prepared biomass sample was dried to a constant mass for 24 h at a temperature of 105 °C, in order to avoid the influence of humidity variations in the starting raw material. A granulometric analysis of the biomass mixture was carried out as well yielding the average sawdust particle diameter of 0.77±0.12 mm. All samples were weighed by using a KERN KB 1200-2 laboratory scale.

Experiments were performed using a total sample mass of 200 g, and the height of the packed bed was 95 mm. Only one experiment, *i.e.* the experiment with maximum reactor loading, was performed with the sample mass of 350 g, and in that case the packed bed height was 190 mm.

Pyrolysis was performed in a laboratory scale, fixed bed reactor at the University of Technology in Banja Luka (Bosnia and Herzegovina), presented in Figure 1.

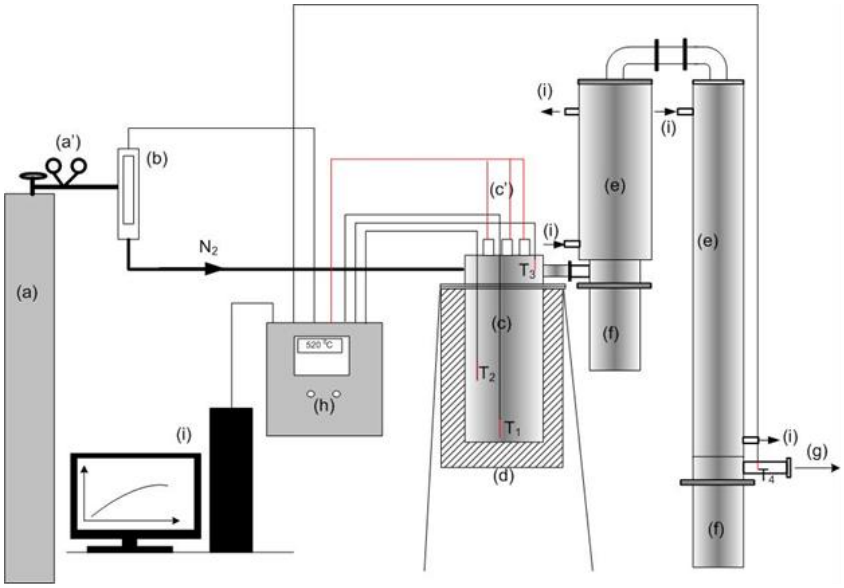

Figure 1 Block diagram of the experimental pyrolysis fixed-bed reactor: a) cylinder with nitrogen gas; b) mass gas flow meter; c) the pyrolysis reactor vessel; d) thermal insulation; e) steam condensation system; f) separation system - vessels for receiving condensate; g) discharge of non-condensable gas into the gas washing system; h) distribution cabinet with the regulation system; i) PC.

A prepared and weighed sample was placed in the reaction vessel (c) and nitrogen was used as the carrier gas, to provide inert atmosphere (a). A gas-flow meter (b) was used to adjust the gas flow (100 ncm^3min^{-1}), and after 10 min, inert atmosphere was accomplished. A PC (i) using CelciuX (EJ1N-TC4A-QQ) (Omron) thermal controller and CX-Thermo (Omron) were used for automatic control and regulation of the system (h) by turning on or off the electric heaters system (c) according to the control loop [25,28]. The thermocouple T1 (Thermocouple type K, Omron, Japan) measured temperature at the bottom part of the reactor and served as a control sensor for the controlling loop of electric heaters *i.e.* as a control variable. The reactor temperature set point was 500 °C. The time that feedstock spent on a set point temperature was considered to be a reaction time. After the chosen reaction time of 45 min, the regulation system was turned off. As the temperature of the reactor fell below 100 °C, the reactor was taken apart and the reaction vessel was disconnected from the reactor (c). The reaction vessel was weighed before and after the pyrolysis reaction and the solid residue was determined from the mass difference. The vessels for receiving condensate (f) were disconnected from condensation system (e) and weighed as well, to determine the mass of condensable products, including a part of the condensate products mass from internal walls of condensation system (e) [28].

The reactor vessel is in the form of a vertical cylinder (101.6×2 mm). The vessel consists of a body (lower part) and a body cover (upper part), with bolted flange joint with gaskets. The body is 200 mm high representing a reaction vessel and it is separated from the upper part and serves as a dosing system. The design enables simple weighing of the raw material and solid residue after the process is completed, so that it is possible to set up material balances relatively easily. A second cylindrical container is attached to the reactor body from the upper side - a cover with a total length of 40 mm. This cover carries three K-type thermocouples and three stainless steel tubes (A304) in which there are cartridge-electric heaters with a total power of 3×350 W. By connecting the cover to the reactor body, the electric heaters and thermocouples are placed in the reactor body. The heaters extend to the bottom of the reactor body, while three thermocouples are arranged in the reactor body, at different heights, as shown in Figure 1. Thermocouples T1, T2, and T3 are located: 7, 90 and 220 mm from the bottom of the reactor body, respectively. The reactor is made of stainless steel (A304) and a 3 cm thick thermal insulation layer of stone wool is applied on the outer wall of the reactor.

Reactor temperature changes were monitored at three characteristic points, while the temperature of non-condensable gases was recorded at the exit from the separation unit. All temperatures were measured by K-type thermos-couples and recorded using CX-Thermo software package (Omron, Japan). Regulation of the operation of the heater, *i.e.,* temperature control was performed using the temperature controller CelciuX (EJ1N-TC4A-QQ) (OMRON, Japan). Adjustment of the PID constants was carried out before the reaction started. Also, the specified constants and other characteristic values in the regulation system were set by using the software. Given the sensitivity of temperature regulation, before each experiment that included a new type of raw material (*i.e.* plastic mixture, bbiomass, and plastic/biomass mixture) measurements were carried out with the self-running option of PID constants (autotuning).

Inert gas flow was measured and regulated by a mass flow meter/regulator (MASS VIEW model MV-304 Mass Flow Regulator, Bronkhorst High-Tech BV, Nederland) with the measurement range 0.04 to 20 $dm^3\ min^{-1}$ and the additional possibility of fine flow regulation. Nitrogen of 99.99 % purity was used as a carrier gas. The total heat consumption was determined based on the electricity consumption, which was measured by the Wolcraft Energy Check 3000 device (Wolcraft GmbH, Germany), which covers the measurement range from 0.001 to 9999 kWh.

3. RESULTS AND DISCUSSION

The developed pilot plant provides the possibility of recording a diagram of the thermal behavior of the reactor (*i.e.* temperatures measured by thermocouples arranged within the reactor and at the exit of the condensation unit).

In Figure 2 a thermal diagram, *i.e.,* the reactor temperature profile is presented, during the empty reactor operation, *i.e.* heating the reactor without any raw material to a temperature of 500 °C for 45 min., at the inert gas flow of 0.1 $cm^3\ min^{-1}$, total heating power of 1050 W and the heating rate of 19.7 °C min^{-1} (PID characteristics of the system were P = 24; I = 306; D = 52.1).

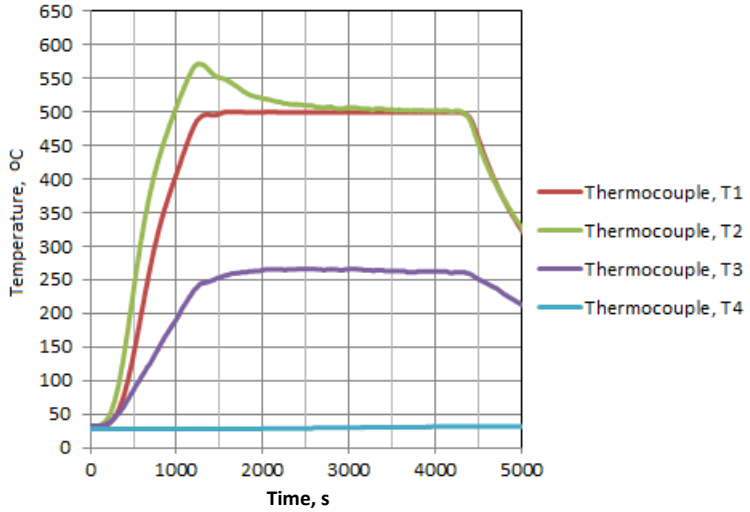

Figure 2. Thermal diagram of the empty reactor (heating rate 19.7 °C min^{-1}, 1050 W, PID constants: P *= 24,* I *= 306,* D *= 52)*

Figure 3 shows the thermal diagram in the pyrolysis experiment with the plastic waste mixture at the same process parameters (500 °C, 45 min, 0.1 cm^3 min^{-1}) and at the same heating conditions, where the heating rate was 12.1 °C min^{-1}.

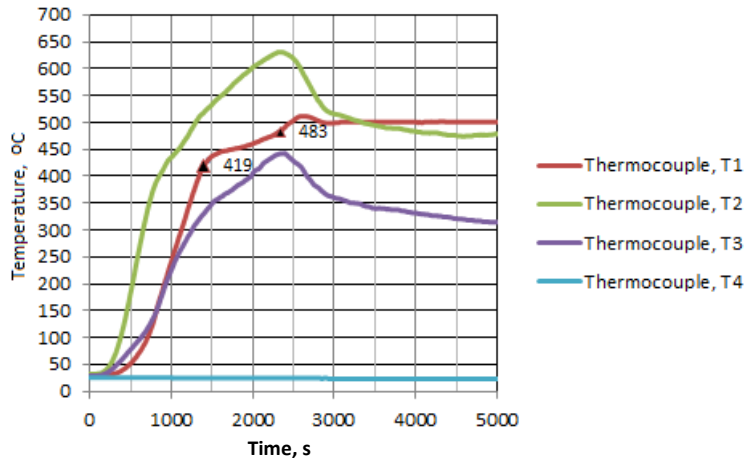

Figure 3. Thermal diagram in the reactor during pyrolysis of the mixture of plastic waste (heating rate 12.1 °C min^{-1}, 1050 W, PID constants: P = 24, I = 306, D = 52)

Both figures show non-uniform temperature distribution. The temperature in the lower part of the reactor (thermocouple T1) is lower than the temperature in the middle part of the reactor (thermocouple T2), which is very evident during pyrolysis (Fig. 3). Still, this is expected behavior, because during the heating phase, plastic is located in the upper and middle part of the reactor (measured by thermocouple T2). During heating, plastic melts, and it comes down towards the reactor bottom. This clears the upper and middle parts of the reactor, which enables intensive heating compared to the bottom part of the reactor. In the lower reactor part energy intensive processes (endothermic processes) are carried out.

The temperature in the upper part of the reactor (measured by thermocouple T3) is the lowest, which is expected. Namely, this part of the reactor, *i.e.* the lid of the reactor body, is practically non-insulated and is partly occupied by inert/non-heating parts of the cartridge-electric heaters. This behavior is additionally influenced by the fact that the carrier gas is introduced in that part of the reactor, which is not subject to pre-heating, *i.e.* the carrier gas enters the system at ambient temperature.

By the comparison of the two figures (Figs 2 and 3), the difference can be clearly observed. During the operation of an empty reactor, the heating of the system was faster *i.e.* a faster rise in temperatures measured by thermocouples T1, T2, and T3 (Fig. 2) occurred. However, during pyrolysis of the raw material (Fig. 3) this temperature increase was

slower. The decrease in the heating rate in the temperature interval from 419 to 483 °C of the lower reactor part (measured by T1) *i.e.* the reactor part where the feedstock material is placed, is particularly characteristic for pyrolysis of plastic. This finding is in accordance with thermogravimetric (TG) and derivative thermogravimetric (DTG) diagrams reported in literature [32,50]. Individual polymers degrade in the following order PS < PET < PP < PE [3]. Only PS decomposition occurs in the range between 350 and 450 °C, while pure PET degrades at temperatures between 390 and 470 °C, and PP, LDPE, and HDPE degrade between 450 and 510 °C [25].

Figure 4 shows the thermal diagram of empty reactor operation and Figure 5. shows the thermal diagram of the reactor filled with the biomass sample, during pyrolysis at 500 °C, time of 45 min, and nitrogen flow rate of 0.1 cm^3 min^{-1} and heating rate 28.6 °C min^{-1}. Both experiments were carried out under identical heating conditions (total heating power: 1050 W, PID characteristics of the system: P = 121, I = 718, D = 122.3), whereby the heating rate of the empty reactor was 15.8 °C min^{-1}.

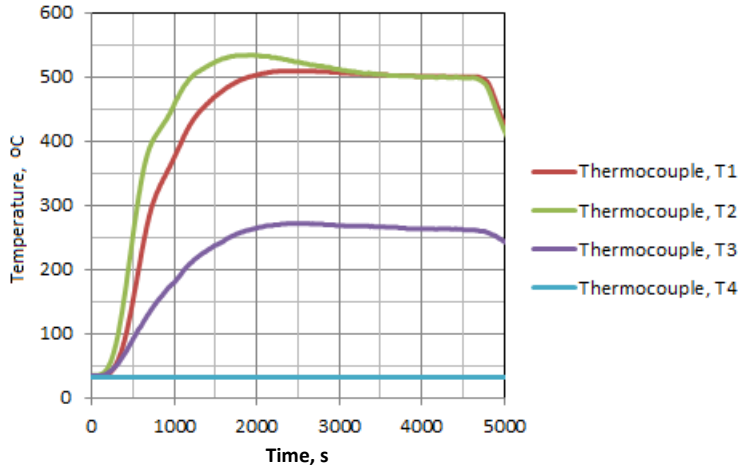

Figure 4. Thermal diagram of the empty reactor (heating rate 15.8 °C min^{-1}, 1050 W, PID constants: P = 121, I = 718, D = 122.3)

Unlike the diagram in Figure 3, the diagram in Figure 5 shows a much faster increase in temperatures measured by thermocouples T3, T2, and T1, at temperatures above 200 °C, and at the same time a faster temperature increases than during the operation of the empty reactor under identical conditions (Fig. 4). This directly implies the existence of exothermic effects in the biomass pyrolysis process, and that the biomass pyrolysis process itself is less energy demanding than plastic pyrolysis. Pyrolysis kinetics of biomass was investigated in literature [43] showing two stages: drying stage and devolatilization stage.

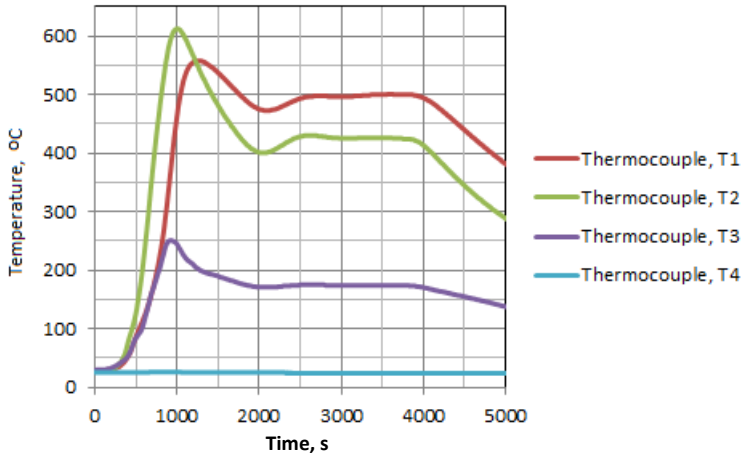

Figure 5. Thermal diagram of the reactor during biomass pyrolysis (heating rate 28.6 °C min^{-1}, 1050 W, PID constants: P = 121, I = 718, D = 122.3)

In the first stage, at temperatures between 50 and 70 °C, the moisture content drops resulting in mass loss. In the temperature range between 130 and 150 °C, TGA/DTG studies provide a flat line as a sign of water removal. And this point (150 °C) is the drying end temperature. During the second, devolatilization stage, biomass undergoes depolymerization and restructuring (mass loss is recorded at temperatures from 150 to 200 °C). After that, thermal chemical reactions occur, and TGA curves show a drop in the interval between 200 and 400 °C. The volatile matter yield depends on temperature and gas atmosphere [43]. It is possible to additionally analyze the obtained thermograms by mathematical methods and based on different slopes of the curves during the operation of the empty and reactor filled with raw materials, at the same operation conditions, to obtain the exact values of the thermal effects in the investigated process.

Considering the above statements, it can be concluded that in the developed pilot plant it is possible, with careful regulation or temperature control of the process to record diagrams that can be used for the purpose of identifying thermally intensive processes, similar to more complex TG and DTG analyses.

Figure 6 shows the thermal diagram of the pyrolysis experiment of a mixture of plastic/biomass in a ratio of 3:1, at 500 °C and a time of 45 min, at the inert gas flow of 0.1 cm^3 min^{-1} and under the conditions of heating waste plastic (total heating power: 1050 W; PID constants: P = 24, I = 306, D = 52.1), while the heating rate was 15.2 °C min^{-1}.

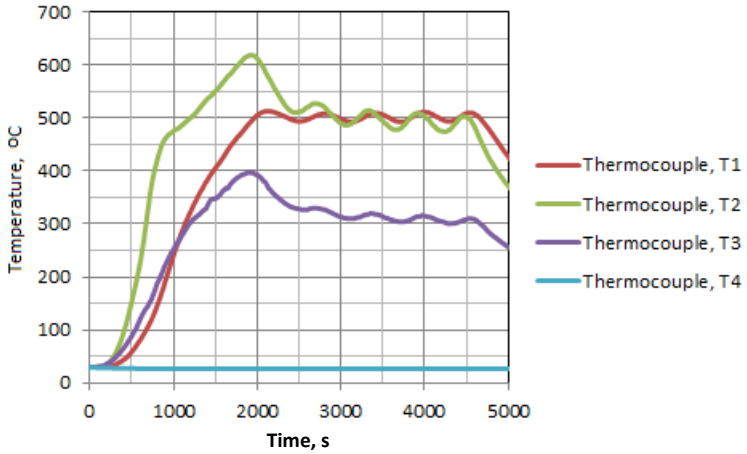

Figure 6. Thermal diagram of the reactor during pyrolysis of plastic/biomass mixture in the ratio 3:1 (heating rate 15.2 °C min^{-1}, 1050 W, PID constants: P = 34, I = 306, D = 52.1)

By comparing the obtained curves with the corresponding ones in Figure 3, a more intense increase in temperature is observed measured by thermocouples T1, T2, and T3, where the characteristic interval (419 to 483 °C), observed during the plastic pyrolysis, is almost completely absent. This means that part of the heat released during the devolatilization of biomass was directly used for the endothermic parts of the plastic pyrolysis process. Thus, it can be concluded that the co-pyrolysis of plastic and biomass, in the examined ratio of 3:1, had a favorable effect in terms of reducing the heat consumption. This behavior was additionally proven by measurement of the total consumption of electricity or heat for the analyzed processes.

From all the thermograms shown above, it can be seen that temperatures measured by thermocouple T3 were lower during the operation of the empty reactor compared to those during the pyrolysis of the investigated raw materials. This could be explained by the fact that the gaseous or steam products of pyrolysis additionally heat up the upper part of the reactor with their sensible heat compared to the conditions during the empty reactor operation.

It can be assumed that different temperatures in the vertical reactor section, above all temperatures measured by T2 and T3, affect the distribution and quality of the products. Namely, higher temperatures in the middle part of the reactor (T3) compared to the lower part of the reactor cause a larger cracking volume of steam products compared to the expected cracking volume, which would have occurred at a lower temperature (T2), *i.e.* under the conditions of a uniform temperature field within the reactor. Examination of the mentioned assumption is the subject of further research and modification of the heating system within the reactor, which will allow comparison of the yield and quality of the products at two different heating modes, *i.e.* at the existing and with the uniform temperature field.

Temperature distribution during the pyrolysis process is in accordance with monitored temperature profiles reported in literature [53], where pyrolysis of PP was carried out in a fixed-bed reactor at different temperatures (300, 400, 500, and 600 °C).

3. 1. Heat consumption and heating dynamics analysis

Table 1 provides values of the consumed electricity for the experiments, presented by the above shown thermal diagrams. The electric heaters are pure so-called "Ohm-consumers". Therefore, one can assume that the measured values of electricity consumption correspond to the heat consumption in the analyzed processes.

Table 1. Heat consumption during pyrolysis of plastic, biomass, and plastic/biomass mixture

Feedstock	Heat consumption, Wh			Specific heat consumption, Wh kg^{-1}
	Reactor filled with feedstock	Empty reactor	Process heat	
Plastic, 200 g	835	482	353	1765 (1386*)
Biomass, 200 g	269	459	-190	-950
Plastic/biomass mixture 3:1, 200 g	702	482	220	1100

*Value for the experiment in which the reactor was filled with 0.35 kg of plastic

Presented data in Table 1 can serve as an assessment of the energy intensity of the process. In the fourth column, the heat consumption of the process is given as a difference between the total heat used for the reactor operation during the pyrolysis of 0.2 kg of the feedstock material and the total heat used for operating the empty reactor under identical conditions. From these data, it can be seen that pyrolysis of plastics is the most energy-demanding process with a total heat consumption of 835 Wh, and the estimated heat consumption of the process of 353 Wh for 0.2 kg of the raw material, *i.e.* 1765 Wh kg^{-1} (6354 kJ kg^{-1}). Pyrolysis of biomass is the least energy-demanding process with a total energy consumption of 269 Wh, and a difference of -190 Wh (-950 W kg^{-1}) compared to the consumption of the empty reactor. This indicated the exothermic nature of the biomass pyrolysis process, and it favors reduction in the heat consumption for the 3:1 plastic/biomass co-pyrolysis process, amounting to 220 Wh for 0.2 kg of the raw material (1100 Wh kg^{-1}).

In order to analyze the possibility of further filling the reactor and the impact on energy consumption, research on the pyrolysis of plastics was carried out with the reactor filled with 0.35 kg of the plastic mixture. The aforementioned tests showed a total heat consumption of 967 Wh, and if the heat consumption of the empty reactor of 482 Wh is taken into account (Table 1), the process heat is 485 Wh, yielding 1386 Wh kg^{-1} (4989 kJ kg^{-1}). In the experiment, the yield in the reactor was the same as in the experiment when the reactor was filled with 0.2 kg of raw material. These results indicate higher reactor efficiency at higher loadings, which is expected considering that lower heat fraction is released through the reactor walls. In practice, the total heat required for the pyrolysis process consists of the heat required to heat the raw material to the appropriate temperature, the heat of depolymerization of the raw material, the heat of evaporation and obtaining gaseous products, the heat for heating the inert gas, and the heat required to maintain the reactor at a given temperature, which includes also heat losses through the reactor walls. Therefore, the analyses of the thermal energy in the developed laboratory scale reactor, which included all the mentioned effects, can serve as an estimate for the thermal analysis of larger pilot, semi-industrial and industrial reactors.

In the work of Xingzhong *et al.* [45] the total energy required for the pyrolysis of PE was 1316.1 kJ kg^{-1}. Also, similar result is presented in literature [46], for the same raw material, theoretical heat consumption was1.075 1075 kJ kg^{-1}. Another study [47] investigated the temperature influence on conversion of polystyrene to liquid oil by using pyrolysis in a fixed-bed reactor. It was concluded that the temperature of 500 °C yielded the maximum oil amount. At the temperatures below 500 °C, wax was produced, and above this temperature gases were the main reaction products [56]. Energy demand of the conventional pyrolysis process ranges between 23 and 30 MJ kg^{-1}, however information on processing scale are lacking. Microwave pyrolysis seems to be more energy efficient in comparison to conventional pyrolysis, because of the fast and selective heating [48]. Energy consumption during microwave pyrolysis is between 5 and 10 MJ kg^{-1} [49]. This agrees with the result obtained in this work (1765 Wh kg^{-1} ~6.35 MJ kg^{-1}), which further indicates that the applied pyrolysis process is more energy efficient than the conventional one (regarding the mentioned

literature values for energy consumption). Furthermore, the results obtained in this work are in the range of energy consumption values for microwave pyrolysis. Considering that the used reactor provides heating directly in the raw material layer, unlike classic batch or fixed-bed reactors, where the heat comes from the outer walls, this type of pyrolysis seems more energy efficient, resulting in lower energy consumption.

The obtained theoretical results differ from the results obtained in this research, primarily because pyrolysis is observed at a temperature lower than 100 °C, without taking into account heat losses and operating conditions of a real processing plant.

By analyzing the thermal diagrams from Figures 3, 4, and 5, i.e., by observing the time required to reach the pyrolysis temperature, the heating rate is obtained, which is presented in Table 2.

Table 2. Heating rates during pyrolysis of plastic, biomass, and plastic/biomass mixture

Feedstock	Heating rate, °C min^{-1}	
	Reactor filled with feedstock	Empty reactor
Plastic	12.1	19.7
Biomass	28.6	15.8
Plastic/biomass mixture 3:1	15	12.1

From the table 2 and the corresponding thermal diagrams, it is clearly seen how the dynamics of reactor heating changes with the change of raw material., even at the same heating conditions (pyrolysis of plastic and pyrolysis of the mixture

4. CONCLUSION

The main conclusions of this work can be summarized as follows.

- The analysis of the thermal behavior of the reactor indicates that in the developed pilot plant it is possible, with careful regulation or temperature control of the process, to record diagrams that can be used for the purpose of detecting thermally intensive processes, similar to more complex TG and DTG analyses. The obtained thermal diagrams of pyrolysis of plastics indicate an extremely endothermic phase of the process in the interval from 419 to 483 °C, while thermal diagrams of biomass pyrolysis indicate an extremely exothermic phase of the process at temperatures higher than 200 °C. The thermal diagram of co-pyrolysis of plastic and biomass in ratio 3:1 indicates a favorable effect of biomass addition in terms of lowering the energy consumption of the process; this is additionally proven by measurements of the total electricity consumption for the analyzed processes.
- Plastic pyrolysis is the most energy-demanding process with the specific heat consumption of 1765 Wh kg^{-1} at a heating rate of 12.1 °C min^{-1}, while the biomass pyrolysis is the least an energy-demanding process with a total consumption of 269 Wh for 0.2 kg of raw material, at a heating rate of 28.6 °C min^{-1}, and specific heat consumption 950 Wh kg^{-1}. The specific heat consumption for the co-pyrolysis of the plastic/biomass mixture was 1100 Wh kg^{-1} at the heating rate of 15.2 °C min^{-1}.
- When the reactor is filled with 0.35 kg of plastic, the reactor shows higher energy efficiency with the specific heat consumption of 1386 Wh kg^{-1}.
- The analyses of heating dynamics and the total energy consumption during the co-pyrolysis of a 3:1 plastic to biomass mixture, shows that it is possible to change the heating rate of the process and the overall energy efficiency of the process by simply choosing the appropriate mixture.

REFERENCES

[1] Miandad R, Barakat MA, Aburiazaiza AS, Rehan M, Nizami AS. Catalytic pyrolysis of plastic waste: A review. *Process Saf Environ Prot*. 2016; 102: 822-38. https://dx.doi.org/10.1016/j.psep.2016.06.022.

[2] Xue Y, Johnston P, Bai X. Effect of catalyst contact mode and gas atmosphere during catalytic pyrolysis of waste plastics. *Energy Convers Manag.* 2017; 142: 441-51. https://dx.doi.org/10.1016/j.enconman.2017.03.071.

[3] Marcilla A, Gómez-Siurana A, Berenguer D. Study of the influence of the characteristics of different acid solids in the catalytic pyrolysis of different polymers. *Appl Catal Gen.* 2006; 301(2): 222-31. https://doi.org/10.1016/j.apcata.2005.12.018

[4] Sharma A, Pareek V, Zhang D. Biomass pyrolysis—A review of modelling, process parameters and catalytic studies. *Renew Sustain Energy Rev*. 2015; 50: 1081-96. https://dx.doi.org/10.1016/j.rser.2015.04.193

[5] Gvero P, Mujanić I, Papuga S, Vasković S, Anatunović R. Review of Synthetic Fuels and New Materials Production Based on Pyrolysis Technologies. In: Pellicer E, Nikolic D, Sort J, Baró M, Zivic F, Grujovic N, et al., editors. *Advances in Applications of Industrial Biomaterials* [Internet]. Cham: Springer International Publishing; 2017; . 65-85. Available from: http://link.springer.com/10.1007/978-3-319-62767-0_4

[6] Almeida D, Marques M de F. Thermal and catalytic pyrolysis of plastic waste. *Polímeros.* 2016; 26(1): 44-51. https://dx.doi.org/10.1590/0104-1428.2100

[7] Gvero P, Papuga S, Mujanic I, Vaskovic S. Pyrolysis as a key process in biomass combustion and thermochemical conversion. *Therm Sci*. 2016; 20(4): 1209-22. https://dx.doi.org/10.2298/TSCI151129154G

[8] Kyaw KT, Hmwe CSS. Effect of various catalysts on fuel oil pyrolysis process of mixed plastic wastes. *Int J. Adv. Eng. Technol.* 2015; 8(5): 9. https://www.proquest.com/openview/5244b40561785593e77c906355ca14f9/1?pq-origsite=gscholar&cbl=1486350

[9] Babu BV. Biomass pyrolysis: a state-of-the-art review. *Biofuels Bioprod Biorefining.* 2008; 2(5): 393-414. https://dx.doi.org/10.1002/bbb.92

[10] Armenise S, SyieLuing W, Ramírez-Velásquez JM, Launay F, Wuebben D, Ngadi N, Rams J, Munoz M. Plastic waste recycling via pyrolysis: A bibliometric survey and literature review. *J Anal Appl Pyrolysis.* 2021; 158: 105265. https://dx.doi.org/10.1016/j.jaap.2021.105265

[11] Kunwar B, Cheng HN, Chandrashekaran SR, Sharma BK. Plastics to fuel: a review. *Renew Sustain Energy Rev.* 2016; 54: 421-8. https://dx.doi.org/10.1016/j.rser.2015.10.015

[12] Vijayakumar A, Sebastian J. Pyrolysis process to produce fuel from different types of plastic - a review. In: *IOP Conf Ser Mater Sci Eng*. Kerala State, India, 2018; 396: 012062. https://dx.doi.org/10.1088/1757-899X/396/1/012062

[13] Lopez G, Artetxe M, Amutio M, Bilbao J, Olazar M. Thermochemical routes for the valorization of waste polyolefinic plastics to produce fuels and chemicals. A review. *Renew Sustain Energy Rev.* 2017 Jun; 73: 346-68. https://dx.doi.org/10.1016/j.rser.2017.01.142

[14] Sharuddin SDA, Abnisa F, Daud WMAW, Aroua MK. Pyrolysis of plastic waste for liquid fuel production as prospective energy resource. In: *IOP Conf Ser Mater Sci Eng.* Banda Aceh, India, 2018; 334: 012001. https://dx.doi.org/10.1088/1757-899X/334/1/012001

[15] Maqsood T, Dai J, Zhang Y, Guang M, Li B. Pyrolysis of plastic species: A review of resources and products. *J Anal Appl Pyrolysis*. 2021; 159: 105295. https://dx.doi.org/10.1016/j.jaap.2021.105295

[16] Aguado J, Serrano DP, Escola JM. Fuels from Waste Plastics by Thermal and Catalytic Processes: A Review. *Ind Eng Chem Res.* 2008; 47(21): 7982-92. https://dx.doi.org/10.1021/ie800393w

[17] Budsaereechai S, Hunt AJ, Ngernyen Y. Catalytic pyrolysis of plastic waste for the production of liquid fuels for engines. *RSC Adv*. 2019; 9(10): 5844-57. https://dx.doi.org/10.1039/C8RA10058F

[18] Suhartono, Kusumo P, Romli A, Aulia MI, Yanuar EM. Fuel Oil from Municipal Plastic Waste through Pyrolysis with and without Natural Zeolite as Catalysts. Hadiyanto, Maryono, Warsito B, editors. *E3S Web Conf*. 2018; 73: 01021. https://dx.doi.org/10.1051/e3sconf/20187301021

[19] Pinto F, Costa P, Gulyurtlu I, Cabrita I. Pyrolysis of plastic wastes 2. Effect of catalyst on product yield. *J Anal Appl Pyrolysis.* 1999; 51: 57-71.

[20] Uthpalani PGI, Premachandra JK, De Silva DSM, Weerasinghe VPA. Pyrolysis as a value added method for plastic waste management: A review on converting LDPE and HDPE waste into fuel [Internet]. In Review; 2022 Jul [cited 2022 Oct 4]. Available from: https://www.researchsquare.com/article/rs-1693804/v1

[21] Kalargaris I, Tian G, Gu S. Combustion, performance and emission analysis of a DI diesel engine using plastic pyrolysis oil. *Fuel Process Technol.* 2017; 157: 108-15. https://dx.doi.org/10.1016/j.fuproc.2016.11.016

[22] Kalargaris I, Tian G, Gu S. The utilisation of oils produced from plastic waste at different pyrolysis temperatures in a DI diesel engine. *Energy*. 2017; 131: 179-85. https://dx.doi.org/10.1016/j.energy.2017.05.024

[23] Kalargaris I, Tian G, Gu S. Investigation on the long-term effects of plastic pyrolysis oil usage in a diesel engine. *Energy Procedia.* 2017; 142: 49-54. https://dx.doi.org/10.1016/j.egypro.2017.12.009

[24] Kalargaris I, Tian G, Gu S. Experimental characterisation of a diesel engine running on polypropylene oils produced at different pyrolysis temperatures. *Fuel.* 2018; 211: 797-803. https://dx.doi.org/10.1016/j.fuel.2017.09.101

[25] Kremer I, Tomić T, Katančić Z, Erceg M, Papuga S, Vuković JP, Schneider DR. Catalytic pyrolysis of mechanically non-recyclable waste plastics mixture: Kinetics and pyrolysis in laboratory-scale reactor. *J Environ Manage.* 2021; 296: 113145. https://dx.doi.org/10.1016/j.jenvman.2021.113145

[26] Kremer I, Tomić T, Katančić Z, Hrnjak-Murgić Z, Erceg M, Schneider DR. Catalytic decomposition and kinetic study of mixed plastic waste. *Clean Technol Environ Policy*. 2021; 23(3): 811-27. https://dx.doi.org/10.1007/s10098-020-01930-y

[27] Kremer I, Tomić T, Katančić Z, Hrnjak-Murgić Z, Erceg M, Vecchio Ciprioti S, Schneider DR. Effect of Zeolite Catalyst on the Pyrolysis Kinetics of Multi-Layered Plastic Food Packaging. *Symmetry.* 2022; 14(7): 1362. https://dx.doi.org/10.3390/sym14071362

[28] Papuga S, Gvero P, Vukic L. Temperature and time influence on the waste plastics pyrolysis in the fixed bed reactor. *Therm Sci.* 2016; 20(2): 731-41. https://dx.doi.org/10.2298/TSCI141113154P

[29] Dewangga PB, Rochmadi, Purnomo CW. Pyrolysis of polystyrene plastic waste using bentonite catalyst.In: *IOP Conf Ser Earth Environ Sci*. Bogor, Indonesia, 2019; 399(1): 012110. https://dx.doi.org/10.1088/1755-1315/399/1/012110

[30] Papuga S, Djurdjevic M, Ciccioli A, Vecchio Ciprioti S. Catalytic Pyrolysis of Plastic Waste and Molecular Symmetry Effects: A Review. *Symmetry.* 2022; 15(1): 38. https://dx.doi.org/10.3390/sym15010038

[31] Fadillah G, Fatimah I, Sahroni I, Musawwa MM, Mahlia TMI, Muraza O. Recent Progress in Low-Cost Catalysts for Pyrolysis of Plastic Waste to Fuels. *Catalysts*. 2021; 11(7): 837. https://dx.doi.org/10.3390/catal11070837

[32] Garcia-Nunez JA, Pelaez-Samaniego MR, Garcia-Perez ME, Fonts I, Abrego J, Westerhof RJM, et al. Historical Developments of Pyrolysis Reactors: A Review. *Energy Fuels.* 2017; 31(6): 5751-75. https://dx.doi.org/10.1021/acs.energyfuels.7b00641

[33] Gholizadeh M, Li C, Zhang S, Wang Y, Niu S, Li Y, et al. Progress of the development of reactors for pyrolysis of municipal waste. *Sustain Energy Fuels*. 2020; 4(12): 5885-915. https://dx.doi.org/10.1039/D0SE01122C

[34] Kabir G, Mohd Din AT, Hameed BH. Pyrolysis of oil palm mesocarp fiber and palm frond in a slow-heating fixed-bed reactor: A comparative study. *Bioresour Technol*. 2017; 241: 563-72. https://dx.doi.org/10.1016/j.biortech.2017.05.180

[35] Wang Z, Cao J, Wang J. Pyrolytic characteristics of pine wood in a slowly heating and gas sweeping fixed-bed reactor. *J Anal Appl Pyrolysis*. 2009; 84(2): 179-84. https://dx.doi.org/10.1016/j.jaap.2009.02.001

[36] Kremer I, Tomić T, Katančić Z, Erceg M, Papuga S, Parlov Vuković J, Schneider DR. Catalytic pyrolysis and kinetic study of real-world waste plastics: multi-layered and mixed resin types of plastics. *Clean Technol Environ Policy*. 2022; 24(2): 677-93. https://dx.doi.org/10.1007/s10098-021-02196-8

[37] Selpiana, Aprianti T, Rayosa I, Fuspitasarie D. Expanded polystyrene and multilayer plastic waste conversion into liquid fuel by the pyrolysis process. In Surakarta, Indonesia; 2018 [cited 2022 Oct 7]. p. 020151. Available from: http://aip.scitation.org/doi/abs/10.1063/1.5054555

[38] Bridgwater AV, Meier D, Radlein D. An overview of fast pyrolysis of biomass. *Org Geochem.* 1999; 30(12): 1479-93. https://dx.doi.org/10.1016/S0146-6380(99)00120-5

[39] Lee CG, Cho YJ, Song PS, Kang Y, Kim JS, Choi MJ. Effects of temperature distribution on the catalytic pyrolysis of polystyrene waste in a swirling fluidized-bed reactor. *Catal Today.* 2003; 79-80: 453-64. https://dx.doi.org/10.1016/S0920-5861(03)00060-9

[40] Pandey U, Stormyr JA, Hassani A, Jaiswal R, Haugen HH, Moldestad BME. Pyrolysis of plastic waste to environmentally friendly products. In 2020 [cited 2022 Aug 15]. p. 61-74. Available from: http://library.witpress.com/viewpaper.asp?pcode=EPM20-007-1

[41] Hartulistiyoso E, Sigiro FAPAG, Yulianto M. Temperature Distribution of the Plastics Pyrolysis Process to Produce Fuel at 450oC. *Procedia Environ Sci.* 2015; 28: 234-41. https://dx.doi.org/10.1016/j.proenv.2015.07.030

[42] Bockhorn H, Hornung A, Hornung U, Jakobströer P. Modelling of isothermal and dynamic pyrolysis of plastics considering non-homogeneous temperature distribution and detailed degradation mechanism. *J Anal Appl Pyrolysis.* 1999; 49(1-2): 53-74. https://dx.doi.org/10.1016/S0165-2370(98)00130-2

[43] Chen D, Zheng Y, Zhu X. In-depth investigation on the pyrolysis kinetics of raw biomass. Part I: Kinetic analysis for the drying and devolatilization stages. *Bioresour Technol.* 2013; 131: 40-6. https://dx.doi.org/10.1016/j.biortech.2012.12.136

[44] Swamardika IBA, Winaya INS, Hartati RS. Utilization plastic waste using pyrolysis fixed bed. In: *IOP Conf. Ser. Mater Sci Eng.* Bali, Indonesia, 2019; 9. https://dx.doi.org/10.1088/1757-899X/539/1/012021

[45] Xingzhong Y. Converting Waste Plastics into Liquid Fuel by Pyrolysis: Developments in China. In: Scheirs J, Kaminsky W, editors. Feedstock Recycling and Pyrolysis of Waste Plastics [Internet]. Chichester, UK: John Wiley & Sons, Ltd; 2006 [cited 2022 Aug 15]. p. 729-55. Available from: https://onlinelibrary.wiley.com/doi/10.1002/0470021543.ch28

[46] Gao F. Pyrolysis of Waste Plastics into Fuels. Dissertation, 2010; Available from: https://ir.canterbury.ac.nz/handle/10092/4303. https://dx.doi.org/10.26021/3251

[47] Abdullah NA, Novianti A, Hakim II, Putra N, Koestoer RA. Influence of temperature on conversion of plastics waste (polystyrene) to liquid oil using pyrolysis process. *IOP Conf Ser Earth Environ Sci.* 2018; 105: 012033. https://dx.doi.org/10.1088/1755-1315/105/1/012033

[48] Job S, Mativenga P, Shuaib NA, Oliveux G, Leeke G, Pickering S. Composites Recycling - Where are we now? *Composites UK*. 2016. https://compositesuk.co.uk/system/files/documents/Recycling%20Report%202016%20-%20Light%20Background.pdf

[49] van Oudheusden AA. Recycling of composite materials. :68. Student thesis. http://resolver.tudelft.nl/uuid:0749ed5c-7aeb-4275-abee-0f904a08ea4d

Analiza termičkog ponašanja reaktora sa nepokretnim slojem u procesu pirolize

Milica Đurđević[1], Saša Papuga[2] i Aleksandra Kolundžija[2]

[1]Mašinski fakultet Banja Luka, Univerzitet u Banjoj Luci, Bosna i Hercegovina
[2]Tehnološki fakultet Banja Luka, Univerzitet u Banjoj Luci, Bosna i Hercegovina

(Naučni rad)

Izvod

Piroliza je termo-hemijski proces u kojem dolazi do razgradnje organskih jedinjenja. Proces se odvija u inertnoj sredini, a može se primeniti na industrijskom, polu-industrijskom i laboratorijskom nivou. Tokom procesa pirolize, kontroliše se temperatura, međutim, studije i radovi koji se bave pirolizom ne naglašavaju gdje se temperatura mjeri i da li je temperaturno polje ujednačeno. U ovom radu se istražuje termičko ponašanje laboratorijskog reaktora sa nepokretnim slojem, kao i potrošnja energije tokom procesa pirolize. Korišćene su tri varijante polaznih sirovina: mješavina plastičnog otpada (uzorak 1), biomasa (uzorak 2) i mješavina plastike i biomase (uzorak 3). Analiza termičkog ponašanja reaktora ukazuje da se uz pažljivu regulaciju ili kontrolu temperature procesa mogu dobiti zavisnosti koje se mogu koristiti u svrhu registracije termički intenzivnih procesa, slično složenijim analizama odnosno termogravimetrijom (TG) ili derivativnom termogravimetrijom (DTG). Pokazalo se da je moguće promijeniti brzinu zagrijavanja i ukupnu energetsku efikasnost procesa jednostavnim odabirom odgovarajuće sirovinske mješavine.

Ključne reči: plastični otpad; reciklaža; termalna reakcija; brzina zagrijavanja; potrošnja energije

Thermal conductivity and microstructure of Bi-Sb alloys

Dragan M. Manasijević, Mirjana S. Milošević, Ljubiša T. Balanović, Uroš S. Stamenković, Miljan S. Marković and Ivana I. Marković

University of Belgrade, Technical Faculty in Bor, Bor, Serbia

Abstract

Four Bi-Sb alloys with compositions $Bi_{79.6}Sb_{20.4}$, $Bi_{56.9}Sb_{43.1}$, $Bi_{39.8}Sb_{60.2}$, $Bi_{18.6}Sb_{81.4}$ have been investigated regarding the microstructures and thermal properties. The microstructure was examined by scanning electron microscopy with energy-dispersive X-ray spectrometry. The light flash method was applied to determine thermal diffusivity and to obtain thermal conductivity in the temperature range 25 to 150 °C, while the indirect Archimedean method was used for determination of densities of the investigated Bi-Sb alloys. The obtained results have shown that the density of the studied alloys decreased monotonically with increasing the antimony content. On the other hand, the specific heat capacity of Bi-Sb alloys increased with the increase in the antimony content as well as with increasing the temperature. Thermal diffusivity of the alloys increased slightly with increasing the temperature. Thermal conductivities of the examined Bi-Sb alloys were determined to be in the range of 3.8 to 7 W m^{-1} K^{-1}, which is lower than thermal conductivities of pure bismuth and antimony. The results obtained in this work represent a contribution to better knowledge of the thermal properties of Bi-Sb alloys, which are of key importance for determining the possibility of their practical application.

Keywords: Bi–Sb system; thermal properties; SEM-EDS; light flash method.

Available on-line at the Journal web address: http://www.ache.org.rs/HI/

ORIGINAL SCIENTIFIC PAPER

UDC: 546.86/.87-034.7: 669.017.16

Hem. Ind. **78(1)** 41-50 (2024)

1. INTRODUCTION

The metal bismuth (Bi) and metalloid antimony (Sb) belong to the group 5A of the periodic table of elements, with the A7 rhombohedral structure. Bismuth is the least toxic heavy metal, but it has poor mechanical and thermal properties and because of that, it is rarely used as a structural material [1,2]. Bismuth alloys are being considered for use as Pb-free high-temperature [3] and low-temperature [4-6] solders due to their suitable melting interval. Antimony found its application as an alloying element in lead alloys (for solder, bearings, cable sheathing, battery grids, and ammunition) and in tin alloys. Antimony is also used as a component of III-V semiconductors such as InSb, AlSb, and GaSb [7].

The Bi-Sb phase diagram is characterized by the existence of a continuous solid solution phase (Bi, Sb) [8]. By adding antimony to bismuth, it is possible to control the structure of the energy bands and the transport properties of the obtained alloys [9,10]. Depending on the antimony content, these alloys can exhibit semimetal behavior (molar ratio of antimony $x_{Sb} < 0.07$), or semiconductor behavior ($0.07 < x_{Sb} < 0.22$), which is interesting from the scientific point of view. For higher antimony contents, the solid solution adopts a semimetal behavior again [11,12]. Because of this, Bi-Sb alloys with less than 20 at.% Sb have the potential for efficient thermoelectric conversion and are of interest from the practical point of view.

Many studies have been performed to investigate the possibility of using Bi-Sb alloys in thermoelectric and thermomagnetic cooling devices [13,14]. These alloys remain the best choice for n type leg of thermocouples used in thermoelectric cooling devices operating at temperatures below 200 K [11].

Thermal and electrical properties of polycrystalline $Bi_{1-x}Sb_x$ (x = 0.10, 0.12 and 0.15) semiconductor alloys were investigated in literature [11]. Electrical resistance, thermoelectric power and thermal conductivity were measured in the temperature range 300 to 500 K. It was found that the thermal conductivity of Bi–Sb alloys is lower than the thermal

Corresponding authors: Miljan S. Marković, University of Belgrade, Technical Faculty in Bor, Vojske Jugoslavije 12, 19210 Bor, Serbia
E-mail: mmarkovic@tfbor.bg.ac.rs
Paper received: 29 August 2023; Paper accepted: 4 January 2024; Paper published: 25 January 2024.
https://doi.org/10.2298/HEMIND230829002M

conductivity of pure bismuth, due to electron scattering because of point defects created by the addition of Sb (when Bi is doped with Sb, it undergoes a semi-metal-semiconductor transition). In this process, additional electron scattering centers and a higher concentration of pores are formed.

$Bi_{1-x}Sb_x$ (x = 0.08 to 0.17) alloys obtained by melting pure elements and subsequent quenching and annealing were investigated regarding semiconductor and thermoelectric properties by measuring the Hall coefficient, electrical resistance and Seebeck coefficient in the temperature range from 20 to 300 K for hardened and annealed samples [10]. Literature values of thermal conductivity for several Bi-Sb alloys of different compositions are given in a compilation of values of thermophysical quantities of pure elements and alloys [15].

In the present study, as a contribution toward a more complete understanding of thermal transport properties of Bi-Sb alloys, four of these alloys with compositions $Bi_{79.6}Sb_{20.4}$, $Bi_{56.9}Sb_{43.1}$, $Bi_{39.8}Sb_{60.2}$, $Bi_{18.6}Sb_{81.4}$ were experimentally examined. Thermal diffusivity and thermal conductivity were obtained in wide composition and temperature ranges using the light flash technique. In addition, microstructure was analyzed by scanning electron microscopy with energy-dispersive X-ray spectrometry (SEM-EDS).

2. EXPERIMENTAL

The alloys were prepared by melting pure Bi (99.99 %, Alfa Aesar, Germany) and Sb (99.999 %, Alfa Aesar, Germany) in evacuated quartz tubes. The samples were re-melted several times to improve homogeneity. The prepared alloys were annealed at 240 °C for one week and after that slowly cooled within the furnace.

A scanning electron microscope (VEGA 3LMU, Tescan, Czech Republic) with the energy-dispersive X-ray spectrometer (X-act, Oxford Instruments, UK) was used to analyze the microstructure and chemical composition of the samples. SEM-EDS analysis was performed with an accelerating voltage of 20 kV. An EDS area and point analysis was used to determine the overall composition of the alloys as well as the compositions of coexisting phases within each alloy. The samples were prepared using a traditional metallographic procedure that included wet grinding, polishing with alumina slurry (granulation 0.3 μm), etching with a diluted solution of ferric chloride in water, and after that cleaning in an ultrasonic bath. Backscattered electron mode (BSE) SEM microstructure images were captured on the surfaces of the prepared samples.

The light flash method was applied by using a TA Instruments compact benchtop apparatus (Discovery Xenon Flash DXF-500, TA Instruments, USA) to measure thermal diffusivity and specific heat capacity in the range 25 to 150 °C. More information on the fundamental theoretical concepts and practical procedures underlying the used flash method can be found in literature [16-19]. The Bi-Sb alloy samples were pressed into round disks (12.7 mm in diameter and 2 mm thick, with two ground plane parallel end-faces). The prepared disc-shaped samples were then placed in the vacuum furnace of the DXF-500 instrument and heated to the desired temperatures (25, 50, 100 and 150 °C) at a constant heating rate (10 °C min^{-1}). The reported results are the average values obtained from three repeated measurements.

Specific heat capacity values were calculated by using the CALPHAD method [20], and densities of the investigated alloys at room temperature were determined by using the indirect Archimedean method [21] with distilled water (ρ = 0.99679 kg m^{-3}) and an electronic instrument (Mettler Toledo, Switzerland).

Thermal conductivity of the alloys was subsequently calculated using the experimentally determined and calculated values of thermal diffusivity, density, and specific heat capacity, following the equation [16]:

$$\lambda = \alpha\rho C_p \quad (1)$$

where λ represents thermal conductivity, α is the measured thermal diffusivity, ρ is the density, and C_p is the calculated specific heat capacity of the studied alloys.

3. RESULTS AND DISCUSSION

3. 1. Microstructure observation

SEM micrographs, illustrating microstructures of the investigated alloys $Bi_{79.6}Sb_{20.4}$, $Bi_{56.9}Sb_{43.1}$, $Bi_{39.8}Sb_{60.2}$, $Bi_{18.6}Sb_{81.4}$ under different magnifications, are given in Figures 1-4.

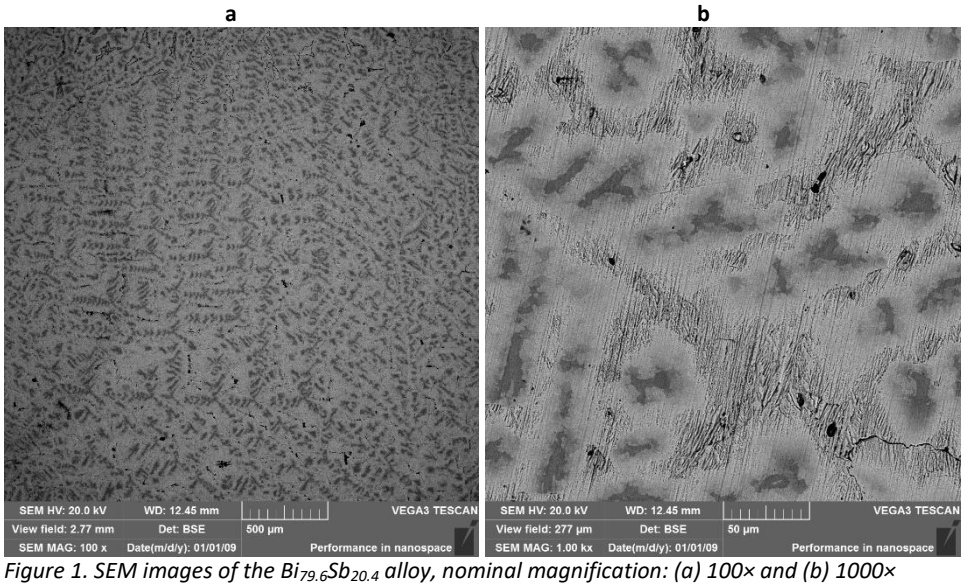

Figure 1. SEM images of the $Bi_{79.6}Sb_{20.4}$ alloy, nominal magnification: (a) 100× and (b) 1000×

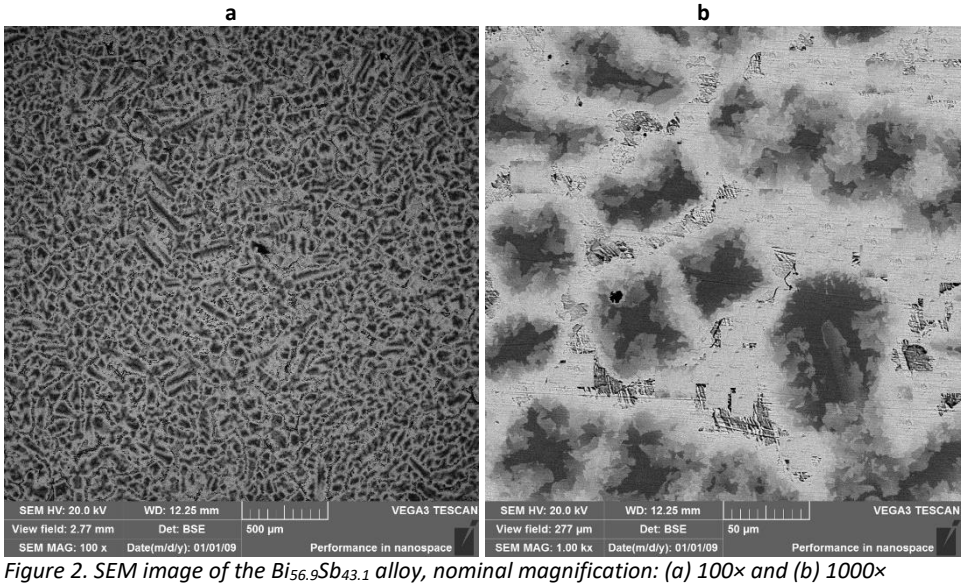

Figure 2. SEM image of the $Bi_{56.9}Sb_{43.1}$ alloy, nominal magnification: (a) 100× and (b) 1000×

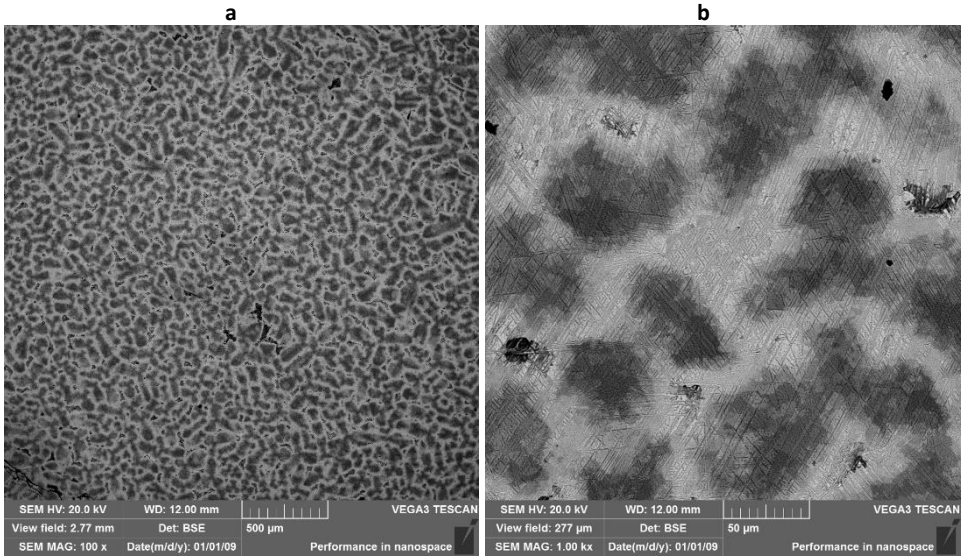

Figure 3. SEM image of the $Bi_{39.8}Sb_{60.2}$ alloy, nominal magnification: (a) 100× and (b) 1000×

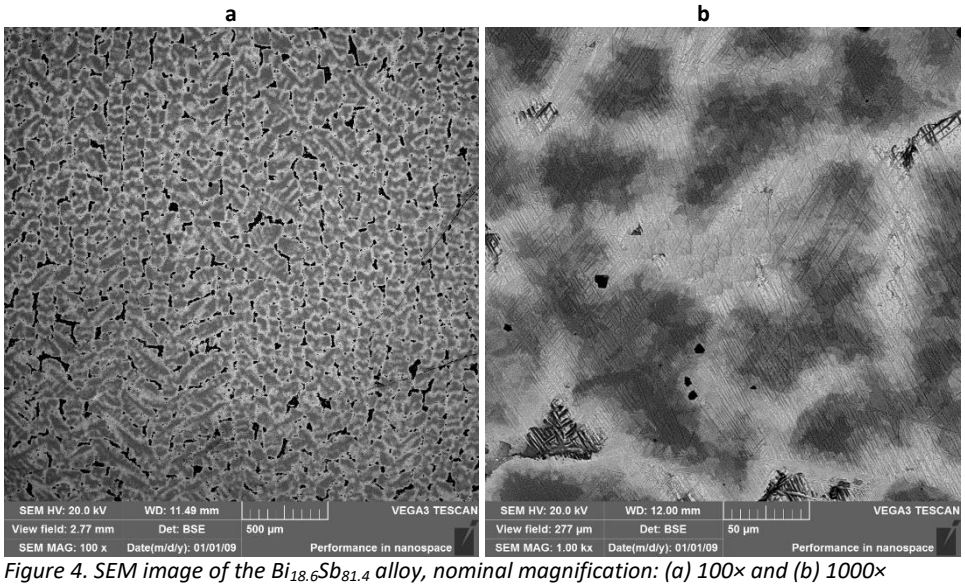

Figure 4. SEM image of the $Bi_{18.6}Sb_{81.4}$ alloy, nominal magnification: (a) 100× and (b) 1000×

Alloys have a highly homogeneous macrostructure that can be seen throughout the samples (Figs. 1-4). However, the microstructure of all four investigated alloys shows inhomogeneity due to coring on solidification. Coring is generally observed in alloys with a noticeable difference between liquidus and solidus temperatures. The liquidus and solidus lines are separated from each other in the Bi–Sb phase diagram resulting in segregation (chemical inhomogeneity) in the melt-grown crystals [10]. The center of each grain, which is the first part to freeze, is rich in the high-melting element (*e.g.* Sb for this Bi–Sb system), whereas the concentration of the low-melting element increases from the central part of the grain to the grain boundary. This is known as a cored structure. Segregation is characterized by an unequal distribution of elements and formation of concentration gradients within the grains.

In order to remove chemical inhomogeneity as the result of segregation, it is necessary to carry out a long-term homogenization annealing. Obviously, annealing at 240 °C, which is temperature just below solidus temperature in the case of the Bi-Sb alloys studied, in the duration of 1 week was not sufficient to fully eliminate segregation.

By the EDS analysis of surfaces of the samples, the overall composition of the investigated Bi-Sb alloys was determined. The obtained values show that there are minor deviations from the planned compositions (20, 40, 60, and 80 % Sb) of the alloys that occurred during the preparation of the samples. The EDS analyses of the grains confirmed the occurrence of crystal segregation. The inner areas of the grains that have a darker shade in the SEM images are areas richer in antimony, while the outer, lighter parts of the grains are richer in bismuth, as given in Table 1.

Elemental SEM-EDS mapping was applied to study the elemental distribution within the studied Bi-Sb alloys. The example of the EDS elemental map for the $Bi_{56.9}Sb_{43.1}$ alloy is given in Figure 5.

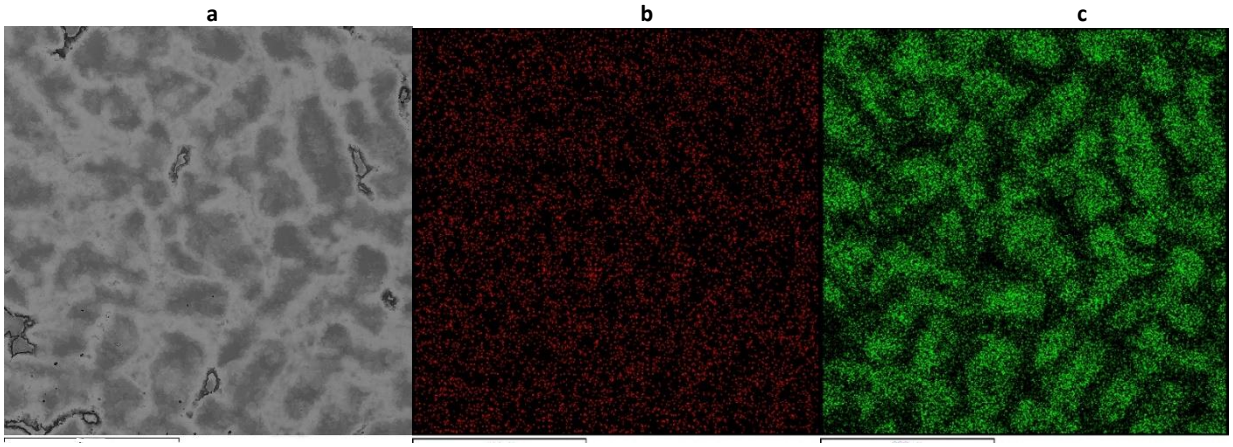

Figure 5. Elemental SEM-EDS mapping for the $Bi_{56.9}Sb_{43.1}$ alloy: (a) microstructure, (b) Bi distribution, (c) Sb distribution (scale bar = 300 µm)

It can be seen that the green contrast for Sb distribution (Fig. 5c) shows high intensity within the regions that correspond to the darker regions on the image of alloy microstructure (Fig. 5a). This analysis confirms that Sb is mainly concentrated in the central parts of the grains exhibiting dark shade on SEM image. On the other hand, Bi is mainly concentrated in the brighter areas shown in the SEM image.

Table 1. The results of the SEM-EDS analysis of the investigated alloys

Overall Sb content, at.%	Microstructure	Identified phase	Region on SEM image	Content, at.%	
				Bi	Sb
20.4	Cored grains of (Bi,Sb) solid solution	(Bi,Sb) solution	dark	49.1	50.9
			gray	60.3	39.7
			bright	84.2	15.8
43.1	Cored grains of (Bi,Sb) solid solution	(Bi,Sb) solution	dark	20.2	79.8
			gray	40.4	59.6
			bright	72.5	27.5
60.2	Cored grains of (Bi,Sb) solid solution	(Bi,Sb) solution	dark	16.2	83.8
			gray	28.7	71.3
			bright	67.2	32.8
81.4	Cored grains of (Bi,Sb) solid solution	(Bi,Sb) solution	dark	5.9	94.1
			gray	26.1	73.9
			bright	40.8	59.2

3. 2. Thermal conductivity of Bi-Sb alloys

Literature values of thermophysical properties of pure Bi and Sb are presented in Table 2.

Table 2. Thermophysical properties of pure Bi and Sb [7]

Metal	Melting point, °C	Latent heat of fusion, J g^{-1}	Density, g cm^{-3} *	Specific heat capacity*, J g^{-1} K^{-1}	Thermal conductivity, W m^{-1} K^{-1}*
Bi	271.4	53.976	9.808	0.122	8.2
Sb	630.7	163.17	6.697	0.207	24.3

*at 25 °C

Bismuth has one of the lowest thermal conductivity among all metals (8.2 W m^{-1} K^{-1} at 25 °C). Antimony has significantly higher values of melting temperature, latent heat of fusion, specific heat capacity and thermal conductivity compared to bismuth, while bismuth has a higher density than antimony.

Table 3 shows the values of specific heat capacity, thermal diffusivity and thermal conductivity for the examined Bi-Sb alloys in the temperature range 25 to 150 °C. Thermal diffusivities were measured by the flash method, while thermal conductivities were calculated using the density and specific heat capacity data of the investigated materials (Eq. 1).

Firstly, alloy densities at room temperature were measured using the buoyancy method based on Archimedes' principle with an estimated uncertainty of ± 1 % [21]. It was assumed that the densities of the alloys are approximately constant in the narrow temperature range studied. Figure 6 shows density values for the investigated Bi-Sb alloys, as well as density values for pure bismuth and antimony at room temperature.

It can be seen that the densities of Bi-Sb alloys lie between the values of densities for pure bismuth and antimony and that the density of the alloys decreases monotonically with increasing the antimony content.

The CALPHAD method [20] and the thermodynamic COST 531 lead-free solder database [22] were used to calculate the specific heat capacities of the alloys under consideration. The calculated specific heat capacity values were checked for accuracy by comparison with the corresponding measured values obtained at room temperature using the light flash technique (pure bismuth and antimony were used as reference materials).

Table 3. Specific heat capacity, thermal diffusivity, and thermal conductivity of the investigated Bi–Sb alloys in the temperature range 25-150 °C

Sb content, at.%	Temperature, °C	Calculated specific heat capacity, J g^{-1} K^{-1}	Thermal diffusivity, mm^2 s^{-1}	Thermal conductivity, W m^{-1} K^{-1}
20.4	25	0.133	3.46±0.10	4.2±0.3
	50	0.134	3.64±0.11	4.4±0.3
	100	0.137	3.85±0.12	4.7±0.3
	150	0.140	3.99±0.12	5.0±0.3
43.1	25	0.148	4.76±0.14	5.9±0.4
	50	0.149	5.00±0.15	6.3±0.4
	100	0.152	5.27±0.16	6.7±0.4
	150	0.155	5.40±0.16	7.0±0.4
60.2	25	0.162	4.01±0.12	5.1±0.3
	50	0.163	4.07±0.12	5.2±0.3
	100	0.166	4.17±0.13	5.4±0.3
	150	0.169	4.24±0.13	5.6±0.3
81.4	25	0.183	2.90±0.09	3.8±0.2
	50	0.185	2.96±0.09	3.9±0.2
	100	0.187	3.05±0.09	4.1±0.2
	150	0.190	3.12±0.09	4.2±0.3

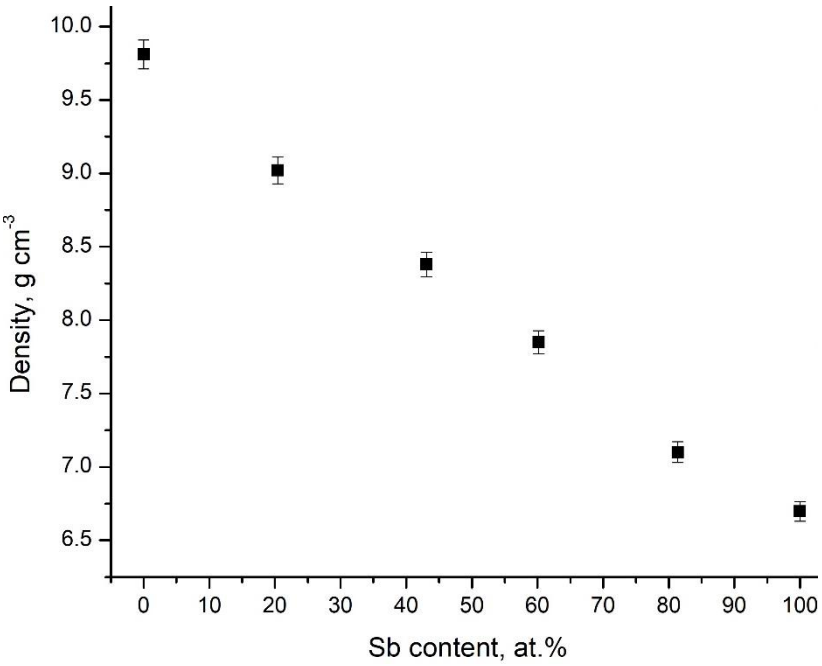

Figure 6. Densities of Bi-Sb alloys depending on composition at 25 °C (data are average of n=3)

Based on the results shown in Table 3, results it can be concluded that the specific heat capacity increases with the increase in antimony content in the alloys. Also, with the increase in temperature, there is an increase in the specific heat capacity of all tested alloys.

Figure 7 shows a comparison of calculated and experimentally determined specific heat capacities of Bi-Sb alloys at 25 °C.

Based on the presented results it can be noted that the specific heat capacity of Bi-Sb alloys increases with increasing the Sb content and temperature. The calculated values of specific heat capacity for $Bi_{79.6}Sb_{20.4}$ and $Bi_{18.6}Sb_{81.4}$ alloys are in very good agreement with the values obtained by the flash method. In the case of $Bi_{56.9}Sb_{43.1}$ and $Bi_{39.8}Sb_{60.2}$ alloys, slightly larger deviations are visible between the calculated values and those obtained by the flash method. Determination of specific heat capacity using the flash method requires the use of a reference material of known specific heat capacity.

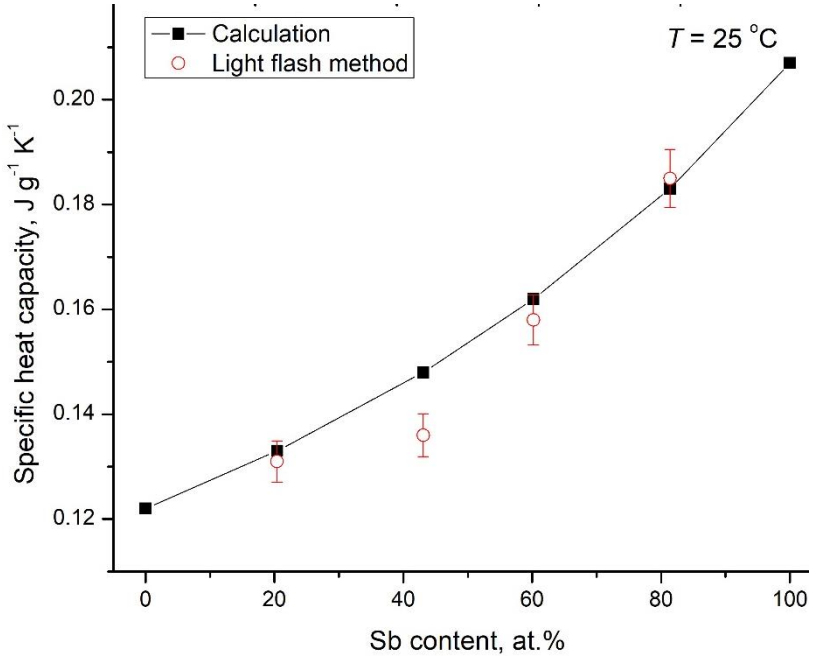

Figure 7. Comparison of calculated and experimentally determined specific heat capacities of Bi-Sb alloys at 25 °C (data are average of n=3)

In the present study, pure bismuth was used as a reference material for measuring the specific heat capacity of $Bi_{79.6}Sb_{20.4}$ and $Bi_{56.9}Sb_{43.1}$ alloys with high bismuth contents. To determine the specific heat capacity of antimony-based alloys $Bi_{39.8}Sb_{60.2}$ and $Bi_{18.6}Sb_{81.4}$, pure antimony was used as a reference material. The reason for the better agreement between the calculated and experimental values of the specific heat capacity for the $Bi_{79.6}Sb_{20.4}$ and $Bi_{18.6}Sb_{81.4}$ alloys can be explained by their greater similarity in terms of specific heat capacity with the reference materials that were used. This leads to the conclusion that coupling of a reference and sample with similar thermal properties might increase the accuracy of the specific heat capacity measurement.

Figure 8 shows the dependence of the experimentally determined thermal diffusivities of the examined Bi – Sb alloys on temperature.

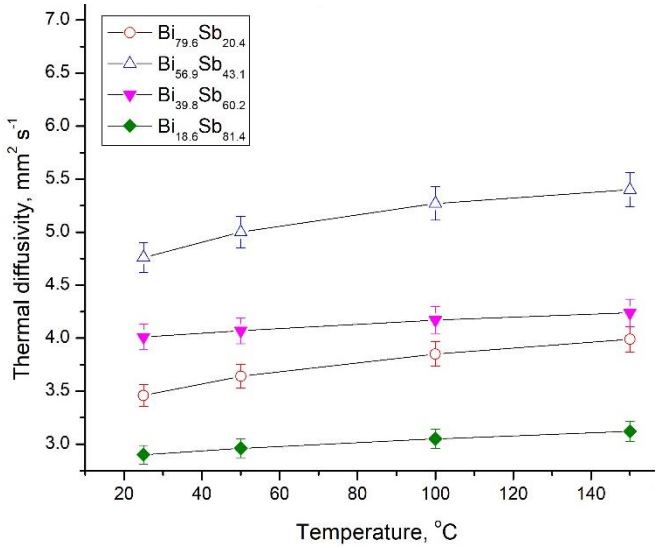

Figure 8. Temperature dependences of the experimentally determined thermal diffusivities of the examined Bi-Sb alloys (data are average of n=3)

It can be observed that with the increase in temperature there is a slight increase in thermal diffusivity.

Based on the results in Table 3, it can be concluded that the thermal conductivity values of the tested Bi-Sb alloys are low and are approximately in the range of 3.8 to 7 W m^{-1} K^{-1}, which is lower than the thermal conductivity of pure bismuth. With an increase in temperature, there is a slight increase in thermal conductivity.

Figure 9 shows a comparison of the obtained thermal conductivity values for the tested Bi-Sb alloys at 25 °C with literature values [11,15].

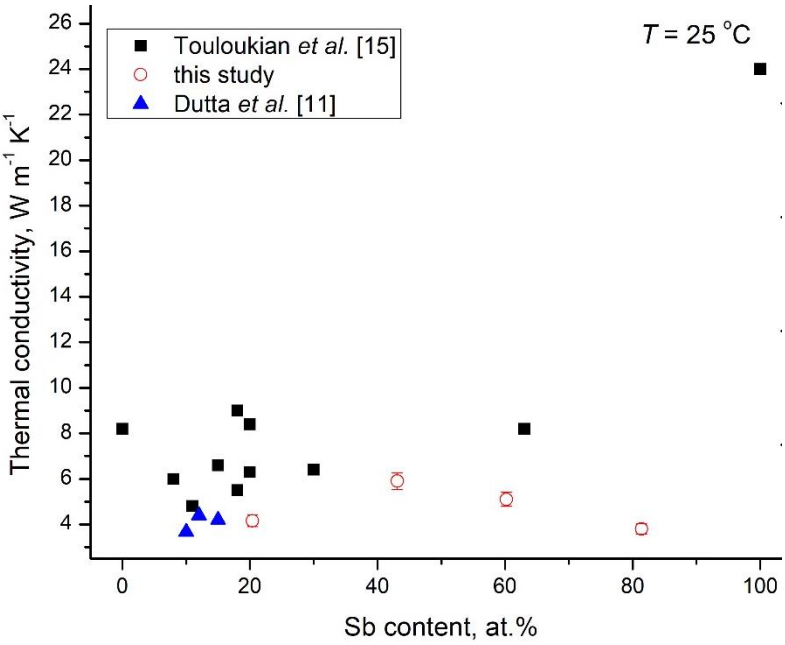

Figure 9. The obtained values of thermal conductivity for the tested Bi-Sb alloys at 25 °C in this study compared to literature values

Based on the literature values, it can be noticed that both studies [11] and [15] generally reported values that did not exceed 10 W m^{-1} K^{-1}, while the investigated alloys generally had higher amounts of Bi. The thermal conductivity values obtained in this work are in relatively good agreement with these literature values. It can be concluded that Bi-Sb alloys have very low thermal conductivities, which are lower than that of pure antimony and significantly lower than the thermal conductivity of pure bismuth.

4. CONCLUSION

Based on the performed experiments and the analysis of the obtained results, the following can be concluded:

a. The microstructure of all examined alloys is similar and consists of large grains of (Bi, Sb) solid solution, indicating that Bi and Sb form a continuous series of solid solutions. The microstructure is inhomogeneous. The reason for this is crystal segregation that appeared during crystal growth during cooling. Annealing at 240 °C for 1 week was not sufficient to remove crystal segregations.
b. Densities of Bi-Sb alloys lie between the values of the densities for pure bismuth and antimony, decreasing monotonically with increasing the antimony content.
c. Thermal diffusivity of Bi-Sb alloys increases slightly with increasing temperature.
d. The specific heat capacity of Bi-Sb alloys increases with increasing the Sb content and with increasing temperature. The values obtained at 25 °C were compared with the values obtained by the flash method and a good agreement was found.
e. With an increase in temperature, there is a slight increase in thermal conductivity. The thermal conductivities of the examined Bi-Sb alloys are low and are in the range of 3.8 to 7 W m^{-1} K^{-1}, which is lower than the thermal conductivity of pure bismuth. Alloys with intermediate antimony content had slightly higher values of thermal diffusivity and thermal conductivity than alloys with low and high antimony contents.

The results presented in this paper are essential for a better understanding of the thermal behavior of the investigated Bi-Sb alloys under different temperature conditions.

Acknowledgements: *The research presented in this paper was performed with the financial support of the Ministry of Science, Technological Development and Innovations of the Republic of Serbia, with the funding of the scientific research work at the University of Belgrade, Technical Faculty in Bor, according to the contract with registration number 451-03-47/2023-01/200131.*

REFERENCES

[1] Spinelli JE, Silva BL, Garcia A. Microstructure, phases morphologies and hardness of a Bi–Ag eutectic alloy for high temperature soldering applications. *Mater Des*. 2014; 58: 338-356. https://doi.org/10.1016/j.matdes.2014.02.026

[2] Song JM, Chuang HY, Wen TX. Thermal and tensile properties of Bi-Ag alloys. *Metall Mater Trans A*. 2007; 38: 1371-1375. https://doi.org/10.1007/s11661-007-9138-1

[3] Yu M, Matsugi K, Xu Z, Choi Y, Yu J, Motozuka S, Nishimura Y, Suetsugu KI. High temperature characterization of binary and ternary Bi alloys microalloyed with Cu and Ag. *Mater Trans*. 2018; 59: 303-310. https://doi.org/10.2320/matertrans.MAW201710

[4] Lee H, Choi K-S, Eom Y-S, Bae H-C, Lee JH. Sn58Bi Solder Interconnection for Low-Temperature Flex-on-Flex Bonding. *ETRI J*. 2016; 38: 1163-1171. https://doi.org/10.4218/etrij.16.0115.0945

[5] Goh Y, Haseeb ASMA, Sabri MFM. Effects of hydroquinone and gelatin on the electrodeposition of Sn–Bi low temperature Pb-free solder. *Electrochim Acta*. 2013; 90: 265-273. https://doi.org/10.1016/j.electacta.2012.12.036

[6] Manasijević D, Balanović Lj, Marković I, Ćosović V, Gorgievski M, Stamenković U, Božinović K. Thermal transport properties and microstructure of the solid Bi-Cu alloys. *Metall Mater Eng*. 2022; 28(3): 503-514. https://doi.org/10.30544/841

[7] ASM International Handbook Committee: Properties and selection: nonferrous alloys and special-purpose materials, 2, ASM international, Materials Park, OH, 1990. https://doi.org/10.31399/asm.hb.v02.9781627081627

[8] Okamoto H. Bi-Sb (bismuth-antimony). *JPED.* 2012; 33: 493-494. https://doi.org/10.1007/s11669-012-0092-2

[9] Rodriguez JE, Cadavid D. Synthesis and thermoelectric properties of polycrystalline Bi-Sb alloys. *Rev Fis*. 2007; 34: 19-27. https://revistas.unal.edu.co/index.php/momento/article/view/40558

[10] Kitagawa H, Noguchi H, Kiyabu T, Itoh M, Noda Y. Thermoelectric properties of Bi–Sb semiconducting alloys prepared by quenching and annealing. *J Phys Chem Solids*. 2004; 65(7): 1223-1227. https://doi.org/10.1016/j.jpcs.2004.01.010

[11] Dutta S, Shubha V, Ramesh TG, D'Sa F. Thermal and electronic properties of Bi1− xSbx alloys. *J Alloys Compd*. 2009; 467(1-2): 305-309. https://doi.org/10.1016/j.jallcom.2007.11.146

[12] Ibrahim AM, Thompson DA. Thermoelectric properties of BiSb alloys. *Mater Chem Phys*. 1985; 12(1): 29-36. https://doi.org/10.1016/0254-0584(85)90034-3

[13] Yim WM, Amith A. Bi-Sb alloys for magneto-thermoelectric and thermomagnetic cooling. *Solid State Electron*. 1972; 15: 1141-1165. https://doi.org/10.1016/0038-1101(72)90173-6

[14] Tanuma S. Thermoelectric power of bismuth-antimony alloys. *J Phys Soc Jpn*. 1961; 16: 2354-2355. https://doi.org/10.1143/JPSJ.16.2354

[15] Touloukian YS, Powell RW, Ho CY, Klemens PG. Thermal Conductivity of Metallic Elements and Alloys. Washington: New York. 1970. http://poplab.stanford.edu/pdfs/Touloukian-v1ThermalConductivityMetallicElementsAlloys-tprc70.pdf

[16] Parker WJ, Jenkins RJ, Butler CP, Abbott GL. Flash Method of Determining Thermal Diffusivity, Heat Capacity, and Thermal Conductivity *J Appl Phys*. 1961; 32: 1679-1684. https://doi.org/10.1063/1.1728417

[17] Manasijević D, Balanović Lj, Marković I, Gorgievski M, Stamenković U, Božinović K. Microstructure, melting behavior and thermal conductivity of the Sn–Zn alloys *Thermochim Acta*. 2021; 702: 178978. https://doi.org/10.1016/j.tca.2021.178978

[18] Manasijević D, Balanović Lj, Marković I, Gorgievski M, Stamenković U, Đorđević A, Minić D, Ćosović V. Structural and thermal properties of Sn–Ag alloys *Solid State Sci*. 2021; 119: 106685. https://doi.org/10.1016/j.solidstatesciences.2021.106685

[19] Božinović KN, Manasijević DM, Balanović LjT, Gorgievski MD, Stamenković US, Marković MS, Mladenović ZD. Study of microstructure, hardness and thermal properties of Sn-Bi alloys/Ispitivanje mikrostrukture, tvrdoce i termijskih karakteristika legura u sistemu Sn-Bi. *Hem Ind.* 2021; 75(4): 227-240 https://doi.org/10.2298/HEMIND210119021B

[20] Lukas HL, Fries SG, Sundman B. Computational Thermodynamics: the Calphad Method, First edition, Cambridge University Press, Cambridge, 2007. https://doi.org/10.1017/CBO9780511804137

[21] Wang L, Xian AP. Density measurement of Sn-40Pb, Sn-57Bi, and Sn-9Zn by indirect Archimedean method, *J Electron Mater*. 2005; 34: 1414-1419. https://doi.org/10.1007/s11664-005-0199-x

[22] Kroupa A, Dinsdale AT, Watson A, Vrestal J, Vizdal J, Zemanova A. The development of the COST 531 lead-free solders thermodynamic database *JOM*. 2007; 59: 20-25. https://doi.org/10.1007/s11837-007-0084-6

Toplotna provodljivost i mikrostruktura Bi-Sb legura

Dragan M. Manasijević, Mirjana S. Milošević, Ljubiša T. Balanović, Uroš S. Stamenković, Miljan S. Marković i Ivana I. Marković

Univerzitet u Belgradu, Tehnički Facutet u Boru, Bor, Srbija

(Naučni rad)

Izvod

Ispitivani su mikrostruktura i termičke osobine Bi-Sb legura sastava $Bi_{79.6}Sb_{20.4}$, $Bi_{56.9}Sb_{43.1}$, $Bi_{39.8}Sb_{60.2}$, $Bi_{18.6}Sb_{81.4}$. Za ispitivanje mikrostrukture pripremljenih legura korišćena je skenirajuća elektronska mikroskopija sa energetsko disperzivnom rendgenskom spektrometrijom. Svetlosno-impulsna metoda je primenjena za merenje toplotne difuzivnosti i za određivanje toplotne provodljivosti. Za određivanje gustine Bi-Sb legura korišćena je indirektna Arhimedova metoda. Dobijeni rezultati pokazuju da se gustina proučavanih legura monotono snižava sa povećanjem sadržaja antimona. Specifični toplotni kapacitet Bi-Sb legura raste sa povećanjem sadržaja Sb i sa povećanjem temperature. Toplotna difuzivnost ispitivanih legura određena je u temperaturnom intervalu od 25 do 150 °C. Toplotna difuzivnost Bi-Sb legura blago raste sa povećanjem temperature. Toplotne provodljivosti ispitivanih Bi-Sb legura su u rasponu od 3,8 do 7 W m^{-1} K^{-1}, što je niže od toplotnih provodljivosti čistog bizmuta i antimona. Rezultati dobijeni u ovom radu predstavljaju doprinos boljem poznavanju toplotnih osobina Bi-Sb legura, koje su od ključnog značaja za određivanje mogućnosti njihove praktične primene.

Ključne reči: Bi-Sb sistem; termičke osobine; SEM-EDS; metoda svetlosnog bljeska

Impact of leaching procedure on heavy metals removal from coal fly ash

Andrija Z. Janković[1], Mirjana R. Ćujić[2], Milica D. Stojković[1], Maja B. Đolić[1], Dragana Z. Živojinović[1], Antonije E. Onjia[1], Mirjana Đ. Ristić[1] and Aleksandra A. Perić Grujić[1]

[1]University of Belgrade, Faculty of Technology and Metallurgy, Belgrade, Serbia
[2]University of Belgrade, Vinča Institute of Nuclear Sciences - National Institute of the Republic of Serbia, Belgrade, Serbia

Abstract

In this work, removal of heavy metals (Cr, Mn, Co, Ni, Cu, Zn, As, Cd, and Pb) from fly ash has been studied using acid leaching and wet oxidation methods. In parallel, microwave-assisted acid digestion was applied for determination of pseudo-total concentrations of heavy metals to estimate the leaching efficiency. Multivariate statistics (Pearson correlation, principal component analysis, and hierarchical cluster analysis) have shown two dominant groups of elements, depending on their characteristics and affinity towards the ash solid phase. Thus, Cr, Zn, Mn, Co, and Ni belong to the group I, while Pb, As, Cd, and Cu belong to the group II. It was demonstrated that the wet oxidation method was more suitable than acid leaching since the reduction in metal concentration was 30 to 75 % compared to 12 to 25 % obtained by acid digestion. The influence of fly ash treatment on the residue characteristics was investigated by X-ray diffractometry and scanning electron microscopy. The analyses revealed surface and structure changes of fly ash after the wet oxidation treatment. Overall, wet oxidation could be an appropriate treatment for heavy metal removal from fly ash, providing a material that could be further used, thus reducing the risk of pollution caused by the disposal of coal combustion fly ash.

Keywords: Waste utilization; wet oxidation; acid leaching; material characterization.

Available on-line at the Journal web address: http://www.ache.org.rs/HI/

ORIGINAL SCIENTIFIC PAPER

UDC: 662.613.13:669.018.291-045.38

Hem. Ind. **78(1)** 51-62 (2024)

1. INTRODUCTION

Ash, bottom and fly presents one of the waste streams generated in the coal combustion process. The amount, characteristics, and potential usage of this waste depend on the coal type and properties of the combustion process. The Republic of Serbia (RS) is dominantly dependent on coal as a resource for electric energy production; the installed capacity is 4,437 MW, and about 24 billion kilowatt hours are generated annually. Nikola Tesla Thermal Power Plants Branch (TENT) is the largest electricity producer in Southeast Europe. The plant has 14 units with a total installed capacity of 3,430 MW. Annually, TENT generates more than 50 % of electricity in Serbia. In line with the waste management hierarchy, which highlights the reuse and recycling of waste, in particular, both in the EU and RS, research is still being carried out regarding the reuse of waste in the process of making construction products containing certain amounts of waste [1]. Approximately 7 million tons of fly ash and slag are produced in thermal power plants in Serbia every year, only 3 % of which is used in the cement industry [2].

Threats to human health and quality of the environment have been mostly the subject of studies/research focusing on coal fly ash (CFA) from Serbian power plants. Single-agent extraction and sequential extraction procedures were used to determine the leaching levels of different metals (Al, As, Be, Cd, Co, Cr, Cu, Fe, Mn, Ni, and Pb) [3]. In a previous study, analysis of CFA, taken from the ash dumps located in the vicinity of the power plant Kostolac using the method of sequential dissolution has been performed to determine the influence aspects of selected heavy metals (V, Cr, Mn, Co, Ni, Cu, Zn, Cd, and Pb) on working and living environments [4]. The isotopic ratios $^{206}Pb/^{207}Pb$ and $^{208}Pb/^{207}Pb$ determined in CFA from Serbian coal-fired power plants present an important contribution to a lead isotopic database fundamental for interpreting different pollution sources [5]. Determination of rare earth elements in CFA leachate from

Corresponding authors: Mirjana Đ. Ristić, University of Belgrade, Faculty of Technology and Metallurgy, Karnegijeva 4, Belgrade, Serbia
E-mail: risticm@tmf.bg.ac.rs
Paper received: 1 September 2023; Paper accepted: 19 December 2023; Paper published: 25 January 2024.
https://doi.org/10.2298/HEMIND230901001J

five Serbian coal-fired thermoelectric power has recently been investigated using dispersive solid-liquid microextraction based on a poly(1,6 hexanediol diacrylate)/graphene sorbent followed by inductively coupled plasma mass spectrometry, ICP-MS [6].

Pollutant emissions from coal and coal waste combustion plants and fly ash landfilling from electricity production were evaluated regarding the environmental risks [7]. This study compared power plants in Serbia Kolubara A, Kostolac B, and Nikola Tesla A, as well as a semi-industrial fluidized bed boiler, as combustion facilities with different combustion regimes, fuel types, and capacities.

In recent research [8], human health risk assessment of potentially harmful substances in fly ashes has been performed by estimating the carcinogenic and non-cancer risks for trace elements and the incremental life cancer risk of seven carcinogenic polycyclic aromatic hydrocarbons (PAHs) associated with different exposure routes.

Samples of coal fly ash from two coal-fired power plants in Serbia (Nikola Tesla and Kostolac) were analyzed and examined as neutralization agents of acid mine drainage [9]. Cotton, cotton/polyester yarn, and fly ash as waste materials from Serbia were used as adsorbents for the removal of certain heavy metals from water [10].

Enhanced coal fly ash leaching can be used to extract valuable element(s) from CFA and to remove toxic element(s) [11]. In the present study, the effect of two methods, acid leaching and wet oxidation, on the removal efficiency of some toxic/hazardous heavy metals from fly ash originating from two Serbian thermal power plants, Nikola Tesla A and Nikola Tesla B, has been investigated. Wet oxidation has been proposed for the first time for this purpose. With this approach, reuse of CFA could be provided, thus reducing the risk of contamination caused by CFA disposal. Bottom ash has been studied, as well, in order to determine fractionation of trace pollutants during the combustion process.

2. MATERIALS AND METHODS

In this work, bottom and fly ash were collected from coal-fired power plants (CPP) in Serbia, Nikola Tesla A and B, located near the Serbian capital, Belgrade. They use lignite as a fuel obtained from the Serbian coal mining complex, RB Kolubara. The CPP Nikola Tesla A, the Serbian largest thermal power plant, has a capacity of 1765 MW and six generation units, while CPP Nikola Tesla B has a total capacity of 1320 MW and two generation units.

Determination of the chemical composition of fly ash and bottom ash was performed by using inductively coupled plasma-optical emission spectrometry (ICP-OES). In specific, prior to the digestion, bottom and fly ash samples were oven-dried at 60 °C for 8 h and then homogenized by using a ball mill. A portion of 0.5 g of the homogenized coal fly ash sample is mixed with 3.0 g lithium tetraborate (≥99.995 %, Sigma-Aldrich, USA) as a fluxing agent, in a platinum crucible. The mixture is then placed in a laboratory furnace and subjected to a controlled temperature ramp up to 1000 °C, a then hold at 1000 °V for 2 h. The obtained homogeneous glass bead is dissolved in a 0.3 % acid solution HCl (ACS reagent grade, Sigma-Aldrich, USA). The resulting solution is analyzed by using the instrument Agilent ICP-OES model 5800 (Agilent Technologies, Santa Clara, CA, USA).

2. 1. Coal ash treatment procedures

Three procedures were used for coal ash treatment: 1) microwave-assisted digestion; 2) acid leaching; and 3) wet oxidation.

In the first method (i.e. microwave-assisted digestion) bottom and fly ash samples (0.5 g) were digested by using high-purity ACS reagent grade mineral acids (nitric, hydrofluoric, and boric) purchased from Sigma-Aldrich (USA). Two-step microwave digestion (Milestone ETHOS LEAN, Milestone Srl, Sorisole, Italy) was carried out. In the first step, 6 mL of concentrated nitric acid and 2 ml of concentrated hydrofluoric acid were added to a Teflon vessel. The digestion conditions for the microwave system were as follows: constant power of 800 W, 10 min at 552 kPa, then 15 min at 827 kPa. The Teflon vessels were then cooled to room temperature and, in the second digestion step, 20 ml of boric acid (5 % w/v) and 20 ml of high purity water (resistivity 18.2 MΩ·cm) were added. In the second step, digestion conditions for the microwave system were as follows: constant power of 800 W, 10 min at 552 kPa, then 15 min at 827 kPa. After digestion, the solution was filtered, and the clear filtrate was diluted to 50 mL with high-purity water obtained from a Milli Q water system (Merck, Darmstadt, Germany).

In the acid leaching method, 1 g of fly ash was burned at 360 °C for 1 h first followed by 650 °C for 1 h. Then 3 ml of concentrated HNO_3 and 5 ml of concentrated $HClO_4$ (ACS reagent grade, Sigma-Aldrich, USA) were added. The beakers were kept on a hot plate (56 to 58 °C). Next, 10 ml of concentrated HCl was added. The solid phase was then separated from the solution. The solution was diluted to 50 ml with high-purity water, while the solid phase was analyzed by X-ray diffractometry (XRD) and scanning electron microscopy (SEM).

For wet oxidation, approximately 0.2 g of fly ash was weighed (the weight was recorded to the nearest 0.1 mg), and approximately 0.2 g of V_2O_5 (ACS reagent grade, Sigma-Aldrich, USA), 8 ml of concentrated HNO_3, and 2 ml of concentrated H_2SO_4 (ACS reagent grade, Sigma-Aldrich, USA) were added. The vessel was placed in a heated sand bath and covered with a watch glass. The temperature was gradually increased to reach 150 °C, which was then maintained for 24 h. After heating, the vessel was cooled and then diluted to a volume of 20 ml with water. The solid phase was separated by centrifuge and further analyzed by XRD and SEM. The liquid phase was transferred into a 100 ml volumetric flask and made up to volume with high purity water.

Bottom ash and fly ash were subjected to microwave digestion to determine distribution of the examined heavy metals between these phases. Only fly ash was treated by acid digestion and wet oxidation, due to the harmful impact on human health and the environment. All experiments were performed in triplicate.

The element concentration in the leachate samples was measured by either ICP-OES, Agilent ICP-OES model 5800 with SPS 4 autosampler (Agilent Technologies, Santa Clara, CA, US) or inductively coupled plasma mass spectrometry (ICP-MS), Thermo Fisher iCAP Q ICP-MS (Thermo Fisher Scientific Inc., Waltham, MA, US). The analysis was repeated three times and the mean was reported as the concentration of heavy metal. All chemicals were of reagent grade. The applied procedure was run without a sample, and the obtained blank values were subtracted from the ICP-OES/ICP-MS measurements of the elements evaluated.

2. 2. Fly ash and residues characterization

Fly ash and leaching/oxidation residues were examined by XRD and SEM.

Diffraction measurements were performed by using a SmartLab Rigaku powder diffractometer (Rigaku Corporation, Tokyo, Japan) that works on the principle of Bragg-Brentan geometry, using an X-ray tube with a copper anticathode, that is, using CuKα radiation with a wavelength of λ = 0.1542 nm. The voltage on the X-ray tube was 40 kV, and the current was 30 mA. Measurements were made in the range of diffraction angles 2θ from 5 to 90° with an angle step of 0.02° and a measurement speed of 2°/min. X-ray phase analysis of the samples was performed on the obtained diffractograms by using the EVA v.9.0 program package [12] and with the help of the PDF-2 crystallographic database [13]. Morphology of fly ash samples before and after leaching/oxidation was observed by TESCAN MIRA 3 XMU field emission scanning electron microscope, FESEM (Tescan, Brno, Czech Republic) operated at 20 keV.
The main steps of applied coal ash treatment procedures are illustrated in Figure 1.

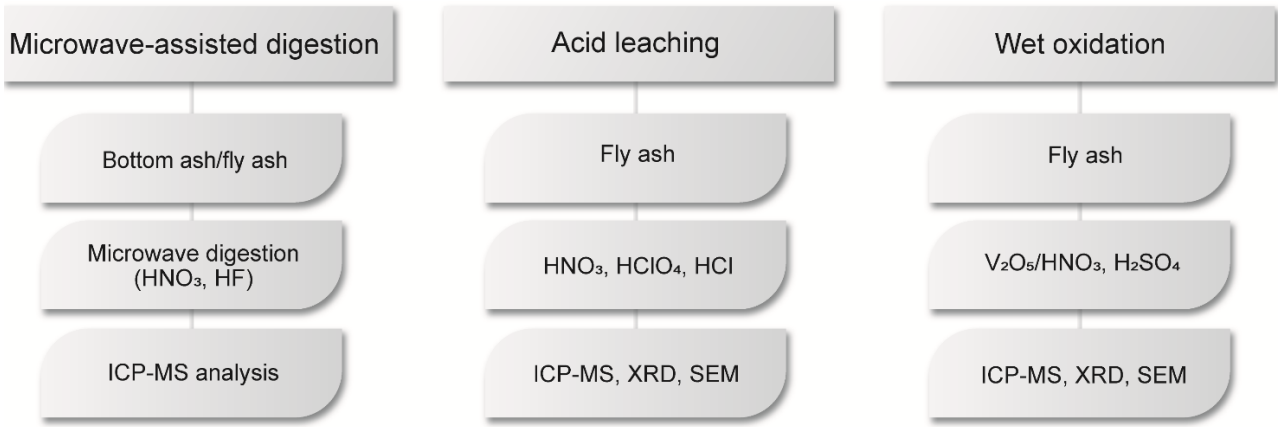

Figure 1. Main steps of applied procedures

3. RESULTS AND DISCUSSION

3. 1. Composition of bottom ash and fly ash

Chemical compositions of examined fly ash and bottom ash are presented in Table 1.

Fly ash from both CPPs is characterized by a high concentration of silica and alumina and a low concentration of calcium. It belongs to class F, according to ASTM C618 [14], since the sum of the percentages of SiO_2 + Al_2O_3 + Fe_2O_3 is 76.13 % (TENT A) and 84.63 % (TENT B), higher than a minimum of 70 %.

Table 1. Chemical composition and loss on ignition (LOI) of the investigated fly ash and bottom ash

	Content, %								
CPP / ash	SiO_2	Al_2O_3	Fe_2O_3	CaO	MgO	K_2O	Na_2O	TiO_2	LOI
TENT A / fly ash	48.1	25.6	2.36	7.1	4.6	6.2	0.7	0.8	3.0
TENT A / bottom ash	27.3	19.4	3.09	3.9	2.0	3.4	0.6	0.5	41.8
TENT B / fly ash	54.3	24.9	5.4	4.0	2.1	4.2	0.7	0.8	1.4
TENT B / bottom ash	41.1	23.2	6.22	2.1	1.4	3.7	0.6	0.7	14.6

Fly ash samples from CPPs TENT A and TENT B were shown to be very similar (Table 1) implying negligible effects of burning conditions; both CPPs use lignite from the RB Kolubara basin. Concerning chemical composition, minor differences in concentrations of Si and Al oxides and Na_2O and TiO_2 concentrations are noticed. TENT A fly ash is slightly enriched in CaO, MgO, and Na_2O and has a slightly higher LOI.

The concentrations of major oxides in fly ashes (Table 1) are similar to those determined in fly ashes sourced from European coal-burning power plants (from Spain, the Netherlands, Italy, and Greece), except for K_2O, which is at a higher concentration in fly ashes examined in this research (6.2 for TENT A and 4.2 for TENT B) compared to 0.4 to 4.0 for fly ashes examined in the research of Moreno *et al*. [15].

The influence of combustion conditions is observed in the bottom ash chemical composition, where the SiO_2 concentration and LOI are significantly different in the two CPP ash samples and indicate incomplete coal combustion in TENT A. LOI of bottom ash from TENT A is almost 3 times higher compared to TENT B / bottom ash.

3. 2. Heavy metal concentration

Contents of selected heavy metals in both fly ash and bottom ash samples originating from coal-fired power plants TENT A and TENT B is presented in Figure 2.

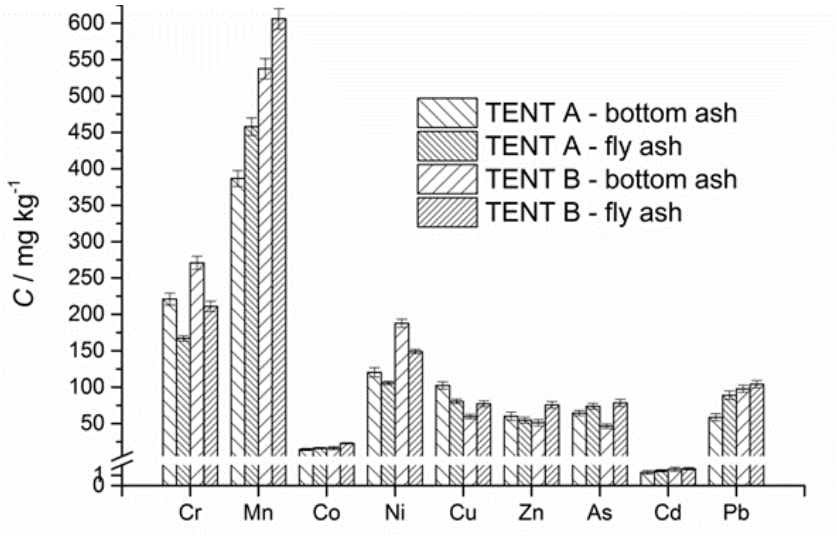

Figure 2. Concentrations of selected heavy metals (triplicate average) in fly ash after microwave-assisted digestion (the error bars represent the standard deviation of the triplicates)

The heavy metal concentration decreases in the order Mn > Cr > > Ni > Cu > As > Pb > Zn > Co > Cd (TENT A) and Mn > Cr > Ni > Cu > Pb > As > Zn > Co > Cd (TENT B), indicating similar patterns. All samples are enriched with Mn, in a concentration range of 386.9 (TENT A bottom ash) and 606 mg kg^{-1} (TENT B fly ash). Concentrations higher than 100 mg kg^{-1} were noticed for Cr and Ni in all samples, while other elements were present at lower concentrations. Elements at the lowest concentrations are Cd, ranging from 1.3 (TENT A bottom ash) to 1.6 mg kg^{-1} (TENT B fly ash) and Co, ranging from 14.6 (TENT B bottom ash) to 23 mg kg^{-1} (TENT B fly ash).

All elements are present in low to middle contents compared to the data reported for European coal combustion fly ashes [15]. The examined fly ashes have the lowest content of Cd (1.4 (TENT A) and 1.6 mg kg^{-1} (TENT B)) and Co (16.3 and 23 mg kg^{-1} in TENT A and TENT B fly ashes, respectively). The range of these heavy metals in European fly ashes is 1-6 mg kg^{-1} for Cd and 20 to 112 mg kg^{-1} for Co [15]. Previously, it has been emphasized that the basic factor influencing the chemical composition of fly ash is the type of basic fuel used [16]. Based on the data presented in Figure 2, trace element concentrations in the native fly ashes studied, it was concluded that the values are similar.

Generally, elements and their compounds can evaporate during coal combustion, and they can be adsorbed and condensed on the surface of coal combustion particles when the temperature decreases [17]. Distribution of various elements between the bottom ash and fly ash depends on the type of boiler, operating conditions, the fuel mix, and the efficiency of flue gas cleaning devices [18] and is greatly influenced by the temperature in the combustion boiler, retention time of feed coal and air supply to the combustion grate [19]. In order to describe the element distribution between fly ash and bottom ash, *f*/*b* value (ratio of element concentration in the fly ash to that in the bottom ash) is calculated. This index is used to detect elements that are volatilized and subsequently condensed totally or partially in the flue gas (high *f*/*b* ratio) or heavy and low-volatile elements that preferably are enriched in bottom ash [20]. For both TENT A and TENT B, the *f*/*b* value for Cr is lower than 0.8 (0.76 and 0.78, for TENT A and TENT B, respectively), suggesting its enrichment in bottom ash in comparison to fly ash. Cr has relatively low vapor pressures and a higher boiling point, so it was retained in the slag or bottom ash [21]. Nickel is depleted in TENT B fly ash (*f*/*b* = 0.79), while Zn is depleted in TENT A fly ash, with the same value of *f*/*b* = 0.79. The results obtained concerning the bottom ash of TENT A enrichment with even 4 elements (Cr, Ni, Cu, and Zn) are in accordance with TENT A bottom ash characteristics; namely, a high value of LOI is an indication of a high amount of unburned carbon, which is the reason for its adsorption affinity.

The concentrations of examined elements in residuals obtained after acid leaching and wet oxidation are presented in Figures 3 and 4, respectively. To easily compare values for different methods, the concentration scale was the same as in Figure 2.

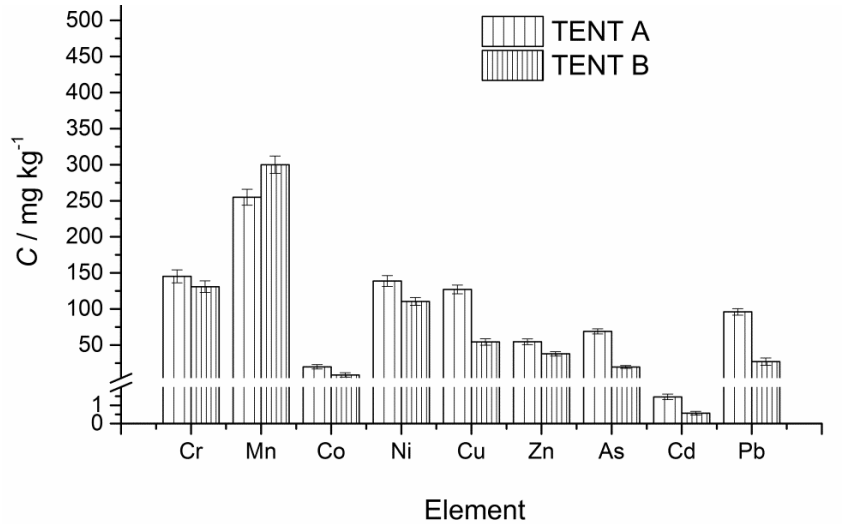

Figure 3. Concentrations of heavy metals (triplicate average) remained in residuals after acid (the error bars represent the standard deviation of the triplicates)

A decrease in the concentration of all examined elements is observed after acid treatment (Figure 3). The highest removal degree by acid digestion is obtained for Mn and for fly ash from both CPPs, 25 % for TENT A and 19.5 % for TENT B. The lowest removal efficiency is obtained for Pb (12.4 %, TENT A).

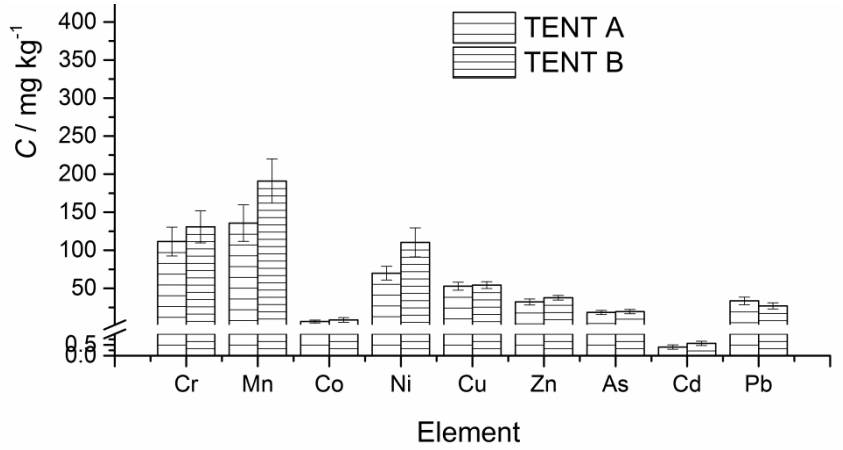

Figure 4. Concentrations of heavy metals remained in residuals after wet oxidation (triplicate average); the error bars represent the standard deviation of the triplicates)

Applying the wet oxidation method showed a significant decrease in the concentration of the examined heavy metals in all tested samples from both CPPs (Figure 4). Considering the degree of concentration decrease, two groups of elements are distinguished: one group in which the degree of removal is from 30 to 50 % (Cr, Ni, Cu, Zn), and the second group in which this degree is in the range 60 to 75 % (Mn, Co, As, Cd and Pb).

In general, wet oxidation showed 2-6 times higher extraction for analyzed heavy metals than acid leaching. Previously, it has been observed that the effect of different acids and acid combinations on fly ash digestion and metal dissolution is metal-dependent [22].

3. 3. Fly ash and residual characterization

Surface compositions of fly ash from TENT A and TENT B, and of residuals obtained after acid leaching and wet oxidation were investigated *via* XRD. Detailed information on the morphology, shape and surface texture of individual particles was obtained using SEM. The phases found in fly ashes and their chemical formulas and symbols are shown in Table 2, while XRD profiles are presented in Figure 5.

Table 2. Mineral name, chemical formula, and symbol

Name of mineral	Chemical formula	Symbol
Quartz	SiO_2	Q
Cristobalite	SiO_2	Cr
Anhydrite	$CaSO_4$	An
Mullite	$Al_{4.64}Si_{1.36}O_{9,68}$	Mu
Anorthoclase	$(Na_{0.7}K_{0.3})(Al_{1.0}2Si_{2.98}O_8)$	Ano
Albite	$(Na,Ca)Al(Si,Al)_3O_8$	Al
Hematite	αFe_2O_3	He
Calcite	$CaCO_3$	C

Fly ashes from both CPPs have shown similar patterns in mineralogical characterization, which is expected considering the same origin of the fuel (lignite, RB Kolubara). The phase analysis results show that in all samples, a few crystalline phases and probably one amorphous phase are present. The dominant crystalline phase in the fly ashes was made of silicates and alumosilicates, such as quartz, mullite, albite, and anorthoclase. Carbonates (calcite), oxide of iron (hematite), and sulfate mineral (anhydrite) were also detected. The types and proportions of metal minerals in coal ash vary depending on their origin [23]. Previously, it was published that magnetite was present in coal fly ash from TENT B [24]. In this research,

as well as in the research of Šešlija *et al.* [25], this mineral was not detected while only weakly magnetic hematite was present. A considerable amount of amorphous matter is present, which is confirmed in results published previously [9,25].

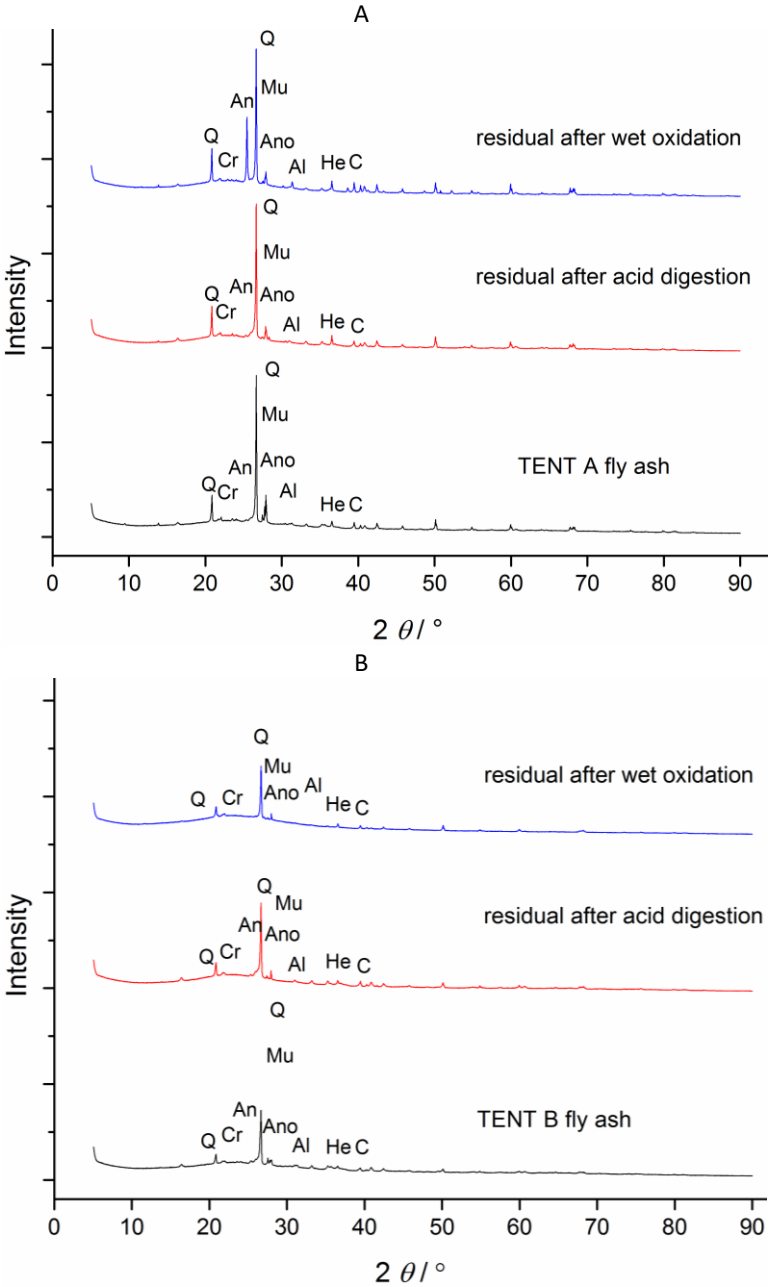

Figure 5. Mineral identification of the initial coal fly ash and the residual after the treatment from: A) TENT A; B) TENT B

Diffraction peak intensities of crystalline phases in the residuals after acid digestion did not change significantly compared to the initial fly ashes, indicating that the crystalline phase types did not change significantly. After wet oxidation, the quartz phase remained the main mineral phase, as it is difficult to dissolve under applied conditions. Also, the crystal phase diffraction peaks of cristobalite and calcite in the residual after this treatment did not change compared to those of the initial fly ash. On the other hand, the XRD analysis of wet oxidation residuals has shown changes in the anorthoclase, albite, and hematite contents.

SEM images of the fly ashes are shown in Figures 6 (TENT A) and 7 (TENT B) together with residuals of acid-treated and wet oxidized fly ash.

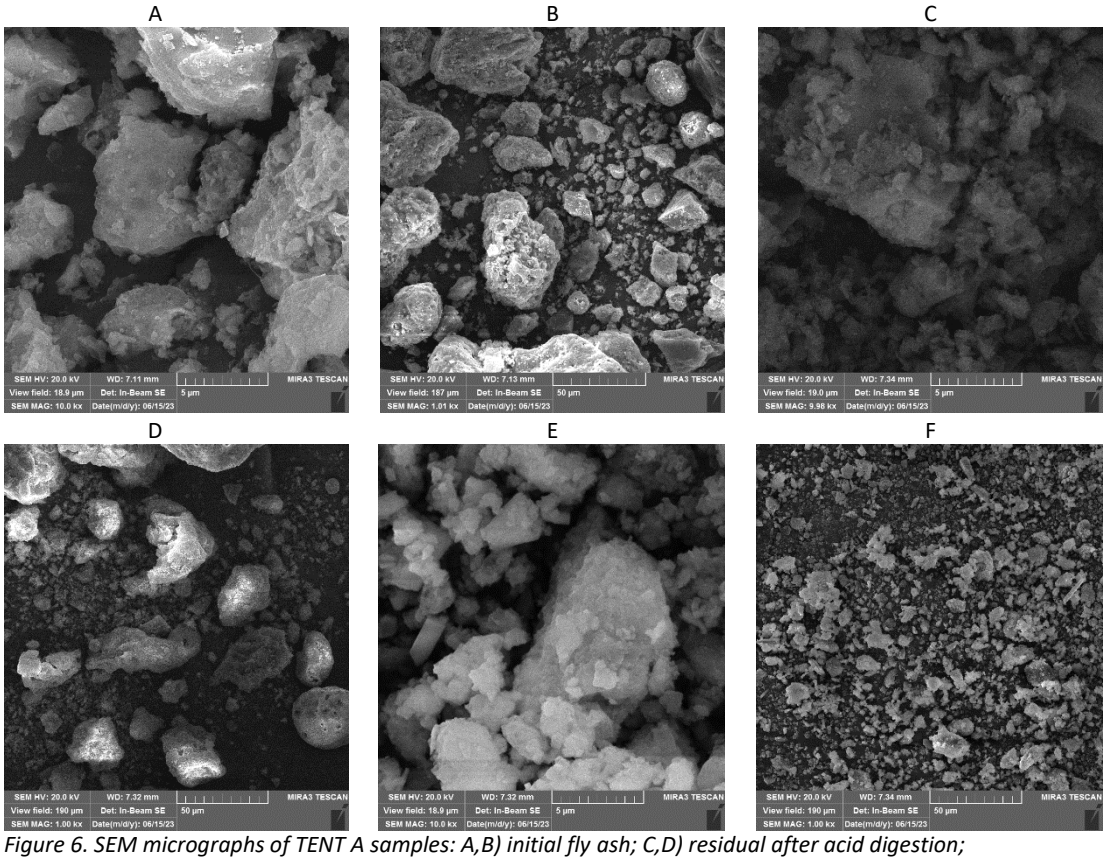

Figure 6. SEM micrographs of TENT A samples: A,B) initial fly ash; C,D) residual after acid digestion; E,F) residual after wet oxidation; (A, C and E: scale bar = 5 μm; B, D and F: scale bar = 50 μm)

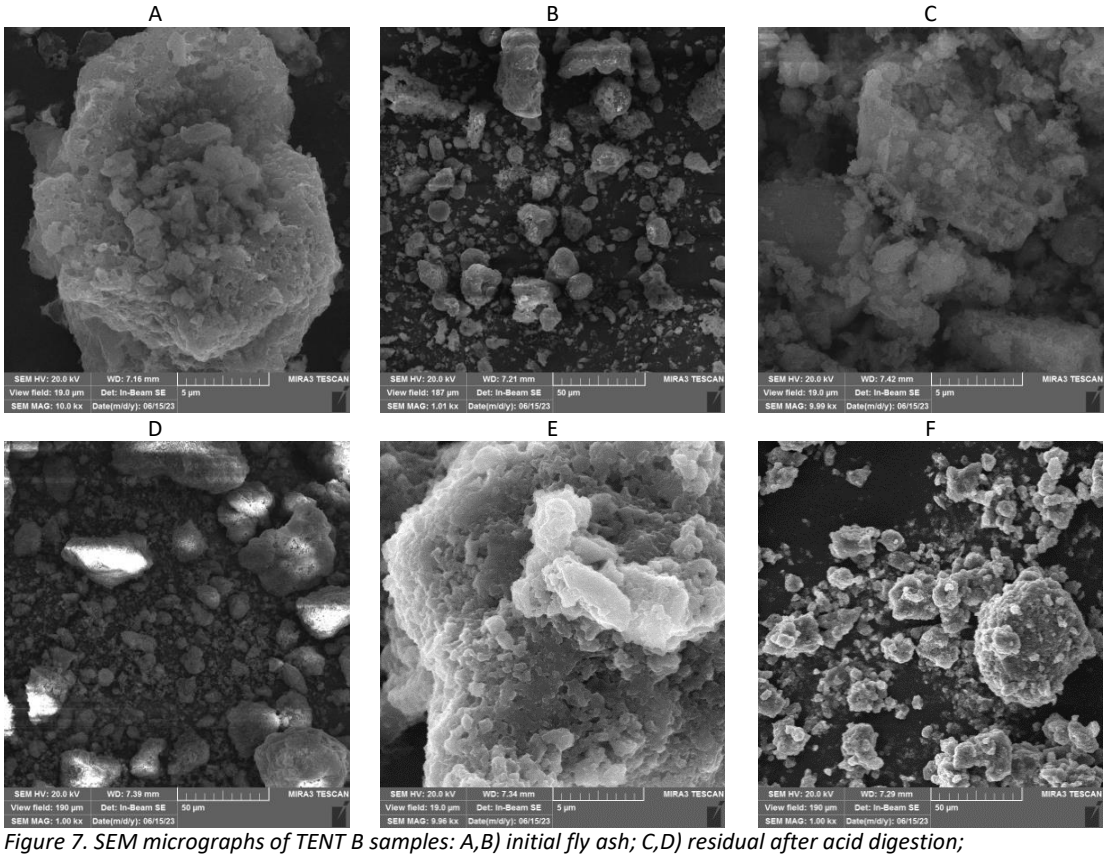

Figure 7. SEM micrographs of TENT B samples: A,B) initial fly ash; C,D) residual after acid digestion; E,F) residual after wet oxidation; (A, C and E: scale bar = 5 μm; B, D and F: scale bar = 50 μm)

SEM images of fly ashes from TENT A and TENT B are similar (Figs 6A and 7A, respectively) showing particles of different sizes and shapes. Similar results were obtained previously by Wang *et al.* [11], where three typical CFA particles were found: spherical, oval, and irregular. For TENT A, the fly ash sample contains few 5 μm particles, while in the TENT B sample, one large particle is noticed, with many small fine particles packed inside and on its surface. The residual of TENT A fly ash after acid digestion had the same morphological pattern as the ash, while wet oxidation resulted in particle structure degradation.

3. 4. Correlation analysis

The experimental data from the chemical analysis after treatment (wet oxidation, acid leaching and microwave digestion of bottom ash/fly ash, TENT A/TENT B) have been used for the correlation analysis. The calculated correlation coefficients are listed in Table 3.

Table 3. Pearson correlation matrix between heavy metal concentrations in coal fly ash samples

	Cr	Mn	Co	Ni	Cu	Zn	As	Cd
Mn	0.997							
Co	0.990	0.987						
Ni	0.972	0.968	0.995					
Cu	0.747	0.767	0.616	0.525				
Zn	0.997	0.988	0.990	0.974	0.707			
As	0.881	0.902	0.821	0.769	0.716	0.848		
Cd	0.968	0.975	0.927	0.888	0.566	0.951	0.970	
Pb	0.968	0.961	0.924	0.884	0.538	0.965	0.925	0.983

Typically, a high correlation was found among all heavy metals because all fly ash samples were obtained by burning the lignite of the same origin. The strongest correlation was found between Pb, Cd, and As, while a very high correlation exists between Cr, Mn, Ni, Zn, and Co.

After performing the correlation analysis, the correlation matrix was checked (*i.e.* the correlation matrix of variables has to have the sufficient number of correlation coefficients above 0.3 to apply factor analysis [26]). Also, justification for performing the factor analysis was confirmed (*i.e.* the Kaiser-Meyer-Olkin (KMO) indicator takes values between 0 and 1, and the smallest value acceptable for good factor analysis (FA) is 0.5 to 0.6 [26,27] and the Bartlett's test of sphericity should be statistically significant, *i.e.* that $p < 0.05$ [28]). Consequently, the principal component analysis (PCA) was applied to the original data set. Two main components were obtained, which can explain the largest variance, over 90 % (Fig. 8). Most heavy metals with very strong correlations are in the first component.

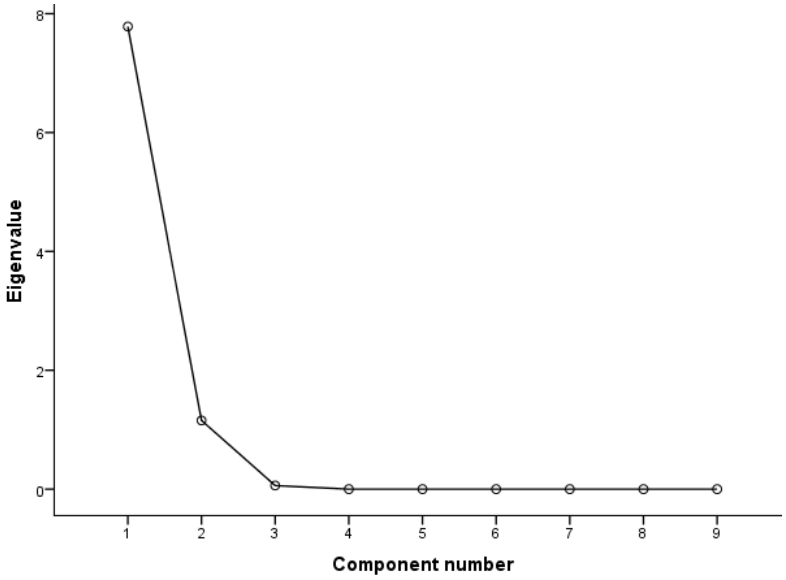

Figure 8. Scree plot of eigenvalues

This scree plot shows that the eigenvalues start to form a straight line after the second principal component. Therefore, the remaining principal components account for a very small proportion of the variability (close to zero) and are probably unimportant. Similar results were obtained by applying cluster analysis to z-transformed data. The dendrogram in Figure 9 shows clusters that coincide with and confirm the result obtained by the PCA analysis. The tested parameters were grouped into two clusters based on their characteristics and affinity towards the solid phase. In cluster I, there are predominantly Cr, Zn, Mn, Co, and, at a slightly greater Euclidean distance, Ni; in the second cluster, Pb, As, and Cd, and as a special one at a slightly greater Euclidean distance, Cu.

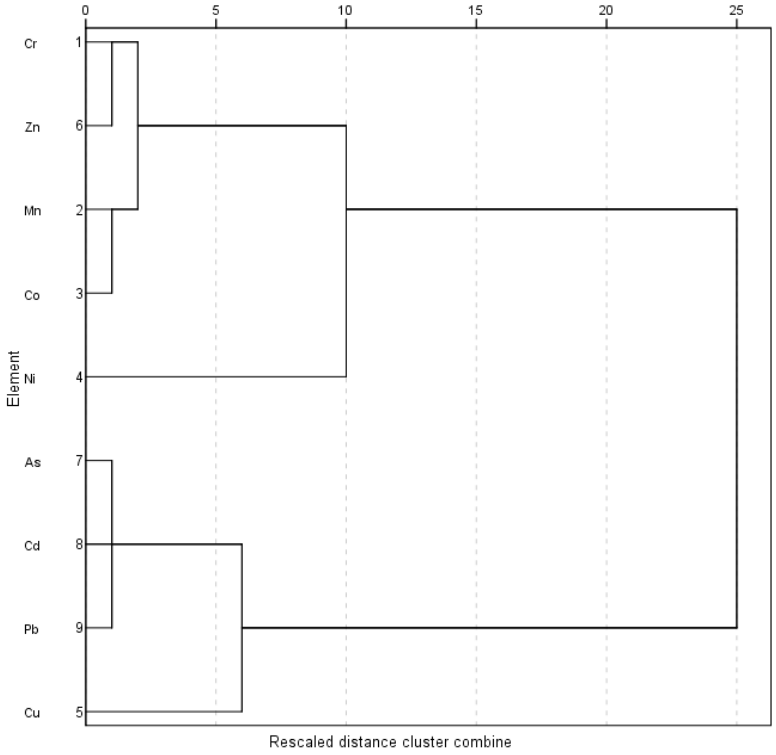

Figure 9. Dendrogram (using Ward linkage) of element grouping in fly ash samples

4. CONCLUSION

The present study investigated contents of selected heavy metals (Cr, Mn, Co, Ni, Cu, Zn, As, Cd, and Pb) in coal bottom and fly ash in samples collected from two Serbian coal-fired power plants, TENT A and TENT B, both using lignite from RB Kolubara. Microwave-assisted acid digestion was applied for sample preparation. The obtained results indicate that burning conditions did not significantly influence the chemical composition, nor the concentration of heavy metals. These concentrations were in the range reported for European coals. A decrease in heavy metal concentration in the fly ash residue has been observed during the heavy metal removal experiments using acid leaching and wet oxidation. The results indicate that wet oxidation is more efficient, with the removal degree in the range of 30 to 75 %; after this treatment, particle structure and surfaces were changed. In this way, material for possible further application can be prepared, and consequently, contamination caused by large amounts of disposed CFA can be reduced.

Acknowledgements: *This work was supported by the Science Fund of the Republic of Serbia within the project "Serbian Industrial Waste towards Sustainable Environment: Resource of Strategic Elements and Removal Agent for Pollutants - SIW4SE" (Contract No. 7743343), Programme Ideas.*

REFERENCES

[1] Šerović R, Jelić I, Matić B, Savić A. Utilization of solidified industrial hazardous waste in construction: A case study. *Hem Ind.* 2023; 77(2): 137-146 https://doi.org/10.2298/HEMIND222610001S.

[2] Vukićević M, Popović Z, Despotović J, Lazarević L. Fly ash and slag utilization for the serbian railway substructure. *Transport.* 2018; 33(2): 389-396 https://doi.org/10.3846/16484142.2016.1252427.

[3] Tasić AM, Sredović Ignjatović ID, Ignjatović LM, Ilić MA, Antić MP. Comparison of sequential and single extraction in order to estimate the environmental impact of metals from fly ash. *J Serb Chem Soc.* 2016; 81(9): 1081-1096 https://doi.org/10.2298/JSC160307038T.

[4] Đorđević D, Stanković M, Krstić N, Dimitrijević V, Anastasijević N, Đorđević M, Nikolić M. Geochemical analysis of Kostolac power plant fly ash: working and living environment influence aspect. *Saf Eng*. 2018; 8(1): 15-20 https://doi.org/10.7562/SE2018.8.01.03.

[5] Đolić M, Ćujić M, Stanišić T, Čičkarić D, Ristić M, Perić Grujić A. Contribution to the Serbian coal ranking and fly ash characterization using Pb isotopic ratio. *Metall Mater Eng*. 2022; 28(4): 675-684 https://doi.org/10.56801/MME931.

[6] Slavković-Beškoski L, Ignjatović L, Bolognesi G, Maksin D, Savić A, Vladisavljević G, Onjia A. Dispersive Solid-Liquid Microextraction Based on the Poly(HDDA)/Graphene Sorbent Followed by ICP-MS for the Determination of Rare Earth Elements in Coal Fly Ash Leachate. *Metals (Basel)*. 2022; 12(5): 791 https://doi.org/10.3390/met12050791.

[7] Buha Marković JZ, Marinković AD, Savić JZ, Mladenović MR, Erić MD, Marković ZJ, Ristić MĐ. Risk Evaluation of Pollutants Emission from Coal and Coal Waste Combustion Plants and Environmental Impact of Fly Ash Landfilling. *Toxics*. 2023; 11(4): 396 https://doi.org/10.3390/toxics11040396.

[8] Buha-Marković J, Marinković A, Savić J, Krstić A, Savić A, Ristić M. Health risk assessment of potentially harmful substances from fly ashes generated by coal and coal waste combustion. *J Serb Chem Soc.* 2023; 88(11): 1161-1173 https://doi.org/10.2298/JSC220130048M.

[9] Petronijević N, Radovanović D, Štulović M, Sokić M, Jovanović G, Kamberović Ž, Stanković S, Stopić S, Onjia A. Analysis of the Mechanism of Acid Mine Drainage Neutralization Using Fly Ash as an Alternative Material: A Case Study of the Extremely Acidic Lake Robule in Eastern Serbia. *Water (Switzerland)*. 2022; 14(20): 3244 https://doi.org/10.3390/w14203244.

[10] Trivunac K, Vukčević M, Maletić M, Karić N, Pejić B, Perić-Grujić A. Waste materials as adsorbents for heavy metals removal from water: Comparative analysis of modification techniques. *Tekst Ind*. 2023; 71(1): 4-10 https://doi.org/10.5937/tekstind2301004T.

[11] Wang N, Sun X, Zhao Q, Yang Y, Wang P. Leachability and adverse effects of coal fly ash: A review. *J Hazard Mater*. 2020; 396: 122725 https://doi.org/10.1016/j.jhazmat.2020.122725.

[12] Bruker-AXS (2013). Crystallography Open Database for DIFFRAC.EVA. https://www.bruker.com/products/x-ray-diffraction-and-elemental-analysis/x-ray-diffraction/xrd-software/eva/cod.html

[13] Powder Diffraction File: PDF-2 (Database), International Center for Diffraction Data (ICDD), Newtown Square, Pennsylvania, USA, 2008.

[14] ASTM-C 618-15: Standard Specification for Coal Fly Ash and Raw or Calcined Natural Pozzolan for Use as a Mineral Admixture in Concrete. 2015

[15] Moreno N, Querol X, Andrés JM, Stanton K, Towler M, Nugteren H, Janssen-Jurkovicová M, Jones R. Physico-chemical characteristics of European pulverized coal combustion fly ashes. *Fuel.* 2005; 84(11): 1351-1363 https://doi.org/10.1016/j.fuel.2004.06.038 .

[16] Strzałkowska E. Morphology, chemical and mineralogical composition of magnetic fraction of coal fly ash. *Int J Coal Geol*. 2021; 240: 103746 https://doi.org/10.1016/j.coal.2021.103746.

[17] Wei Q, Song W. Mineralogical and chemical characteristics of coal ashes from two high-sulfur coal-fired power plants in Wuhai, Inner Mongolia, China. *Minerals* 2020; 10(4): 323 https://doi.org/10.3390/min10040323.

[18] Dahl O, Nurmesniemi H, Pöykiö R, Watkins G. Heavy metal concentrations in bottom ash and fly ash fractions from a large-sized (246 MW) fluidized bed boiler with respect to their Finnish forest fertilizer limit values. *Fuel Process Technol*. 2010; 91(11): 1634-1639 https://doi.org/10.1016/j.fuproc.2010.06.012.

[19] Tang Q, Liu G, Zhou C, Sun R. Distribution of trace elements in feed coal and combustion residues from two coal-fired power plants at Huainan, Anhui, China. *Fuel*. 2013; 107: 315-322 https://doi.org/10.1016/j.fuel.2013.01.009.

[20] Dai S, Zhao L, Peng S, Chou C-L, Wang X, Zhang Y, Li D, Sun Y. Abundances and distribution of minerals and elements in high-alumina coal fly ash from the Jungar Power Plant, Inner Mongolia, China. *Int J Coal Geol*. 2010; 81(4): 320-332 https://doi.org/10.1016/j.coal.2009.03.005.

[21] da Silva EB, Li S, de Oliveira LM, Gress J, Dong X, Wilkie AC, Townsend T, Ma LQ. Metal leachability from coal combustion residuals under different pHs and liquid/solid ratios. *J Hazard Mater*. 2018; 341 (September): 66-74 https://doi.org/10.1016/j.jhazmat.2017.07.010.

[22] Ramanathan T, Ting YP. Selection of wet digestion methods for metal quantification in hazardous solid wastes. *J Environ Chem Eng*. 2015; 3(3): 1459-1467 https://doi.org/10.1016/j.jece.2015.05.006.

[23] Ramakrishna C, Thenepalli T, Nam SY, Kim C, Ahn JW. The brief review on coal origin and distribution of rare earth elements in various coal ash samples. *KSEE*. 2018; 27(2): 61-69 https://doi.org/10.5855/ENERGY.2018.27.2.061.

[24] Hredzák S, Tomanec R, Matik M, Šepelák V, Václavíková M. Magnetic separation and analysis of products obtained from coal-fired power plant fly ashes of Nikola Tesla B (Serbia). *J Min Met*. 2006; 42 A: 55-68 https://www.jmma.tfbor.bg.ac.rs/Volumes/2006/06.pdf.

[25] Šešlija M, Rosić A, Radović N, Vasić M, Đogo M, Jotić M. Physiproperties of fly ash and slag from the power plants. *Geol Croat.* 2016; 69(3): 317-324 https://doi.org/10.4154/gc.2016.26.
[26] Tabachnick BG, Fidel SL. Using multivariate statistics. 7th ed., New York, NY: Pearson; 2018. ISBN 978-0134790541
[27] Kaiser HF, A second generation little jiffy. *Psychometrika*. 1970; 35(4): 401-415 https://doi.org/10.1007/BF02291817.
[28] Bartlett MS. A note on the multiplying factor for various chi square approximations. *J R Stat Soc, B:Stat*. 1954; 16: 296-298 https://doi.org/10.1111/j.2517-6161.1954.tb00174.x.

Uticaj metode izluživanja na uklanjanje teških metala iz letećeg pepela

Andrija Z. Janković[1], Mirjana R. Ćujić[2], Milica D. Stojković[1], Maja B. Đolić[1], Dragana Z. Živojinović[1], Antonije E. Onjia[1], Mirjana Dj. Ristić[1] i Aleksandra A. Perić Grujić[1]

[1]Univerzitet u Beogradu, Tehnološko-metalurški fakultet, Beograd, Srbija
[2]Univerzitet u Beogradu, Institut za nuklearne nauke Vinča – Institut od nacionalnog značaja za Republiku Srbiju, Beograd, Srbija

(Naučni rad)

Izvod

Uklanjanje teških metala (Cr, Mn, Co, Ni, Cu, Zn, As, Cd i Pb) iz elektrofilterskog pepela proučavano je korišćenjem metoda kiselog luženja i vlažne oksidacije. Paralelno je primenjena i kisela digestija uz pomoć mikrotalasne pećnice za određivanje pseudoukupnih koncentracija teških metala u cilju procene efikasnosti luženja. Multivarijantna statistika (Pearsonova korelacija, analiza glavnih komponenti i hijerarhijska klaster analiza) pokazala je dve dominantne grupe elemenata u zavisnosti od njihovih karakteristika i afiniteta prema čvrstoj fazi pepela. Grupe I (Cr, Zn, Mn, Co i Ni) i II (Pb, As, Cd i Cu) su međusobno diskriminisane. Pokazalo se da je metoda vlažne oksidacije prikladnija od kiselog luženja jer je smanjenje koncentracija metala bilo 30-75 % u poređenju sa 12-25 % dobijenih kiselom digestijom. Takođe je ispitan uticaj tretmana letećeg pepela na karakteristike čvrstog ostatka metodama rendgenske difrakcije i skenirajuće elektronske mikroskopije. Ovim metodama su otkrivene promene na površini i u strukturi letećeg pepela nakon tretmana vlažnom oksidacijom. Vlažna oksidacija se može smatrati kao moguća metoda za tretman u cilju uklanjanje teških metala iz letećeg pepela, obezbeđujući materijal koji bi se mogao dalje koristiti i smanjujući rizik od zagađenja izazvanog odlaganjem letećeg pepela.

Ključne reči: iskorišćenje otpada; vlažna oksidacija; izluživanje kiselinom; karakterizacija materijala

Natural deep eutectic solvents for turbidity removal from synthetic pharmaceutical wastewater

Adeeb Hayyan[1], Siti Nuratikah Nabila binti Suratmin[1], Fathiah Mohamed Zuki[1], M. Zulhaziman M. Salleh[2], Jehad Saleh[3], Waleed Al Abdulmonem[4], Abdullah S. M. Aljohani[5], Ahmad GH. Aldaihani[6], Khaled H. Alkandari[1], Mohd Roslan Mohd Nor[7], Andrew T. H. Yeow[1] and Wan Jefrey Basirun[8]

[1]*Department of Chemical Engineering, Faculty of Engineering, Universiti Malaya, Kuala Lumpur, Malaysia*
[2]*Department of Chemical and Process Engineering, Faculty of Engineering and Built Environment, Universiti Kebangsaan Malaysia, Bangi, Selangor, Malaysia*
[3]*Chemical Engineering Department, King Saud University, Riyadh, Saudi Arabia*
[4]*Department of Pathology, College of Medicine, Qassim University, Buraydah, Saudi Arabia*
[5]*Department of Veterinary Medicine, College of Agriculture and Veterinary Medicine, Qassim University, Buraydah, Saudi Arabia*
[6]*School of Engineering, University of Liverpool, Liverpool, UK*
[7]*Halal Research Group, Academy of Islamic Studies, Universiti Malaya, Kuala Lumpur, Malaysia*
[8]*Department of Chemistry, Faculty of Science, University of Malaya, Kuala Lumpur, Malaysia*

Abstract

Contamination of water resources by active pharmaceutical ingredient wastes is among major environmental concerns. To prevent major disruptions of aquatic life, an efficient and environmentally-friendly turbidity removal procedure of common contaminants such as paracetamol should be established. In this study, several natural deep eutectic solvents (NADESs) were screened to reduce the turbidity of simulated water contaminated with paracetamol below the standard turbidity limit recommended by the National Water Quality Standards for Malaysia (50 NTU). The optimal operating parameters (NADES dosage, stirring time and operating pH) were determined. Under optimized conditions, stearic acid-based NADES achieved the highest turbidity removal of 97.5 %. High coagulation performances were investigated based on molecular interaction using COSMO-RS (COnductor like Screening MOdel for Real Solvents) σ-profile and σ-potential (histogram of charge density distribution over molecular surface) and showed high affinity between the NADES compounds and paracetamol. Thus, NADESs are promising candidates for turbidity removal of paracetamol from water and are viable in further investigations for effluent treatment applications.

Keywords: Active pharmaceutical ingredients; flocculation; coagulation; wastewater treatment.

Available on-line at the Journal web address: http://www.ache.org.rs/HI/

ORIGINAL SCIENTIFIC PAPER

UDC: 632.153:661.12:543.316

Hem. Ind. **78(1)** 63-72 (2024)

1. INTRODUCTION

Substantial efforts in research and industrialisation have been carried out to establish effective treatment and purification of industrial wastewater to meet the increasing public demand of clean water. These efforts include various techniques which were conducted for removal of pollutants from wastewater with high efficiency such as liquid-liquid extraction (LLE), aqueous biphasic systems, adsorption, and application of liquid membranes [1-3]. Wastewater treatment plants usually involve physical, chemical, and biological treatments to minimize and remove pollutants from water. Individual wastewater treatment methods that are classified as primary, secondary and tertiary treatment methods are integrated into a set of systems to achieve a certain degree of contaminant elimination [4]. Industrially, the treatment of wastewater utilizes numerous chemical substances such as activated carbon, chlorine, ozone, and ionic

Corresponding authors: *Adeeb Hayyan, Department of Chemical Engineering, Faculty of Engineering, Universiti Malaya, Kuala Lumpur, Malaysiaand **M. Zulhaziman M. Salleh, Department of Chemical and Process Engineering, Faculty of Engineering and Built Environment, Universiti Kebangsaan Malaysia, Bangi, Selangor, Malaysia

E-mail: *adeeb@um.edu.my; **zulhaziman@ukm.edu.my

Paper received: 25 March 2023; Paper accepted: 2 January 2024; Paper published: 26 February 2024.
https://doi.org/10.2298/HEMIND230325005H

liquids (ILs) [5]. However, such chemical substances pose challenges in terms of manufacturing/operating costs, material reusability and recyclability, and environmental impact during disposal when exhausted [6]. Therefore, further studies are required towards development of advanced water purification processes using sustainable, renewable low-cost materials.

Importance of utilization of natural deep eutectic solvents (NADESs) in extraction of pollutants from wastewater has been widely explored in numerous studies such as purification of water contaminated with bisphenol-A (BPA) using hydrophobic deep eutectic solvents (DESs) [7], a circular approach to purify water contaminated with ciprofloxacin by using hydrophobic DESs [8], synthesis and characterization of DESs and hydrophobic application for micro-extraction of environmental water samples [9], development of hydrophobic DESs for extraction of pesticides from aqueous environments [10] and separation and pre-concentration of parabens from water samples by liquid-liquid micro-extraction [11]. The outcomes of these studies reveal that DESs are one of many viable and effective alternative materials in removing pollutants of high concern, such as BPA, pesticides and active pharmaceuticals ingredients (APIs) from wastewater. However, the ability of DESs to remove turbidity of wastewater induced by paracetamol content has not been studied yet despite its exacerbating impact towards the environment due to the increased production and consumption by humans.

In this study, NADESs are employed as cost-effective materials acting as the coagulant stage in API wastewater treatment. Specifically, NADESs were studied as alternative solvents regarding the ability to decrease the turbidity of water contaminated with paracetamol to below the standard turbidity limit recommended by the National Water Quality Standards for Malaysia (50 NTU). The optimal conditions were achieved by manipulating experimental parameters such as the dosage of NADESs, stirring time and pH of the water system. Furthermore, the interactions between the NADES constituents and paracetamol were investigated and inferred using COSMO-RS. Ultimately, this study demonstrates DESs as a viable and effective alternative in water purification technologies by method of extraction of pollutants.

2. MATERIALS AND METHODS

NADESs were synthesised from the following chemical constituents: stearic acid (SA, Merck, Malaysia, ≥97 %), levulinic acid (LA, Sigma Aldrich, Malaysia, ≥98 %), malonic acid (MA, Sigma Aldrich, Malaysia, ≥99 %), and choline chloride (ChCl, Sigma Aldrich, Malaysia, ≥98 %). Synthetic wastewater samples contaminated with acetaminophen (paracetamol, Merck, Malaysia, ≥99 %) were prepared by dissolving paracetamol in distilled water yielding an acetaminophen solution of 10 g L^{-1} concentration. An electronic turbidity meter (HI 98703, Hanna Instruments, Woonsocket RI, USA) was used to measure the initial and final turbidity readings of the synthetic wastewater. The solution pH was adjusted by adding either 0.1 M sodium hydroxide solution or 0.1 M hydrochloric acid solution, and was measured using a digital pH meter (Mettler Toledo Seven Compact, Switzerland).

2. 1. Preparation of NADESs

NADESs were prepared according to similar procedures published in prior literature [12]. Briefly, the NADESs were prepared by mixing a hydrogen bond donor (HBD) and hydrogen bond acceptor (HBA) constituent at specific component molar ratios as listed in Table 1. The obtained mixtures were stirred vigorously at 60 – 65 °C using a hot plate magnetic stirrer until a homogenous liquid is formed.

Table 1. Molar ratios of chemical constituents used to prepare the NADESs, hydrogen bond acceptor is choline chloride

Hydrogen bond donor (HBD)	Molar ratio	Abbreviation of NADES
Stearic acid (SA)	1:2	ChCl:SA
Malonic acid (MA)	1:1	ChCl:MA
Levulinic acid (LA)	1:2	ChCl:LA

2. 2. Optimisation of experimental parameters

The list of NADESs prepared in Table 1 and its individual constituents were screened as natural coagulants for turbidity removal, and the compounds with acceptably high efficiency in turbidity removal were selected for further optimisation.

The dosage of NADESs was optimised as follows: initially, 2 g of NADESs were added to 500 mL of simulated wastewater at pH 6.0. Flash mixing mode (coagulation) was first performed at a stirring rate of 200 rpm for 5 min. Subsequently, slow mixing at a stirring rate of 150 rpm was conducted for 15 min. After the stirring procedures, the treated wastewater was allowed to sit for 30 min, at which the treated wastewater was sampled by pipetting a sample out from the beaker at a predetermined depth below the water surface. The final turbidity reading was recorded by using the turbidity meter. The experiment was conducted in triplicates to obtain the average value. The experimental procedures were repeated with different increasing dosages of NADESs (10, 16, 20 and 40 g L^{-1}). The coagulation efficiency is represented by the turbidity removal efficiency (TRE) from wastewater and is calculated based on equation (1):

$$\text{TRE}=\frac{T_0 - T}{T_0}100 \quad (1)$$

where T_0 is the turbidity of paracetamol-contaminated wastewater before extraction and T is the turbidity of paracetamol-contaminated wastewater after extraction.

Optimisation of stirring time was conducted by using the optimised dosage of NADESs on turbidity removal. The effect of stirring time was investigated for 10, 15, 25 and 30 min. Finally, the optimal pH of the wastewater system was investigated for pH 4, 7, 9 and 11 using the pre-determined optimum conditions of NADES dosages and stirring time.

3. RESULTS AND DISCUSSION

3. 1. Screening of NADESs as potential coagulants

Screening of NADESs and its individual constituents was conducted prior to the optimisation step and the results are presented in Figure 1. At the pre-optimisation stage, the highest turbidity reduction was achieved by ChCl:SA (90 %), followed by ChCl:LA (85 %) and ChCl:MA (84 %). Additionally, the individual organic acid constituent of the NADESs exhibited some level of performance in turbidity removal. For example, LA as a standalone compound achieved a TRE of 77 %, whereas MA achieved the lowest TRE value out of the three acid constituents at 57 %. In the further optimisation analysis, the individual constituents were excluded from further optimisation based on the turbidity removal performance of the NADESs. The NADESs were used as new coagulants for the turbidity removal of simulated wastewater samples contaminated with paracetamol.

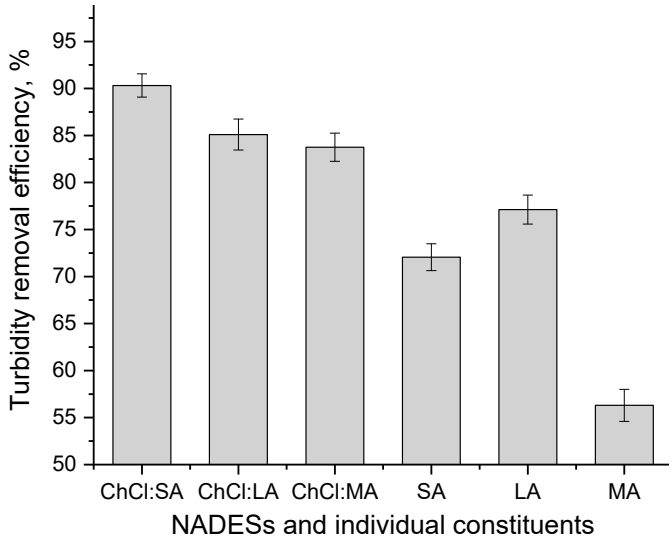

Figure 1. Screening of NADESs and its individual constituents in relation to its turbidity removal performance (data are average of n=3)

3. 2. Dosage effect of NADESs

The effect of NADES dosages on the turbidity removal is shown in Figure 2. Each NADES resulted in different optimum dosages that efficiently reduced turbidity of the wastewater. The optimum dosage of ChCl:SA NADES was determined

as 16 g L^{-1}, where the turbidity reading of the wastewater was decreased from 400 NTU to 10 NTU, corresponding to a TRE of 97 %. On the other hand, the ChCl:LA NADES achieved a high TRE value of 94 % at the lowest optimum dosage among the three NADESs at 10 g L^{-1}. Comparatively, ChCl:MA NADES required the highest optimum NADES dosage of 20 g L^{-1} to achieve 96 % TRE. The optimum dosage depends on the coagulant's molecular weight, ionic character and degree of ionization. Ultimately, low coagulation and flocculation efficiencies are due to the insufficient or excessive dosages of DESs. Larger dosages could either agitate the sedimentation process causing re-suspension of aggregated particles [13].

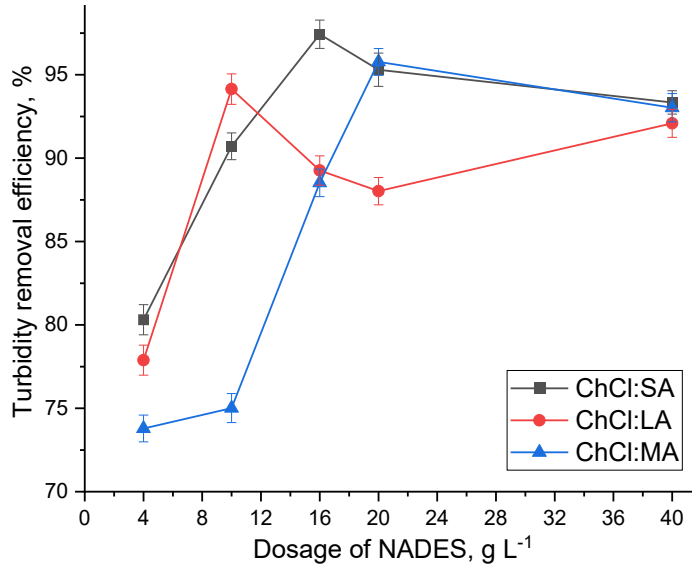

Figure 2. Effect of NADES dosage on turbidity removal efficiency of synthetic paracetamol contaminated wastewater (data are average of n = 3)

3. 3. Effects of stirring time

Effects of stirring time on the turbidity removal are presented in Figure 3. For the ChCl:SA NADES, the optimum stirring time was determined at 20 min where the turbidity decreases from around 400 NTU to 11 NTU, corresponding to a TRE value of 97 %.

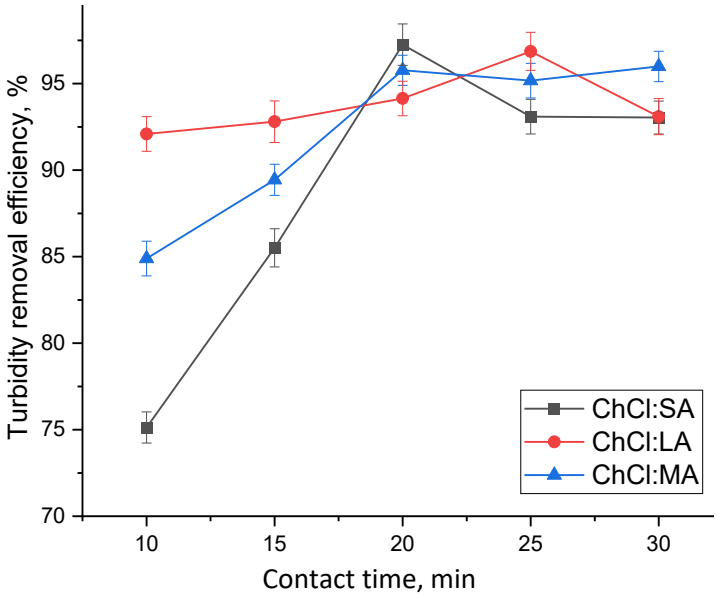

Figure 3. Effect of stirring time on turbidity removal efficiency of synthetic paracetamol contaminated wastewater using optimized NADES dosages (data are average of n = 3)

Similar TRE performances can be achieved by using the ChCl:LA NADES at the optimum stirring time of 25 min. The ChCl:MA NADES achieved a maximum of 96 % TRE at the optimal stirring time of 30 min, which was the longest stirring time out of the three NADESs investigated. In the present study, the coagulation and flocculation steps are assumed to occur in stages and the stirring time was observed to affect both processes. However, the coagulation is unaffected by excessive mixing, but inadequate mixing can result in the incomplete coagulation phase. Typically, the contact time for rapid-mixing is allowed for 1–3 min, while the design of flocculation contact times may vary from 15–60 min according to the equipment design.

3. 4. Effects of pH of the wastewater system

Effects of the solution pH on the turbidity removal are shown in Figure 4. The optimum pH for stearic acid and levulinic acid-based DES is pH 6 where the turbidity level can be reduced from around 400 NTU to 11 NTU and 13 NTU. pH 7 was the optimal pH value for the turbidity removal using ChCl:MA where the turbidity was reduced from around 400 NTU to 16 NTU. Hence, it can be concluded that choline chloride-based deep eutectic solutions can perform well in the pH range of 6-7. The surface charge of the coagulants is affected by the pH of the water. The surface of coagulated paracetamol particles is negative at high pH, resulting in a lower turbidity removal. When H^+ ions are added, pH steadily decreases with the turbidity, resulting in a relatively clear supernatant. This is due to the increasing concentration of hydrogen ions in the suspension which neutralises some of the negative charges on the coagulated paracetamol particles [14].

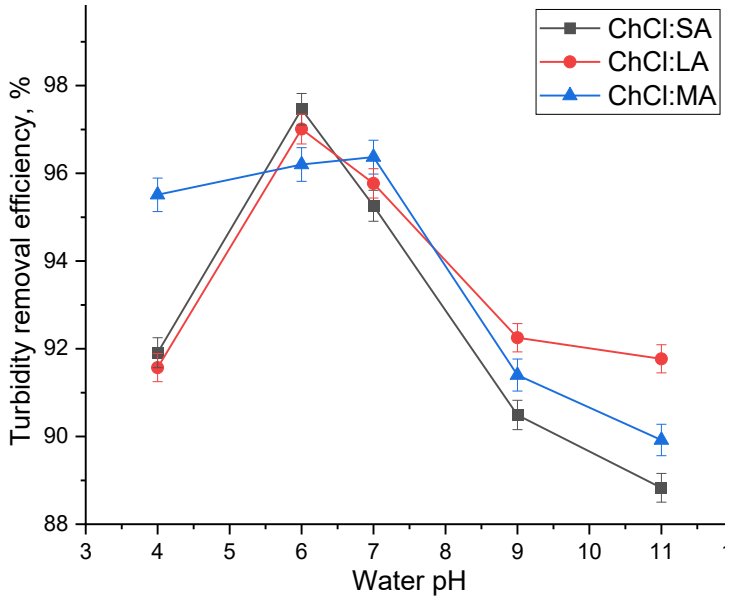

Figure 4. Effects of wastewater pH on turbidity removal efficiency using optimized NADES dosages and stirring time (data are average of n = 3)

3. 5. Performance comparison of NADESs under optimal conditions

Turbidity removal efficiencies of the NADESs and their individual constituents at the optimised conditions are illustrated in Figure 5. The optimized NADES dosage, stirring time and water pH of each NADES employed in this study are presented in Table 2. The highest turbidity reduction was achieved by ChCl:SA (97.5 %), followed by ChCl:LA (97.0 %) and ChCl:MA (96.4 %). The NADES constituent components were also efficient in removing the turbidity of wastewater with the turbidity reduction efficiency ranging from 87 to 93 %. Similar trends were observed at the screening stage, where malonic acid alone was less efficient in the turbidity removal compared to stearic and levulinic acids at their optimal conditions. Comparatively, the effects of various ChCl-based NADESs were previously studied for the turbidity removal in a bentonite suspension [13,14]. Carboxylic acids such as citric, lactic and malic acids were used as the HBD components of the NADESs revealing high removal efficiencies of up to 100 %. The results from this study

showed comparable removal efficiencies with NADESs based on other types of carboxylic acids as their constituents. Furthermore, these results suggest that the fatty acids alone could perform well in removing turbidity.

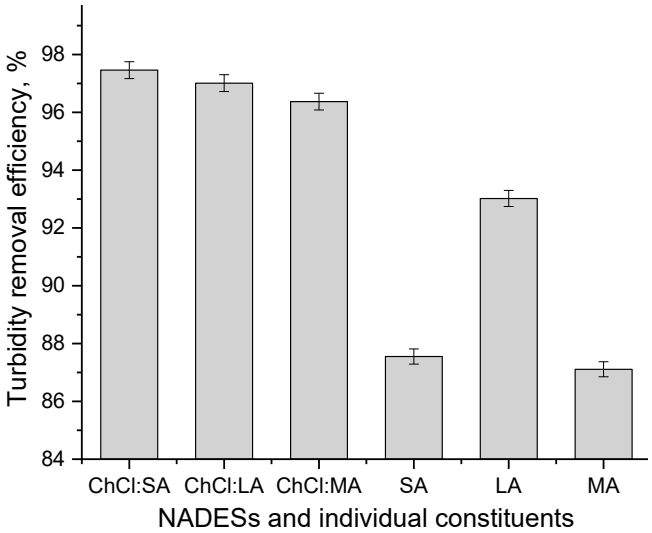

Figure 5. Comparison of turbidity removal efficiencies of NADESs and their individual constituents under optimal conditions (data are average of n = 3)

Table 2. Optimized NADES dosage, stirring time and wastewater pH for the removal of turbidity in paracetamol contaminated wastewater

	ChCl:SA	ChCl:LA	ChCl:MA
Dosage, g L^{-1}	16	10	20
Stirring time, min	20	25	30
pH of water system	6	6	7

3. 6. Investigation of molecular interactions between the pollutant and NADES

The performance of coagulants in this work can be explained by interactions between molecules with respect to the COSMO-RS *σ*-profile and *σ*-potential (histogram of charge density distribution over molecular surface). The validity of this approach was explained in detail in literature [15] and was reported in many recent studies involving molecular interactions analysis [16-18]. In the *σ*-profile, the molecule is considered adequately polar to induce hydrogen bonding as the screening charge density exceeds ±0.84 e nm^{-2}. A higher *σ* absolute value shows that the compound is a stronger HBD or HBA. On the other hand, the *σ*-potential indicates affinity of a component in a mixture towards another. In the *σ*-potential plot, a higher negative *μ* (*σ*) value indicates enhanced attraction between the molecules, whereas a higher positive value indicates increased repulsion between the molecules. In the horizontal axis, an increase in the negative and positive values for the hydrogen bonding threshold (±0.84 e nm^{-2}) indicates the region of a molecule where interactions between the HBDs and HBAs occur, respectively. The *σ*-profile and *σ*-potential of all species involved in this study are depicted in Figures 6 and 7, respectively.

In the turbidity reduction process, the coagulation mechanism can be inferred from interactions between paracetamol and the coagulants. Firstly, it is relevant to observe solvation effects in a mixture of paracetamol and water. As seen in Figure 6, water molecule possesses both donor and acceptor abilities via the hydrogen bonding between hydrogen atoms and the oxygen atom, respectively. Paracetamol possesses several peaks in the non-polar region due to the presence of the benzene ring and methyl group within the molecular structure. Additionally, paracetamol also exhibits peaks in the polar regions, which may be responsible for the hydrogen bonding with water observed from the similar peaks in the *σ*-profile of water. However, the non-polar surface of paracetamol makes it sparingly soluble in water at ambient temperature. Therefore, a competition can be expected between the water–paracetamol interaction and their corresponding self-associations, *i.e.* water–water and paracetamol–paracetamol interactions.

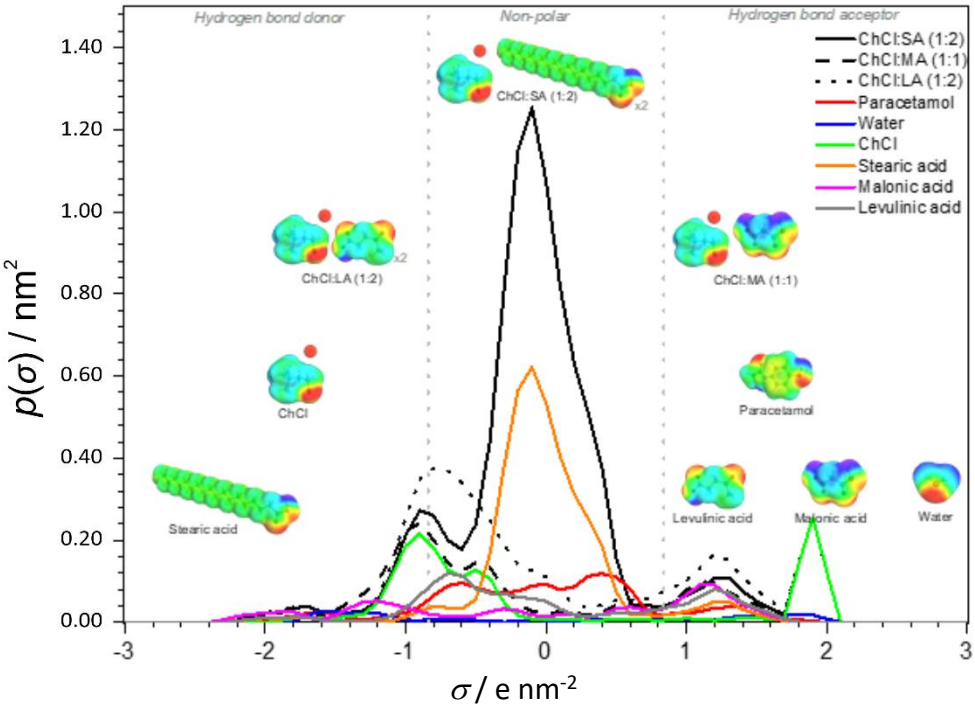

Figure 6. Plot of *σ*-profiles for the NADESs and their individual constituents, paracetamol, and water

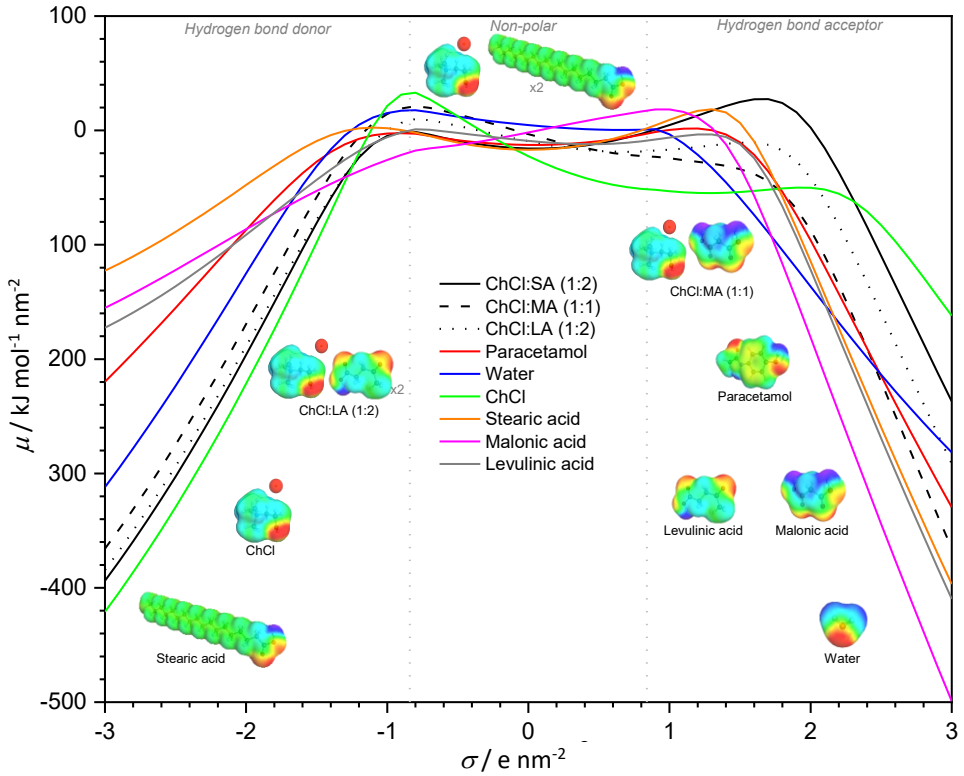

Figure 7. Plot of σ-potentials for the NADESs and their individual constituents, paracetamol, and water

From the paracetamol accumulation in water, a net negative charge can be expected from the colloids as paracetamol has more peaks in the hydrogen bond acceptor region. This explains the coagulation effect from the neutralization of opposite charges upon the introduction of coagulants, and consequently decreasing the turbidity of

water. This also suggests that the coagulant should have high hydrogen bond donor ability or being highly electro-negative *i.e.* exhibiting the peaks or the curve in the left side of the σ-profile. The σ-potential of both molecules also explains similar molecular interactions, where the interactions occur mainly in the polar regions.

By comparing the σ-profiles of the coagulants involved in this study, the presence of choline chloride brought significant peaks in the hydrogen bond donor region, *i.e.* at around -0.9 e nm^{-2}. This peak interacts well with the peaks of paracetamol in the hydrogen bond acceptor region, *i.e.* 1.4 e nm^{-2}. In addition, the peaks of malonic acid (1.1 e nm^{-2}), levulinic acid (1.2 e nm^{-2}) and stearic acid (1.2 e nm^{-2}) on the right side of the σ-profiles indicate significant polar interactions with the polarized peak of paracetamol on the left side (1.6 e nm^{-2}). On the other hand, the coagulants that consists of stearic acid (pure stearic acid and ChCl:SA (1:2)) show an obvious peak in the non-polar region. This peak is due to the presence of linear – CH_2 carbon chains in stearic acid, while the higher peak observed in the NADES form is due to its double molar ratio. However, as seen in the σ-potential, the non-polar attractions between the coagulants and paracetamol are very small compared to that in the polar region. Thus, it can be concluded that coagulants with straight carbon chains can be used to treat paracetamol contaminated water as long as they contain strong polar moieties. In the σ-potential plots, all coagulants showed attractive interaction in the polar regions, and relatively small attractions in the non-polar region. In the hydrogen bond acceptor region, paracetamol shows high affinity towards coagulants with negative μ values at the hydrogen bond donor region. From the investigations of the three NADESs, the attraction behaviour towards paracetamol increases in the order of ChCl:SA (1:2) > ChCl:LA (1:2) > ChCl:MA (1:1). This order is consistent with the performance of turbidity removal efficiency depicted previously in Figure 5. Furthermore, when comparing this specific region with all coagulants involved, the attraction behaviour at this region increased in the order of ChCl > ChCl:SA (1:2) > ChCl:LA (1:2) > ChCl:MA (1:1) >> levulinic acid > malonic acid > stearic acid. This ranking is almost identical to our experimental turbidity removal efficiency results, where ChCl is the only coagulant that showed significant deviation. Thus, it can be assumed that the polarity of coagulants with respect to the hydrogen bond donor ability influences the efficiency of turbidity removal.

4. CONCLUSION

High turbidity removal performances were demonstrated by using NADESs in this study. In a simulated wastewater containing paracetamol, ChCl:SA yielded the highest turbidity removal performances at 97.5 %, closely followed by ChCl:LA and ChCl:MA at 97.0 and 96.4 %, respectively at its optimized operating conditions. Optimal conditions were also applied for application of the individual fatty acid constituents. Under optimal conditions, the constituent components can also work efficiently on reducing turbidity of paracetamol-contaminated wastewater at a TRE range from 87–93 %. As a result, NADESs have been demonstrated to be able to reduce the turbidity of water to a lower value, in comparison to their individual components. The proposed NADESs can be categorized as promising solvents for the removal of turbidity caused by paracetamol in water and are preferable as novel coagulants owing to the simplicity of synthesis and application. As a preliminary study in applying NADESs for turbidity removal, these novel coagulants (ChCl-DES) require further studies in effluent treatment applications.

Acknowledgements: *This work was financially supported by the Ministry of Higher Education, Malaysia through the Grant provided under the Fundamental Research Grant Scheme FRGS/1/2023/TK05/UKM/02/5, and the Universiti Malaya, RU Geran-Fakulti program – GPF015A-2023.*

REFERENCES

[1] Crini G, Lichtfouse E. Advantages and disadvantages of techniques used for wastewater treatment. *Environ Chem Lett.* 2019; 17(1): 145-155. https://doi.org/10.1007/s10311-018-0785-9

[2] Yao T, Gan Y, Li Q, Tan M, Shi X. Removal and recovery of triphenylmethane dyes from wastewater with temperature-sensitive magnetic ionic liquid aqueous two-phase system. *J Clean Prod*. 2021; 328: 129648. https://doi.org/10.1016/j.jclepro.2021.129648

[3] Imdad S, Dohare RK. A Critical Review on Heavy Metals Removal Using Ionic Liquid Membranes from The Industrial Wastewater. *Chem Eng Process*. 2022; 173: 108812. https://doi.org/10.1016/j.cep.2022.108812

[4] Sundararaman S, Aravind Kumar J, Deivasigamani P, Devarajan Y. Emerging pharma residue contaminants: Occurrence, monitoring, risk and fate assessment – A challenge to water resource management. *Sci Total Environ*. 2022; 825: 153897. https://doi.org/10.1016/j.scitotenv.2022.153897

[5] Sgroi M, Anumol T, Vagliasindi FGA, Snyder SA, Roccaro P. Comparison of the new Cl_2/O_3/UV process with different ozone- and UV-based AOPs for wastewater treatment at pilot scale: Removal of pharmaceuticals and changes in fluorescing organic matter. *Sci Total Environ*. 2021; 765: 142720. https://doi.org/10.1016/j.scitotenv.2020.142720

[6] Gadipelly C, Pérez-González A, Yadav GD, Ortiz I, Ibáñez R, Rathod VK, Marathe KV. Pharmaceutical Industry Wastewater: Review of the Technologies for Water Treatment and Reuse. *Ind Eng Chem Res*. 2014; 53(29): 11571-11592. https://doi.org/10.1021/ie501210j

[7] Florindo C, Monteiro NV, Ribeiro BD, Branco LC, Marrucho IM. Hydrophobic deep eutectic solvents for purification of water contaminated with Bisphenol-A. *J Mol Liq*. 2020; 297: 111841. https://doi.org/10.1016/j.molliq.2019.111841

[8] Florindo C, Lima F, Branco LC, Marrucho IM. Hydrophobic Deep Eutectic Solvents: A Circular Approach to Purify Water Contaminated with Ciprofloxacin. *ACS Sustain Chem Eng*. 2019; 7(17): 14739-14746. https://doi.org/10.1021/acssuschemeng.9b02658

[9] Qu Q, Lv Y, Liu L, Row KH, Zhu T. Synthesis and characterization of deep eutectic solvents (five hydrophilic and three hydrophobic), and hydrophobic application for microextraction of environmental water samples. *Anal Bioanal Chem*. 2019; 411(28): 7489-7498. https://doi.org/10.1007/s00216-019-02143-z

[10] Florindo C, Branco LC, Marrucho IM. Development of hydrophobic deep eutectic solvents for extraction of pesticides from aqueous environments. *Fluid Phase Equilibr*. 2017; 448: 135-142. https://doi.org/10.1016/j.fluid.2017.04.002

[11] Ge D, Wang Y, Jianga Q, Dai E. A Deep Eutectic Solvent as an Extraction Solvent to Separate and Preconcentrate Parabens in Water Samples Using in situ Liquid-Liquid Microextraction. *J Brazil Chem Soc*. 2019; 30(6): 1203-1210. https://doi.org/10.21577/0103-5053.20190014

[12] Elgharbawy AAM, Hayyan A, Hayyan M, Mirghani MES, Salleh HM, Rashid SN, Ngoh GC, Liew SQ, Nor MR, bin Mohd Yusoff MYZ, Alias Y. Natural Deep Eutectic Solvent-Assisted Pectin Extraction from Pomelo Peel Using Sonoreactor: Experimental Optimization Approach. *Processes*. 2019; 7(7). https://doi.org/10.3390/pr7070416

[13] Al-Risheq DIM, Nasser MS, Qiblawey H, Ba-Abbad MM, Benamor A, Hussein IA. Destabilization of stable bentonite colloidal suspension using choline chloride based deep eutectic solvent: Optimization study. *J Water Process Eng*. 2021; 40: 101885. https://doi.org/10.1016/j.jwpe.2020.101885

[14] Al-Risheq DIM, Nasser MS, Qiblawey H, Hussein IA, Benamor A. Choline chloride based natural deep eutectic solvent for destabilization and separation of stable colloidal dispersions. *Sep Purif Technol*. 2021; 255: 117737. https://doi.org/10.1016/j.seppur.2020.117737

[15] Klamt A. *COSMO-RS: From Quantum Chemistry to Fluid Phase Thermodynamics and Drug Design*. 1st ed., Amsterdam, Netherlands: Elsevier; 2005.

[16] Foong CY, Zulkifli MFM, Wirzal MDH, Bustam MA, Nor LHM, Saad MS, Abd Halim NS. COSMO-RS prediction and experimental investigation of amino acid ionic liquid-based deep eutectic solvents for copper removal. *J Mol Liq*. 2021; 333: 115884. https://doi.org/10.1016/j.molliq.2021.115884

[17] Hu W, Shang Z, Wei N, Hou B, Gong J, Wang Y. Solubility of benorilate in twelve monosolvents: Determination, correlation and COSMO-RS analysis. *J Chem Thermodyn*. 2021; 152: 106272. https://doi.org/10.1016/j.jct.2020.106272

[18] Khan AS, Ibrahim TH, Rashid Z, Khamis MI, Nancarrow P, Jabbar NA. COSMO-RS based screening of ionic liquids for extraction of phenolic compounds from aqueous media. *J Mol Liq*. 2021; 328: 115387. https://doi.org/10.1016/j.molliq.2021.115387

Prirodni duboki eutektički rastvarači za uklanjanje zamućenosti iz sintetičke farmaceutske otpadne vode

Adeeb Hayyan[1], Siti Nuratikah Nabila binti Suratmin[1], Fathiah Mohamed Zuki[1], M. Zulhaziman M. Salleh[2], Jehad Saleh[3], Waleed Al Abdulmonem[4], Abdullah S. M. Aljohani[5], Ahmad GH. Aldaihani[6], Khaled H. Alkandari[1], Mohd Roslan Mohd Nor[7], Andrew T. H. Yeow[1] and Wan Jefrey Basirun[8]

[1]*Department of Chemical Engineering, Faculty of Engineering, Universiti Malaya, Kuala Lumpur, Malaysia*

[2]*Department of Chemical and Process Engineering, Faculty of Engineering and Built Environment, Universiti Kebangsaan Malaysia, Bangi, Selangor, Malaysia*

[3]*Chemical Engineering Department, King Saud University, Riyadh, Saudi Arabia*

[4]*Department of Pathology, College of Medicine, Qassim University, Buraydah, Saudi Arabia*

[5]*Department of Veterinary Medicine, College of Agriculture and Veterinary Medicine, Qassim University, Buraydah, Saudi Arabia*

[6]*School of Engineering, University of Liverpool, Liverpool, UK*

[7]*Halal Research Group, Academy of Islamic Studies, Universiti Malaya, Kuala Lumpur, Malaysia*

[8]*Department of Chemistry, Faculty of Science, University of Malaya, Kuala Lumpur, Malaysia*

(Naučni rad)

Izvod

Kontaminacija vodnih resursa otpadom aktivnih farmaceutskih sastojaka je među glavnim problemima životne sredine. Da bi se sprečili veliki poremećaji u prirodnim vodama, treba uspostaviti efikasan i ekološki prihvatljiv postupak uklanjanja zamućenja od strane uobičajenih zagađujućih materija, kao što je paracetamol. U ovoj studiji je istraživana upotreba nekoliko prirodnih dubokih eutektičkih rastvarača u cilju smanjivanja zamućenosti simulirane vode kontaminirane paracetamolom ispod standardne granice zamućenosti koju preporučuju Nacionalni standardi kvaliteta vode u Maleziji (50 NTU). Određeni su optimalni radni parametri (količina eutektičkih rastvarača, vreme mešanja i radna pH vrednost). Pod optimizovanim uslovima, korišćenje eutektičkog rastvarača na bazi stearinske kiseline dovelo je do najvećeg smanjenja zamućenosti od 97,5 %. Visoke performanse koagulacije su ispitivane na osnovu molekularne interakcije, korišćenjem COSMO-RS (CONductor like Screening MOdel for Real Solvents) σ-profila i σ-potencijala (histogram raspodele gustine naelektrisanja preko molekularne površine) i pokazali su visok afinitet između eutektičkih rastvarača i paracetamola. Zaključeno je da su eutektički rastvarači obećavajući kandidati za uklanjanje zamućenosti vode izazavane prisustvom paracetamola i prikladni su u daljim istraživanjima tretmana otpadnih voda.

Ključne reči: Aktivni farmaceutski sastojci; flokulacija; koagulacija; tretman otpadnih voda

Doktorske disertacije hemijsko–tehnološke struke odbranjene na univerzitetima u Srbiji u 2023. godini

TEHNOLOŠKO-METALURŠKI FAKULTET, UNIVERZITET U BEOGRADU

	Ime i prezime	Naslov	Mentor/i
1.	**Kumar Amit**	Razvoj i karakterizacija plazma sistema na atmosferskom pritisku za preradu otpadne vode	Dr Dragan Povrenović Dr Wolfgang Gernjak
2.	**Stefan Dikić**	Termomehanička prerada i transformaciono ponašanje mikrolegiranih čelika	Dr Dragomir Glišić Dr Sanja Martinović
3.	**Stefan Pavlović**	Sinteza i karakterizacija nanostrukturnog heterogenog katalizatora na bazi kalcijum-oksida valorizacijom čvrstih otpadnih materijala i njegova aktivnost u metanolizi suncokretovog ulja	Dr Ljiljana Mojović Dr Dalibor Marinković
4.	**Nela Petronijevi**	Ispitivanje mehanizma neutralizacije kiselih rudničkih voda korišćenjem flotacijske jalovine i letećeg pepela	Dr Željko Kamberović
5.	**Daniel Mijailović**	Porozne elektrode na bazi ugljeničnih vlakana i spinela prelaznih metala za primenu u skladištenju električne energije	Dr Petar Uskoković
6.	**Salih Rabab**	Lignin mikrosfere kao adsorbenti za uklanjanje tekstilnih boja i nosači za imobilizaciju enzima	Dr Aleksandar Marinković Dr Katarina Banjanac
7.	**Vesna Marjanović**	Primena polimernih nanokompozita modifikovanih getitom i magnetitom za uklanjanje selenata iz vode	Dr Maja Đolić Dr Marija Šljivić-Ivanović
8.	**Snežana Mihajlović**	Modifikacija i primena otpadnih prediva pamuka za uklanjanje jona teških metala iz vodenih rastvora	Dr Katarina Trivunac
9.	**Marija Ječmenica Dučić**	Primena kompozitnih ugljeničnih elektroda za elektrohemijsko uklanjanje organskih boja iz vodenih rastvora – eksperimentalni i teorijski pristup	Dr Milica Gvozdenović
10.	**Barbara Kalebić**	Površinska modifikacija i funkcionalizacija prirodnog zeolita - klinoptilolita	Dr Nevenka Rajić Dr Lidija Ćurković
11.	**Lana Putić**	Modifikacija funkcionalnih svojstava tekstilnih membrana	Dr Snežana Stanković Dr Jasna Stajić Trošić
12.	**Petar Batinić**	Kontrolisano otpuštanje folne kiseline iz sistema lipozom-biopolimerni film	Dr Branko Bugarski Dr Dušan Mijin
13.	**Zorica Jauković**	Razvoj i primena metode analize odabranih sterola i steroidnih hormona u prirodnim i otpadnim vodama tečnom hromatografijom sa tandem masenom spektrometrijom	Dr Svetlana Grujić
14.	**Vukašin Ugrinović**	Kompozitni hidrogelovi na bazi interpenetrirajućih mreža vinilnih i prirodnih polimera i nanočestica kalcijum-fosfata: sinteza, svojstva u primena u biomedicini	Dr Đorđe Veljović Dr Vesna Panić
15.	**Teodora Nedić**	Kontaminacija životne sredine usled prekomerne primene komponenata za koordinaciju izolacije na niskonaponskom nivou i mogućnost njene minimizacije	Dr Aco Janićijević Dr Predrag Kolarž
16.	**Ahmad Hakky Mohammad**	Optimizacija procesa adsorpcije zagađujućih materija iz vodenih rastvora primenom biomase *Pontederia crassipes*	Dr Mirjana Kijevčanin
17.	**Eleonora Gvozdić**	Razvoj i primena HPLC–MS/MS metode za ispitivanje prisustva veštačkih zaslađivača kao indikatora komunalnog zagađenja vode i sedimenata	Dr Svetlana Grujić
18.	**Danijela Prokić**	Uticaj modifikacije površine ugljeničnih materijala na njihova svojstva i adsorpciju odabranih estrogenih hormona iz vode	Dr. Tatjana Đurkić

TEHNIČKI FAKULTET U BORU, UNIVERZITET U BEOGRADU

Ime i prezime	Naslov	Mentor
1. Nebojsa Vučićević	Razvoj modela za optimizaciju emisije polutanata nastalih u procesu sagorevanja i detonacije ubojnih sredstava	Dr Milovan Vuković
2. Vladimir Nikolić	Definisanje modela za određivanje Bondovog radnog indeksa izučavanjem meljivosti sirovina nestandardne krupnoće	Dr Milan Trumić
3. Damir Ilić	Integrisani model za prioritizaciju strategija implementacije sistema bespilotnih vazduhoplova u svrhu tehnološkog razvoja u Republici Srbiji	Dr Isidora Milošević
4. Njegoš Dragović	Identifikacija i analiza faktora koji utiču na usvajanje i realizaciju projekata u oblasti korišćenja obnovljivih izvora energije	Dr Milovan Vuković
5. Jelena Velimirović	Razvoj višekriterijumskog modela za utvrđivanje prioriteta zamene energetske opreme primenom intervalnih dijagrama uticaja	Dr Đorđe Nikolić
6. Jelena Petrović	Hemometrijska karakterizacija teških metala u zemljištu i izdancima pionirskih vrsta koje rastu u blizini zagađenih voda u neposrednoj okolini rudarsko-metalurškog kompleksa u Boru: Aspekti fitoekstrakcije i biomonitoringa	Dr Slađana Alagić
7. Aleksandar Krstić	Razvoj i implementacija hibridnog višeodzivnog modela u fazi okruženju za optimizaciju parametara procesa tehnološkog postupka ekstruzije	Dr Đorđe Nikolić
8. Đuro Ćokeša	Istraživanje interakcije arsena i huminskih kiselina iz zemljišta	Dr Snežana Šerbula

TEHNOLOŠKI FAKULTET, UNIVERZITET U NOVOM SADU

Ime i prezime	Naslov	Mentor
1. Jelena Lubura	Modelovanje, simulacija i optimizacija dobijanja gumenih proizvoda na osnovu različitih kaučukovih smeša	Dr Oskar Bera
2. Milica Perović	Proteini leblebije (*Cicer arietinum* L.) - enzimska ekstrakcija, karakterizacija i modifikacija u nanostrukture pogodne za unapređenu primenu	Dr Mirjana Antov
3. Maja Milošević	Izdvajanje, karakterizacija i enzimska modifikacija pektinskog polisaharida muskatne tikve (*Curcubita moschata*)	Dr Mirjana Antov

TEHNOLOŠKI FAKULTET U LESKOVCU, UNIVERZITET U NIŠU

Ime i prezime	Naslov	Mentor/i
1. Aleksandra Mičić	Primena sorbenata na bazi pamučnog otpada iz odevne industrije u obradi obojenih voda	Dr Dragan Đorđević
2. Jelena Mitrović	Antioksidativni potencijal polifenola i ulja semena koprive (*Urtica dioica* L.) i karakterizacija proizvoda od pšeničnog brašna sa dodatkom semena koprive	Dr Nada Nikolić
3. Jovana Stepanović	Istraživanje deformacionih karakteristika teksturiranih multifilamentnih poliesterskih pređa	Dr Dušan Trajković